LIBRARY
ROYAL AIRCRAFT ESTABLISHMENT
BEDFORD.

R. & M. No. 2882
(13,655, 14,139)
A.R.C. Technical Report

MINISTRY OF SUPPLY

AERONAUTICAL RESEARCH COUNCIL
REPORTS AND MEMORANDA

Low-Speed Tests on 45-deg Swept-back Wings

PART I. PRESSURE MEASUREMENTS ON WINGS OF ASPECT RATIO 5

By

J. WEBER, Dr.rer.nat.
and
G. G. BREBNER, M.A.

PART II. BALANCE AND PRESSURE MEASUREMENTS ON WINGS OF DIFFERENT ASPECT RATIOS

By

D. KÜCHEMANN, Dr.rer.nat.,
J. WEBER, Dr.rer.nat.
and
G. G. BREBNER, M.A.

Crown Copyright Reserved

LONDON: HER MAJESTY'S STATIONERY OFFICE
1958

PRICE £1 12s. 6d. NET

Low-Speed Tests on 45-deg Swept-back Wings

Parts I and II

By

J. WEBER, Dr.rer.nat.,

D. KÜCHEMANN, Dr.rer.nat.

and

G. G. BREBNER, M.A.

COMMUNICATED BY THE PRINCIPAL DIRECTOR OF SCIENTIFIC RESEARCH (AIR), MINISTRY OF SUPPLY

*Reports and Memoranda No. 2882**

May, 1951

PART I

Pressure Measurements on Wings of Aspect Ratio 5

By

J. WEBER, Dr.rer.nat.

and

G. G. BREBNER, M.A.

Summary.—This report contains the results of pressure measurements on three 45-deg swept-back wings with constant chord and aspect ratio 5, over an incidence range up to 10 deg. Chordwise and spanwise lift distributions are given, mostly near the centre where, on two of the wings, modifications had been made to the section shape. It was found that altering the thickness distribution in the centre did not affect the loading but that approximately straight isobars could be obtained at values of C_L below about 0·1. By the incorporation of twist and camber in the central part the distortion of the lift distribution in the centre could be avoided at one particular incidence, and thus the same chordwise distribution obtained over most of the span.

Twist and camber alone do not improve the isobar pattern and therefore a thickness modification would be needed to give the desired lift distribution and isobar pattern at one particular incidence.

1. *Introduction.*—This report deals with part of the work done in an investigation of the chordwise and spanwise lift distribution of swept-back wings, and gives results of pressure measurements on three wings of aspect ratio 5 at incidences up to 10 deg. One wing had the same symmetrical section throughout the span. Another had a modification to its thickness distribution in the central part designed to straighten the isobars near the centre at zero incidence.

* R.A.E. Report Aero. 2374, received 4th January, 1951.

R.A.E. Report Aero. 2419, received 13th July, 1951.

The tests were made to find out how far this could be achieved, and whether there were any effects on the lift distribution. The third wing was designed with twist and camber in the central part to give approximately the same chord and spanwise lift distribution up to about mid-semispan at a C_L value of about $0 \cdot 15$. The test was intended to check the design method and to show the influence of such modifications on the isobar pattern.

2. *Details of Models and Tests.*—Pressure measurements have been made on three wings of 45-deg sweep and aspect ratio 5 in the No. 2, $11\frac{1}{2}$-ft $\times$ $8\frac{1}{2}$-ft Wind Tunnel at the Royal Aircraft Establishment during October and November 1949. All the wings had an identical plan-form, with constant chord up to $0 \cdot 90$ semispan. The wing tip had a curved leading edge and a straight trailing edge swept at 45 deg (Fig. 1). The wing chord was 20 inches and the span 98 inches, *i.e.*, $0 \cdot 71$ of the tunnel breadth.

The three wings will be called A, B and C. Wing A had the same section along wind throughout its span. This section was RAE 101, 12 per cent thickness/chord ratio, which has its maximum thickness at $0 \cdot 31$ chord. Co-ordinates are given in Table 1.

Wing B had the same basic section as wing A but the thickness distribution was modified in the central part of the wing. The thickness/chord ratio remained 12 per cent but the position of maximum thickness was moved forward to $0 \cdot 20$ chord on the centre-line where the modification was greatest. At $y/c = 0 \cdot 06$ and $y/c = 0 \cdot 14$, the shift of maximum thickness was respectively $0 \cdot 50$ and $0 \cdot 25$ times the shift at the centre, and it decreased to zero at $y/c = 0 \cdot 40$. The profile section at the centre was calculated from Ref. 1 to give at zero incidence the same pressure distribution as that at about mid-semispan. The co-ordinates of the modified section at two spanwise stations are given in Table 1.

Wing C also had the same basic section as wing A beyond $1 \cdot 00$ chord from the centre. Inboard of this section the thickness distribution remained the same, but the chord-line had a negative camber and a positive twist designed by the formulae given in Ref. 2, in order to give a chordwise load distribution approximately the same as that at mid-semispan at an incidence of about $2 \cdot 8$ deg. The camber and twist were greatest at the centre, decreasing to $0 \cdot 50$ and $0 \cdot 25$ their centre values at $y/c = 0 \cdot 13$ and $y/c = 0 \cdot 30$ respectively, and to zero at $y/c = 1 \cdot 00$; the co-ordinates of two spanwise positions are given in Table 1.

On all three wings, pressure measurements were made by means of flush holes on both upper and lower wing surfaces at several spanwise stations, (*see* Fig. 1). The copper tubes from these holes were led out through perspex tips. To complete the spanwise distribution up to the tip, another set of measurements was made at the section $y/c = 2 \cdot 20$ with a plain wooden tip, using a perforated copper tube sunk below the wing surface and covered with wax. This was the section at which the leading edge started to curve. The fairing for the tubes coming from the wing tip was not present for these readings; so that they are not strictly comparable with the other sections.

The range of incidence covered was from 0 deg to $+10$ deg for wings A and B, and from $-3 \cdot 8$ deg to $+10 \cdot 2$ deg for wing C. Since the ratio of wing span to tunnel breadth was $0 \cdot 71$, the tunnel correction to incidence varies along the span, being different at the various pressure measuring lines. Account has been taken of this by using the calculations of Bazjanac[3] (1943). These apply to an elliptical tunnel of ratio $1{:}\sqrt{2}$ in which a wing of span $1/\sqrt{2}$ times the major axis is represented by a single horseshoe vortex. The corrections given by this method for $\alpha = 10$ deg (measured) are $+0 \cdot 7$ deg at the tip and $+0 \cdot 4$ deg at the centre.

The wind speed was 163 ft/sec throughout the tests, giving a Reynolds number of $1 \cdot 68 \times 10^6$ based on wing chord.

3. *Results*.—3.1. *Wing with Constant Section* (Tables 2 to 4, Figs. 2 to 7).—Table 2 gives the measured values of C_p on upper and lower surfaces. It will be seen that the values for $\alpha = 0$ deg are not the same on both surfaces, but this small variation is not systematic and cannot be corrected by a shift of incidence. When evaluating the pressure differences between upper and lower surfaces, the pressure differences at zero incidence were subtracted from the corresponding pressure differences at non-zero incidences.

The chordwise load distributions are plotted in Figs. 2 and 3. Fig. 2, in conjunction with Fig. 6, shows how this distribution varies along the span. Three distinct regions are apparent, one from about $0 \cdot 2$ to $0 \cdot 8$ semispan in which the type of chordwise distribution is the same, the central part where the local lift decreases near the nose and increases in the rear part of the section, and the part near the tip where the local lift is concentrated towards the nose. The chordwise lift distribution is also influenced by the finite thickness of the wing as can be seen from the comparison of calculated distributions for thin and thick profiles in Fig. 3. The pressure distribution of the given thick profile was calculated by the method of Riegels[5,6] which replaces the wing by a distribution of sources and vortices. Finite thickness tends to increase the local lift coefficient.

The local values of the normal force and tangential force coefficients have been worked out by integrating graphically the chordwise pressure distribution and from these values the local lift and drag coefficients have been calculated.

The spanwise distribution of local lift coefficient, C_L, is given in Table 3 and in Figs. 4 and 5. Compared with the spanwise distribution for an unswept wing of the same plan-form and aspect ratio, there is a marked decrease of C_L at the centre and an increase near the tip. Fig. 5 also shows the additional lift near the tip, increasing with incidence (*see* also Fig. 13). This is due to the end-plate effect mentioned in Ref. 4. The values of local lift coefficient plotted against incidence (Fig. 4) do not lie on a straight line, the divergence increasing with distance from the centre. This is due to the effect of the boundary layer which also affects the type of spanwise loading as shown in Fig. 5. Fig. 5 shows that the boundary layer reduces the loading across the whole span. The reduction is smallest at the centre section.

The position of the aerodynamic centre is plotted in Fig. 6 and shows clearly the three regions already mentioned. Incidence has little effect on this position within the range tested.

The total lift coefficient obtained by graphical integration is given in Table 4. The value, $3 \cdot 40$, of the total lift slope is nearly that calculated (Ref. 2) for a wing with constant sectional lift slope, which corresponds to omitting centre and tip effects. The distributions of drag coefficients derived from the pressure measurements are given in Fig. 7, along with the spanwise distribution of induced drag, C_{Di}, calculated from the measured C_L distribution. A comparison of C_D and C_{Di} shows that C_D is greater than C_{Di} at the centre and less near the tip. This effect exists at zero lift (Ref. 7), and, due to the distorted chordwise lift distributions (Figs. 2 and 3), it increases with incidence. These positive and negative drag forces occur even in potential flow where they counterbalance each other and give no contribution to the total drag. Since the boundary layer also affects the pressure distribution, C_D will contain a positive contribution due to the boundary layer. The total drag $\bar{C}_D$ is therefore different from the total induced drag $\bar{C}_{Di}$.

3.2. *Wing with Modified Thickness Distribution*.—(Tables 5 and 6, Figs. 8 to 10).—The pressure distribution at several sections in the central part of the wing at zero incidence, and the corresponding isobar patterns are shown in Figs. 8 and 9. It can be seen that the isobars remain straight up to about $0 \cdot 1$ chord from the centre-line but they continue to curve at the centre. This is mainly because the profile of the centre section was calculated on the assumption that neighbouring sections would have the same profile, whereas in fact it changes gradually to the basic section shape. In the front part of the chord the thickness decreases in a spanwise direction until the basic section is reached, and in the rear part it increases. This accounts for the differences between the measured pressure distribution and the calculated distribution at the centre. It is doubtful whether there exists a profile shape which gives the 'sheared wing' distribution up to the centre section, and therefore even a more exact three-dimensional calculation in the central part might not achieve the required result. Since the peak suction line is straight up to the centre, the present approximation might be sufficient for practical purposes.

There is still a considerable improvement in the isobar pattern at small incidences, for example $\alpha = 2$ deg in Fig. 9. At higher incidences, from 4 deg upwards, the isobars are distorted near the centre because of the change in chordwise lift distribution there. The chordwise lift distribution at the centre is influenced only very slightly by the thickness modification (Fig. 8). Therefore the local lift coefficient, spanwise lift distribution and aerodynamic centre position are the same as for the wing with constant section.

3.3. *Wing with Camber and Twist.*—(Tables 7 and 8, Figs. 11 to 14).—Incidence in this case refers to the incidence of the unmodified part of the wing. At zero incidence there is a lift at the centre (Fig. 11), the resultant effect of the positive twist and negative camber, producing a sharp peak in the lift distribution at the front and a flat section of small negative lift behind. The change of lift for a given change of incidence is the same for this wing as for the uncambered wings (Fig. 11). This means that the lift components due to incidence, twist, and camber are additive. At the design incidence of 2·8 deg the total chordwise lift distribution at the centre is similar to that at mid-semispan (Fig. 12). The spanwise load distribution is nearly constant up to about 0·60 semispan. At higher incidences, the decrease in local lift coefficient in the inner part of the wing would be expected to reappear. Fig. 13 shows that this is delayed, the local lift near mid-semispan being reduced by the boundary-layer effects previously mentioned (*see* also Fig. 5).

The camber and twist move the position of the aerodynamic centre further forward than that of the constant section wing (Fig. 13). At 2·8 deg incidence the chordwise position of the aerodynamic centre is nearly the same for all spanwise stations. At higher incidences the chordwise position in the central part moves back towards that for the constant section wing.

The sharp peak in the lift distribution at zero incidence mentioned above (Fig. 11) is due to an increase in negative pressure on the upper surface near the nose, but this is not sufficient to compensate for the distortion at the centre due to thickness (Fig. 14) and the isobar pattern is not improved.

It was shown in section 3.2 that the lift effects are nearly independent of the pressure distribution at no lift, which can be modified near the centre by altering the chordwise position of the maximum thickness of the section. Similarly, from Fig. 11, the twist and camber applied near the centre of the wing affect the no-lift curve, but the pressure distribution due to change of α is unchanged.

It would therefore appear that a wing could be designed in which both types of variable are used to get a wing with the desired isobar pattern and lift distribution at some given C_L.

4. *Further Work.*—This wing was cut down successively to aspect ratios 3 and 2, and the results of the tests on aspect ratio effects follow in Part II of this paper.

NOTATION

x,y,z	Rectangular co-ordinates ; x-axis in direction of the main flow, y-axis spanwise ; z-axis upwards ; origin at leading edge
$c(y)$	Local wing chord
$\bar{c}$	Mean chord
b	Span
φ	Angle of sweep
α	Angle of incidence
C_p	$= (p - p_0)/q_0$, pressure coefficient
ΔC_p	Difference of pressure coefficients on upper and lower surface
$C_N(y)$	Coefficient of local normal force $= -\int_0^1 \Delta C_p(x,y)\, d\left(\frac{x}{c(y)}\right)$
$C_T(y)$	Coefficient of local tangential force $= \int_{\substack{\text{around}\\ \text{profile}}} C_p(x,y)\, d\left(\frac{z(x)}{c(y)}\right)$
$C_L(y)$	Local lift coefficient $= C_N \cos\alpha - C_T \sin\alpha$
$C_D(y)$	Local drag coefficient $= C_N \sin\alpha + C_T \cos\alpha$
C_{Di}	Coefficient of induced drag
$\bar{C}_L$	Coefficient of total lift $= \int_0^1 C_L(y)\frac{c(y)}{\bar{c}}\, d\left(\frac{y}{b/2}\right)$
$\bar{C}_D$	Coefficient of total drag as integrated from pressure measurements $= \int_0^1 C_D(y)\frac{c(y)}{\bar{c}}\, d\left(\frac{y}{b/2}\right)$
$C_m(y)$	Coefficient of local pitching moment with respect to the local quarter-chord point $= \int_0^1 \Delta C_p(x,y)\left(\frac{x}{c(y)} - 0\cdot 25\right) d\left(\frac{x}{c(y)}\right) + \int_{\substack{\text{around}\\ \text{profile}}} C_p(x,y)\frac{z(x)}{c(y)}\, d\left(\frac{z(x)}{c(y)}\right)$
h	x co-ordinate of local aerodynamic centre $= \left(0\cdot 25 - \frac{C_m(y)}{C_N(y)}\right)c(y)$

REFERENCES

No.	*Author*	*Title, etc.*
1	D. Küchemann	Design of wing junction, fuselage and nacelles to obtain the full benefit of sweptback wings at high Mach number. A.R.C. 11,035. 1947. (To be published.)
2	D. Küchemann	A simple method of calculating the spanwise and chordwise loadings on thin swept wings. A.R.C. 13,758. 1950.
3	D. Bazjanac	Investigations by means of the electrical analogy on the influence of the jet boundaries in wind tunnels on aerofoil measurements. Diss. Zürich, 1943. Summary in: F. W. Riegels: Wind tunnel corrections for incompressible flow. M.O.S. Göttingen Monograph D_3 4.1. M.A.P. Völkenrode R and T 958.
4	J. Weber	Low speed measurements of the pressure distributions and overall forces on wings of small aspect ratio and 53 deg sweepback. A.R.C. 12,878. 1949.
5	F. W. Riegels	The pressure distribution along an aerofoil profile. M.O.S. Göttingen Monograph E.3. M.A.P. Völkenrode, R and T 925.
6	J. Weber	A simple method for calculating the chordwise pressure distribution on two-dimensional and swept wings for aerofoil sections of finite thickness. A.R.C. 13,757. 1950.
7	J. Weber	Low speed measurements of the pressure distribution near the tips of swept back wings at no lift. A.R.C. 12,421. 1949. (To be published.)

TABLE 1

Co-ordinates of Profile Sections

(Co-ordinates in per cent chord and referred to chord-line of unmodified aerofoil)

x	Original section (Wing A)	Wing B with modified thickness distribution		Wing C with twisted and cambered centre section			
		$y/c = 0$	$y/c = 0 \cdot 1$	$y/c = 0$		$y/c = 0 \cdot 13$	
				upper surface	lower surface	upper surface	lower surface
0	0	0	0	5·48	+5·48	2·74	+2·74
1·25	1·64	2·72	1·86	6·60	3·32	4·12	0·84
2·50	2·30	3·53	2·61	7·03	2·43	4·67	+0·07
5	3·19	4·45	3·58	7·59	1·21	5·39	−0·99
7·5	3·83	5·03	4·20	7·96	+0·30	5·90	−1·76
10	4·33	5·43	4·69	8·23	−0·43	6·28	−2·38
15	5·06	5·86	5·39	8·57	−1·55	6·82	−3·30
20	5·56	6·00	5·83	8·73	−2·39	7·15	−3·97
30	6·00	5·73	5·96	8·58	−3·42	7·29	−4·71
40	5·76	4·92	5·52	7·84	−3·68	6·80	−4·72
50	5·12	3·80	4·76	6·75	−3·49	5·94	−4·30
60	4·24	2·72	3·70	5·47	−3·01	4·86	−3·62
70	3·22	1·80	2·64	4·09	−2·35	3·66	−2·78
80	2·15	1·00	1·62	2·69	−1·61	2·42	−1·88
90	1·07	0·40	0·72	1·32	−0·82	1·20	−0·94
100	0	0	0	0	0	0	0

TABLE 2

Pressure Coefficients on Wing A with Constant Section Shape

$\varphi = 45$ deg $\qquad A = 5 \cdot 0$

$y = 0$

Upper surface $\qquad C_p$

x/c	α (deg) 0	2·1	4·2	6·2	8·3	10·4
0	+1·010	+1·010	+0·980	+0·935	+0·865	+0·785
0·01	0·450	0·330	+0·190	+0·020	−0·165	−0·340
0·03	0·200	+0·095	−0·035	−0·180	−0·315	−0·460
0·08	+0·020	−0·085	−0·185	−0·290	−0·400	−0·505
0·15	−0·105	−0·195	−0·275	−0·375	—	−0·550
0·225	−0·175	−0·260	—	−0·415	−0·475	−0·560
0·35	−0·250	−0·315	−0·380	−0·455	−0·520	−0·590
0·50	−0·225	−0·275	−0·325	−0·380	−0·435	−0·475
0·65	−0·165	−0·205	−0·240	−0·285	−0·325	−0·350
0·75	−0·110	−0·140	−0·170	−0·205	−0·240	−0·250
0·85	−0·075	—	—	−0·150	−0·175	−0·185
0·95	−0·010	−0·025	−0·035	−0·055	−0·070	−0·065

Lower surface $\qquad C_p$

x/c	α (deg) 0	2·1	4·2	6·2	8·3	10·4
0·01	+0·520	+0·640	+0·745	+0·825	0·885	0·945
0·03	0·230	0·350	0·460	0·565	0·650	0·745
0·08	+0·005	+0·110	0·210	0·305	0·380	0·480
0·15	−0·095	−0·005	0·090	0·180	0·260	0·345
0·225	−0·155	−0·080	+0·005	+0·090	0·170	0·250
0·35	−0·245	−0·170	−0·095	−0·020	0·055	0·130
0·50	−0·220	−0·160	−0·095	−0·035	0·025	0·090
0·65	−0·165	−0·110	−0·060	−0·020	0·025	0·080
0·75	−0·120	−0·080	−0·035	+0·005	0·045	0·090
0·85	−0·060	−0·035	−0·005	0·025	0·060	0·100
0·95	−0·030	0	+0·025	+0·045	0·065	0·090

TABLE 2—*continued*

$y/c = 0 \cdot 1$ $2y/b = 0 \cdot 041$

Upper surface C_p

x/c	α (deg) 0	2·1	4·2	6·2	8·3	10·4
0	+0·545	+0·525	+0·425	+0·250	+0·025	−0·260
0·01	+0·180	−0·015	−0·235	−0·505	−0·800	−1·155
0·03	−0·015	−0·185	−0·370	−0·585	−0·805	−1·055
0·08	−0·120	−0·250	−0·375	−0·515	−0·660	−0·790
0·15	−0·195	−0·305	−0·400	−0·510	−0·600	−0·690
0·225	−0·245	−0·340	−0·415	−0·510	−0·580	−0·660
0·35	−0·245	−0·310	−0·385	−0·445	−0·515	−0·575
0·50	−0·185	−0·250	−0·280	−0·325	−0·375	−0·415
0·65	−0·115	−0·145	−0·180	−0·220	−0·250	−0·275
0·75	−0·065	−0·090	−0·120	−0·140	−0·170	−0·185
0·85	−0·010	−0·025	−0·040	−0·055	−0·075	−0·080
0·95	+0·060	+0·055	+0·050	+0·045	+0·040	+0·040

Lower surface C_p

x/c	α (deg) 0	2·1	4·2	6·2	8·3	10·4
0·01	+0·220	+0·375	+0·480	+0·540	0·565	0·535
0·03	+0·040	0·190	0·315	0·420	0·490	0·565
0·08	−0·110	+0·020	+0·130	0·235	0·325	0·420
0·15	−0·200	−0·105	−0·005	0·095	0·180	0·285
0·225	−0·225	−0·140	−0·055	+0·035	0·115	0·195
0·35	−0·250	−0·185	−0·115	−0·040	0·030	0·105
0·50	−0·205	−0·150	−0·095	−0·035	0·020	0·085
0·65	−0·125	−0·100	−0·050	−0·010	0·040	0·085
0·75	−0·060	—	—	+0·035	0·065	0·105
0·85	−0·025	0	+0·030	0·050	0·075	0·100
0·95	+0·050	+0·060	+0·060	+0·080	0·090	0·110

TABLE 2—*continued*

$y/c = 0 \cdot 2$ $2y/b = 0 \cdot 082$

Upper surface C_p

	α (deg)					
x/c	0	2·1	4·2	6·2	8·3	10·4
0	+0·490	+0·440	+0·270	−0·020	−0·375	−0·870
0·01	+0·155	−0·080	−0·355	−0·705	−1·085	−1·510
0·03	−0·055	−0·260	−0·485	−0·740	−1·015	−1·335
0·08	−0·170	−0·315	−0·465	−0·630	−0·795	−0·930
0·15	−0·240	−0·355	−0·465	−0·590	—	−0·780
0·225	−0·265	−0·365	−0·455	−0·550	−0·615	−0·695
0·35	−0·260	−0·335	−0·400	−0·450	−0·520	−0·570
0·50	−0·195	−0·245	−0·275	−0·320	−0·370	−0·395
0·65	−0·090	−0·130	−0·155	−0·190	−0·215	−0·235
0·75	−0·040	−0·065	−0·090	−0·100	−0·115	−0·135
0·85	+0·015	−0·005	−0·020	−0·025	−0·035	−0·040
0·95	+0·065	+0·060	+0·060	+0·055	+0·050	+0·050

Lower surface C_p

	α (deg)					
x/c	0	2·1	4·2	6·2	8·3	10·4
0·01	+0·205	+0·375	+0·480	+0·525	0·530	0·485
0·03	0	+0·170	0·310	0·415	0·500	0·550
0·08	−0·175	−0·035	+0·085	0·200	0·310	0·395
0·15	−0·240	−0·135	−0·025	0·075	0·170	0·265
0·225	−0·260	−0·170	−0·080	+0·005	0·090	0·180
0·35	−0·265	−0·200	−0·120	−0·055	0·015	0·095
0·50	−0·205	−0·145	−0·085	−0·030	0·015	0·085
0·65	−0·080	−0·045	−0·020	+0·010	0·035	0·090
0·75	−0·055	−0·020	0	0·020	0·055	0·095
0·85	+0·005	+0·025	+0·040	0·050	0·075	0·105
0·95	+0·060	+0·070	+0·075	+0·075	0·080	0·100

TABLE 2—*continued*

$y/c = 0 \cdot 4$ $2y/b = 0 \cdot 163$

Upper surface C_p

x/c	α (deg) 0	2·1	4·2	6·2	8·3	10·4
0	+0·490	+0·400	+0·165	−0·250	−0·770	−1·450
0·01	+0·125	−0·155	−0·485	−0·920	−1·415	−1·990
0·03	−0·060	−0·300	−0·550	−0·865	−1·185	−1·570
0·08	−0·200	−0·365	−0·540	−0·735	−0·925	−1·080
0·15	−0·265	−0·390	−0·520	−0·665	−0·775	−0·920
0·225	−0·265	−0·370	−0·465	−0·530	−0·635	−0·725
0·35	−0·265	−0·335	−0·400	−0·465	−0·535	−0·580
0·50	—	−0·190	−0·235	−0·275	−0·315	−0·340
0·65	−0·080	−0·095	—	−0·160	—	−0·190
0·75	−0·030	−0·050	−0·060	−0·075	−0·090	−0·095
0·85	+0·010	−0·005	−0·005	−0·010	−0·015	−0·020
0·95	+0·065	+0·060	+0·060	+0·055	+0·045	+0·040

Lower surface C_p

x/c	α (deg) 0	2·1	4·2	6·2	8·3	10·4
0·01	+0·130	+0·330	+0·455	+0·505	0·480	0·365
0·03	−0·075	+0·125	0·280	0·405	0·485	0·530
0·08	−0·215	−0·055	+0·085	0·210	0·310	0·405
0·15	−0·260	−0·145	−0·030	0·075	0·175	0·265
0·225	−0·275	−0·185	−0·085	+0·005	0·090	0·180
0·35	−0·265	−0·200	−0·125	−0·055	0·015	0·090
0·50	−0·165	−0·135	−0·070	−0·025	0·030	0·080
0·65	−0·070	−0·035	−0·010	+0·025	0·055	0·095
0·75	−0·025	0	+0·020	0·040	0·065	0·095
0·85	0	+0·030	0·040	0·050	0·065	0·085
0·95	+0·060	+0·065	+0·065	+0·070	0·060	0·080

TABLE 2—*continued*

$y/c = 0 \cdot 6$ $2y/b = 0 \cdot 245$

Upper surface C_p

x/c	α (deg)					
	0	2·1	4·2	6·2	8·3	10·4
0	—	+0·425	+0·220	−0·185	−0·740	−1·445
0·01	+0·125	−0·165	−0·505	−0·960	−1·475	−2·065
0·03	−0·065	−0·305	−0·615	−0·905	−1·280	−1·710
0·08	−0·195	−0·360	−0·535	−0·745	−0·950	−1·100
0·15	−0·260	−0·385	−0·505	−0·655	−0·755	−0·905
0·225	−0·270	−0·370	−0·465	−0·535	−0·655	−0·750
0·35	−0·250	−0·315	−0·370	—	−0·460	−0·520
0·50	−0·145	−0·160	−0·205	−0·250	−0·275	—
0·65	−0·055	−0·075	−0·100	−0·115	−0·130	−0·140
0·75	−0·020	−0·035	−0·050	−0·060	−0·060	−0·070
0·85	+0·025	+0·020	+0·015	+0·015	+0·010	0
0·95	+0·070	+0·070	+0·070	+0·070	+0·080	+0·035

Lower surface C_p

x/c	α (deg)					
	0	2·1	4·2	6·2	8·3	10·4
0·01	+0·090	+0·325	+0·450	+0·510	0·480	0·370
0·03	−0·065	+0·150	0·300	0·425	0·500	0·530
0·08	−0·220	−0·055	+0·085	0·225	0·325	0·410
0·15	−0·260	−0·135	−0·025	0·090	0·195	0·275
0·225	−0·265	−0·165	−0·075	+0·030	0·120	0·210
0·35	−0·250	−0·180	−0·110	−0·035	0·035	0·105
0·50	−0·175	−0·125	−0·065	−0·005	0·045	0·090
0·65	−0·060	−0·020	0	+0·020	0·060	0·095
0·75	−0·005	+0·020	+0·035	0·060	0·080	0·100
0·85	—	0·040	0·055	0·070	0·080	0·090
0·95	+0·070	+0·075	+0·085	+0·085	0·075	0·075

TABLE 2—*continued*

$y/c = 0 \cdot 9$ $2y/b = 0 \cdot 367$

Upper surface C_p

x/c	α (deg) 0	2·1	4·2	6·3	8·4	10·5
0	+0·505	+0·450	+0·270	−0·100	−0·635	−1·305
0·01	+0·115	−0·200	−0·565	−1·055	−1·660	−2·305
0·03	−0·055	−0·315	−0·595	−0·960	−1·375	−1·715
0·08	−0·185	−0·360	−0·545	−0·765	−0·945	−1·205
0·15	−0·250	−0·385	−0·515	−0·650	−0·780	−0·935
0·225	−0·260	−0·360	−0·460	−0·540	−0·650	−0·740
0·35	−0·245	−0·315	−0·345	−0·410	−0·470	−0·525
0·50	−0·145	—	−0·185	−0·230	−0·255	−0·275
0·65	−0·055	−0·080	−0·100	−0·115	−0·125	−0·125
0·75	—	—	−0·030	−0·035	−0·040	−0·055
0·85	+0·020	+0·015	+0·015	+0·020	+0·010	−0·020
0·95	+0·075	+0·080	+0·080	+0·080	+0·060	+0·015

Lower surface C_p

x/c	α (deg) 0	2·1	4·2	6·3	8·4	10·5
0·01	+0·100	+0·325	+0·465	+0·515	0·480	0·360
0·03	−0·090	+0·135	0·295	0·425	0·505	0·535
0·08	−0·200	−0·035	+0·115	0·240	0·355	0·435
0·15	−0·255	−0·130	−0·015	0·105	0·200	0·285
0·225	−0·260	−0·160	−0·065	+0·035	0·120	0·195
0·35	−0·240	−0·170	−0·105	−0·030	0·040	0·100
0·50	−0·140	−0·095	−0·035	+0·010	0·060	0·100
0·65	−0·050	−0·030	+0·005	0·040	0·065	0·085
0·75	−0·020	+0·005	0·025	0·050	0·065	0·075
0·85	+0·035	0·050	0·060	0·075	0·085	0·085
0·95	+0·070	+0·075	+0·080	+0·080	0·070	0·055

TABLE 2—*continued*

$y/c = 1 \cdot 25$ $2y/b = 0 \cdot 510$

Upper surface C_p

x/c	α (deg) 0	2·1	4·2	6·3	8·4	10·5
0	+0·495	+0·510	+0·380	+0·095	−0·365	−0·995
0·01	+0·155	−0·150	−0·515	−1·015	−1·650	−2·335
0·03	−0·065	−0·330	−0·620	−0·990	−1·385	−1·885
0·08	−0·200	−0·380	−0·575	−0·800	−1·015	−1·235
0·15	−0·240	−0·380	−0·505	−0·650	−0·770	−0·915
0·225	−0·250	−0·355	−0·445	—	−0·610	−0·710
0·35	−0·235	−0·310	−0·345	−0·410	−0·470	−0·520
0·50	−0·140	—	−0·190	−0·225	−0·250	−0·260
0·65	−0·055	−0·080	−0·095	−0·110	−0·115	−0·115
0·75	−0·010	−0·025	−0·030	−0·035	−0·035	−0·055
0·85	+0·035	+0·030	+0·025	+0·030	+0·025	−0·025
0·95	+0·080	+0·085	+0·085	+0·085	+0·060	−0·025

Lower surface C_p

x/c	α (deg) 0	2·1	4·2	6·3	8·4	10·5
0·01	+0·110	+0·350	+0·480	+0·525	0·490	0·325
0·03	−0·040	+0·180	0·355	0·460	0·525	0·530
0·08	−0·185	−0·015	+0·130	0·265	0·370	0·445
0·15	−0·245	−0·115	0	0·120	0·220	0·295
0·225	−0·255	−0·155	−0·060	+0·045	0·125	0·200
0·35	−0·235	−0·165	−0·095	−0·010	0·045	0·100
0·50	−0·150	−0·105	−0·035	+0·020	0·065	0·090
0·65	−0·060	−0·025	0	0·030	0·060	0·075
0·75	−0·010	+0·015	+0·030	0·055	0·065	0·080
0·85	+0·030	0·045	0·055	0·070	0·070	0·070
0·95	+0·070	+0·070	+0·075	+0·070	0·055	0·040

TABLE 2—*continued*

$y/c = 1 \cdot 6$ $2y/b = 0 \cdot 653$

Upper surface C_p

x/c	α (deg)					
	0	2·1	4·2	6·3	8·5	10·6
0	+0·500	+0·410	+0·170	−0·290	−0·920	−1·685
0·01	+0·130	−0·200	−0·575	−1·125	−1·750	−2·445
0·03	−0·090	−0·345	−0·640	−1·010	−1·420	−1·795
0·08	−0·225	−0·405	−0·595	−0·820	−1·000	−1·255
0·15	−0·250	−0·385	−0·510	−0·640	−0·770	−0·915
0·225	−0·255	−0·355	−0·445	−0·545	−0·645	−0·725
0·35	−0·240	−0·300	−0·355	−0·420	−0·465	−0·490
0·50	−0·140	−0·175	−0·205	−0·230	−0·245	−0·245
0·65	−0·060	−0·080	−0·090	−0·100	−0·110	−0·120
0·75	0	−0·010	−0·015	−0·020	−0·035	−0·065
0·85	+0·030	+0·025	+0·025	+0·025	+0·010	−0·020
0·95	+0·080	+0·085	+0·085	+0·085	+0·060	+0·060

Lower surface C_p

x/c	α (deg)					
	0	2·1	4·2	6·3	8·5	10·6
0·01	+0·135	+0·355	+0·475	+0·520	0·470	0·335
0·03	−0·045	+0·180	0·335	0·460	0·515	0·530
0·08	−0·180	−0·010	0·125	0·255	0·350	0·435
0·15	−0·230	−0·100	+0·010	0·130	0·220	0·300
0·225	−0·255	−0·160	−0·065	+0·030	0·110	0·190
0·35	−0·240	−0·175	−0·110	−0·035	0·025	0·090
0·50	−0·145	−0·110	−0·040	+0·005	0·045	0·085
0·65	−0·040	−0·010	+0·010	0·035	0·055	0·075
0·75	−0·005	+0·005	0·025	0·045	0·055	0·065
0·85	+0·035	0·045	0·055	0·070	0·070	0·070
0·95	+0·075	+0·080	+0·085	+0·085	0·075	0·070

TABLE 2—*continued*

$y/c = 2\cdot20$ $\qquad$ $2y/b = 0\cdot898$

Upper surface $\quad C_p$

x/c	α (deg) 0	4·3	10·7
0	+0·430	+0·250	−1·375
0·01	−0·015	−0·425	−1·835
0·03	−0·150	−0·530	−1·480
0·08	−0·195	−0·510	−0·895
0·15	−0·220	−0·440	−0·715
0·225	−0·230	−0·380	−0·600
0·35	−0·205	−0·300	−0·385
0·50	−0·120	—	−0·180
0·65	−0·030	−0·045	−0·055
0·75	0	0	0
0·85	+0·050	+0·050	+0·040
0·95	+0·110	+0·110	+0·100

Lower surface $\quad C_p$

x/c	α (deg) 0	4·3	10·7
0·01	−0·065	+0·345	+0·325
0·03	−0·215	+0·160	0·380
0·08	−0·265	−0·005	0·240
0·15	−0·255	−0·075	0·140
0·225	−0·275	−0·125	+0·050
0·35	−0·230	−0·100	−0·035
0·50	−0·140	−0·055	+0·005
0·65	−0·055	0	0·030
0·75	−0·015	+0·010	0·035
0·85	+0·035	0·035	0·055
0·95	+0·075	+0·070	+0·070

$y/c = 2\cdot33$ $\qquad$ $2y/b = 0\cdot949$

Upper surface $\quad C_p$

x/c	α (deg) 0	2·1	4·3	6·4	8·6	10·7
0	+0·060	+0·025	−0·085	−0·285	−0·560	−0·880
0·025	−0·060	−0·215	−0·420	−0·700	−1·030	−1·375
0·05	−0·115	−0·245	−0·425	−0·650	−0·905	−1·170
0·10	−0·160	−0·260	−0·390	−0·560	−0·745	−0·915
0·15	−0·185	−0·270	−0·380	−0·520	−0·665	−0·795
0·25	−0·175	−0·240	−0·320	−0·425	−0·520	−0·595
0·35	−0·160	−0·210	−0·265	−0·330	−0·400	−0·440
0·50	−0·090	−0·120	−0·150	−0·190	−0·240	−0·270
0·70	+0·005	−0·005	−0·020	−0·045	−0·055	−0·055

Lower surface $\quad C_p$

x/c	α (deg) 0	2·1	4·3	6·4	8·6	10·7
0·025	−0·075	+0·060	+0·095	+0·085	+0·020	−0·085
0·05	−0·100	+0·005	+0·070	0·090	0·075	+0·025
0·10	−0·155	−0·065	0	0·040	0·055	0·050
0·15	−0·175	−0·090	−0·035	+0·010	0·045	0·045
0·25	−0·185	−0·115	−0·065	−0·020	+0·015	0·045
0·35	−0·160	−0·120	−0·080	−0·040	−0·015	0·005
0·50	−0·065	−0·045	−0·030	0	+0·015	0·035
0·70	+0·005	+0·035	+0·050	+0·060	+0·065	+0·070

TABLE 3

Coefficients of Local Normal Force, Tangential Force, Lift, Drag and Aerodynamic Centre Position

Wing A with constant section shape

$\varphi = 45$ deg $\qquad A = 5 \cdot 0$

C_N

	$2y/b$									
α (deg)	0	0·041	0·082	0·163	0·245	0·367	0·510	0·653	0·898	0·949
2·1	0·120	0·121	0·127	0·129	0·129	0·129	0·131	0·125	—	0·087
4·2	0·239	0·243	0·249	0·254	0·251	0·250	0·251	0·246	0·192	0·170
6·3	0·357	0·360	0·368	0·374	0·374	0·372	0·376	0·364	—	0·254
8·4	0·476	0·479	0·484	0·493	0·492	0·491	0·491	0·477	—	0·336
10·5	0·592	0·595	0·599	0·605	0·608	0·601	0·595	0·582	0·410	0·395

C_T

	$2y/b$									
α (deg)	0	0·041	0·082	0·163	0·245	0·367	0·510	0·653	0·898	0·949
0	0·044	0·014	0·007	0·002	0	−0·001	0	−0·001	−0·009	−0·010
2·1	0·043	0·012	0·005	−0·001	−0·003	−0·004	−0·003	−0·004	—	−0·012
4·2	0·042	0·007	−0·002	−0·010	−0·012	−0·012	−0·013	−0·014	−0·016	−0·020
6·3	0·039	−0·001	−0·013	−0·024	−0·027	−0·029	−0·030	−0·031	—	−0·033
8·4	0·035	−0·012	−0·027	−0·044	−0·047	−0·050	−0·050	−0·053	—	−0·050
10·5	0·030	−0·025	−0·045	−0·067	−0·071	−0·074	−0·075	−0·082	−0·067	−0·069

C_L

	$2y/b$									
α (deg)	0	0·041	0·082	0·163	0·245	0·367	0·510	0·653	0·898	0·949
2·1	0·118	0·121	0·126	0·129	0·129	0·129	0·131	0·125	—	0·087
4·2	0·235	0·241	0·248	0·253	0·251	0·251	0·251	0·246	0·192	0·171
6·3	0·351	0·358	0·367	0·374	0·375	0·373	0·377	0·365	—	0·256
8·4	0·466	0·476	0·483	0·494	0·494	0·493	0·493	0·480	—	0·340
10·5	0·577	0·589	0·597	0·607	0·611	0·605	0·599	0·587	0·415	0·401

TABLE 3—*continued*

C_D

α (deg)	2y/b 0	0·041	0·082	0·163	0·245	0·367	0·510	0·653	0·898	0·949
0	0·044	0·014	0·007	0·002	0	−0·001	0	−0·001	−0·009	−0·010
2·1	0·047	0·016	0·010	0·004	0·002	+0·001	0·002	+0·001	—	−0·009
4·2	0·059	0·025	0·016	0·009	0·007	0·006	0·006	0·004	−0·002	−0·007
6·3	0·078	0·039	0·028	0·017	0·015	0·012	0·012	0·009	—	−0·005
8·4	0·104	0·058	0·045	0·029	0·026	0·023	0·022	0·016	—	−0·001
10·5	0·138	0·084	0·065	0·044	0·041	+0·037	0·035	+0·026	+0·009	+0·004

h/c

α (deg)	2y/b 0	0·041	0·082	0·163	0·245	0·367	0·510	0·653	0·898	0·949
0 extrapol.	0·368	0·320	0·291	0·265	0·253	0·243	0·240	0·236	0·217	0·273
2·1	0·368	—	—	—	—	—	—	0·234	—	—
4·2	0·367	0·319	0·293	0·265	0·254	0·242	0·242	0·235	0·219	0·267
6·3	0·362	0·316	0·287	0·264	0·254	0·240	0·240	0·233	—	0·267
8·4	0·363	0·319	0·291	0·264	0·252	0·241	0·237	0·234	—	0·261
10·5	0·362	0·319	0·292	0·265	0·251	0·239	0·237	0·233	0·205	0·254

TABLE 4

Coefficients of Total Lift and Drag from Pressure Measurements

Wing A

α (deg)	$\bar{C}_L$	$\bar{C}_D$
2·1	0·121	—
4·2	0·238	0·005
6·3	0·350	0·012
8·4	0·456	0·022
10·5	0·559	0·035

TABLE 5

Pressure Coefficients on Wing B with Modified Thickness Distribution at the Centre

$\varphi = 45$ deg $\qquad A = 5 \cdot 0$

$y = 0$

Upper surface $\qquad C_p$

x/c	α (deg)					
	0	2·1	4·2	6·2	8·3	10·4
0	+1·005	+1·005	+0·995	+0·950	+0·910	+0·845
0·01	0·510	0·410	+0·295	+0·155	+0·030	−0·120
0·03	+0·225	+0·110	−0·015	−0·165	−0·285	−0·440
0·08	−0·100	−0·205	−0·310	−0·430	−0·535	−0·645
0·15	−0·165	−0·250	−0·335	−0·440	−0·525	−0·605
0·225	−0·240	−0·320	−0·400	−0·490	−0·565	−0·640
0·35	−0·250	−0·315	−0·380	−0·450	−0·510	−0·575
0·50	−0·180	−0·230	−0·270	−0·325	−0·370	−0·425
0·65	−0·105	−0·145	−0·180	−0·220	−0·250	−0·285
0·75	−0·070	−0·105	−0·130	−0·165	−0·190	−0·220
0·95	+0·035	+0·025	+0·020	+0·005	0	−0·015

Lower surface $\qquad C_p$

x/c	α (deg)					
	0	2·1	4·2	6·2	8·3	10·4
0·01	+0·540	+0·650	+0·745	+0·825	0·890	0·945
0·03	+0·165	0·285	0·400	0·510	0·605	0·685
0·08	−0·105	+0·010	0·125	0·225	0·320	0·405
0·15	−0·165	−0·065	+0·035	0·130	0·215	0·290
0·225	−0·240	−0·145	−0·055	+0·035	0·125	0·200
0·35	−0·240	−0·165	−0·085	−0·005	0·065	0·135
0·50	−0·195	−0·135	−0·065	0	0·065	0·120
0·65	−0·120	−0·065	−0·015	+0·035	0·085	0·135
0·75	−0·070	−0·030	+0·015	0·055	0·100	0·140
0·85	−0·045	−0·005	0·020	0·035	0·080	0·145
0·95	+0·020	+0·040	+0·055	+0·075	0·105	0·120

TABLE 5—*continued*

$y/c = 0{\cdot}1$ $\qquad$ $2y/b = 0{\cdot}041$

Upper surface $\qquad$ C_p

	α (deg)					
x/c	0	2·1	4·2	6·2	8·3	10·4
0	+0·470	+0·465	+0·395	+0·245	+0·035	−0·250
0·01	0·150	−0·020	−0·210	−0·475	−0·735	−1·030
0·03	−0·070	−0·235	−0·410	−0·630	−0·830	−1·060
0·08	−0·185	−0·305	−0·440	−0·585	−0·730	−0·905
0·15	−0·245	−0·350	−0·455	−0·580	−0·685	−0·760
0·225	−0·265	−0·350	−0·440	—	−0·580	−0·650
0·35	−0·240	−0·310	−0·380	—	−0·455	−0·525
0·50	−0·180	−0·205	−0·245	−0·295	−0·335	−0·385
0·65	−0·075	−0·110	−0·135	−0·170	−0·200	−0·235
0·75	−0·050	−0·070	−0·090	−0·115	−0·135	−0·165
0·85	+0·010	−0·005	−0·020	−0·035	−0·050	−0·060
0·95	—	—	—	—	—	—

Lower surface $\qquad$ C_p

	α (deg)					
x/c	0	2·1	4·2	6·2	8·3	10·4
0·01	+0·140	+0·285	+0·410	+0·495	0·550	0·565
0·03	−0·075	+0·090	0·230	0·350	0·450	0·510
0·08	−0·200	−0·070	+0·060	0·180	0·280	0·360
0·15	−0·255	−0·145	−0·040	0·065	0·165	0·245
0·225	−0·270	−0·175	−0·085	+0·010	0·100	0·170
0·35	−0·250	−0·175	−0·105	−0·025	0·050	0·110
0·50	−0·165	—	−0·060	+0·020	—	0·105
0·65	−0·080	−0·035	+0·005	0·050	0·095	0·130
0·75	−0·040	−0·005	0·035	0·070	0·110	0·135
0·85	0	+0·030	0·060	0·085	0·115	0·135
0·95	+0·035	+0·055	+0·070	+0·085	0·100	0·110

TABLE 5—*continued*

$y/c = 0 \cdot 4$ $2y/b = 0 \cdot 163$

Upper surface C_p

x/c	α (deg) 0	2·1	4·2	6·2	8·3	10·4
0	+0·495	+0·440	+0·245	−0·140	−0·640	−1·295
0·01	+0·115	−0·155	−0·490	−0·920	−1·365	−1·900
0·03	−0·045	−0·275	−0·540	−0·855	−1·190	−1·620
0·08	−0·200	−0·365	−0·545	−0·740	−0·950	−1·130
0·15	−0·240	−0·360	−0·490	—	—	−0·830
0·225	−0·265	−0·365	−0·460	−0·540	−0·610	−0·725
0·35	−0·250	−0·325	−0·395	−0·445	−0·505	−0·575
0·50	−0·170	—	−0·210	−0·255	−0·290	−0·335
0·65	−0·055	−0·080	−0·105	−0·130	−0·145	−0·175
0·75	−0·010	−0·025	−0·035	−0·050	−0·060	−0·085
0·85	+0·035	+0·030	+0·025	+0·015	+0·010	−0·015
0·95	+0·065	+0·070	+0·080	+0·075	+0·070	+0·040

Lower surface C_p

x/c	α (deg) 0	2·1	4·2	6·2	8·3	10·4
0·01	+0·090	+0·300	+0·440	+0·515	0·515	0·445
0·03	−0·130	+0·085	0·260	0·390	0·480	0·520
0·08	−0·230	−0·070	+0·080	0·205	0·315	0·395
0·15	−0·270	−0·140	−0·020	0·095	0·195	0·275
0·225	−0·285	−0·175	−0·075	+0·025	0·115	0·185
0·35	−0·265	−0·185	−0·110	−0·035	0·040	0·100
0·50	−0·180	−0·125	−0·060	−0·005	0·055	0·085
0·65	−0·070	−0·025	+0·005	+0·040	0·075	0·110
0·75	−0·040	−0·010	0·020	0·040	0·065	0·095
0·85	+0·025	+0·050	0·065	0·075	0·100	0·110
0·95	+0·060	+0·075	+0·080	+0·080	0·085	0·085

TABLE 6

Coefficients of Local Normal Force, Tangential Force, Lift, Drag and Aerodynamic Centre Position

Wing B with modified thickness distribution at the centre

$\varphi = 45$ deg $A = 5 \cdot 0$

C_N

α (deg)	$2y/b$		
	0	0·041	0·163
2·1	0·121	0·122	0·136
4·2	0·239	0·244	0·263
6·3	0·358	0·362	0·387
8·4	0·475	0·475	0·511
10·5	0·591	0·588	0·631

C_T

α (deg)	$2y/b$		
	0	0·041	0·163
0	0·064	+0·010	0
2·1	0·063	0·009	−0·003
4·2	0·062	+0·005	−0·012
6·3	0·059	−0·002	−0·025
8·4	0·055	−0·012	−0·043
10·5	0·050	−0·024	−0·064

C_L

α (deg)	$2y/b$		
	0	0·041	0·163
2·1	0·119	0·122	0·136
4·2	0·234	0·243	0·263
6·3	0·349	0·360	0·387
8·4	0·462	0·472	0·512
10·5	0·572	0·583	0·632

C_D

α (deg)	$2y/b$		
	0	0·041	0·163
0	0·064	0·010	0
2·1	0·067	0·014	0·002
4·2	0·079	0·023	0·008
6·3	0·098	0·038	0·018
8·4	0·125	0·057	0·033
10·5	0·156	0·084	0·051

h/c

α (deg)	$2y/b$		
	0	0·041	0·163
0 extrapol.	0·353	0·318	0·265
2·1	—	—	—
4·2	0·355	0·316	0·265
6·3	0·355	0·318	0·265
8·4	0·356	0·319	0·266
10·5	0·357	0·320	0·266

TABLE 7

Pressure Coefficients on Wing C with Twisted and Cambered Centre Section

$\varphi = 45$ deg $\qquad A = 5$

$y = 0$

Upper surface $\qquad C_p$

x/c	α (deg)							
	−4·0	−1·9	−0·1	+2·3	+4·4	+6·4	+8·5	+10·6
0	+1·00	+0·985	+0·965	+0·905	+0·830	+0·740	+0·620	+0·505
0·01	0·370	0·235	+0·115	−0·070	−0·240	−0·415	−0·590	−0·755
0·03	0·160	+0·040	−0·060	−0·215	−0·345	−0·490	−0·615	−0·735
0·08	0·055	−0·050	−0·125	−0·250	−0·350	−0·450	−0·535	−0·635
0·15	+0·035	−0·055	−0·120	−0·220	−0·290	−0·375	−0·445	−0·520
0·225	−0·035	−0·115	−0·185	−0·270	−0·340	−0·420	−0·500	−0·575
0·35	−0·075	−0·145	−0·200	−0·270	−0·335	−0·395	−0·460	−0·510
0·50	−0·110	−0·170	−0·220	−0·275	−0·325	−0·380	−0·435	−0·480
0·65	−0·070	−0·115	−0·155	−0·205	−0·240	−0·280	−0·320	−0·350
0·75	−0·045	−0·085	−0·115	−0·160	−0·190	−0·225	−0·250	−0·275
0·85	−0·015	−0·050	−0·070	−0·105	−0·125	−0·150	−0·175	−0·190
0·95	+0·015	0	−0·015	−0·040	−0·045	−0·065	−0·075	−0·080

Lower surface $\qquad C_p$

x/c	α (deg)							
	−4·0	−1·9	−0·1	+2·3	+4·4	+6·4	+8·5	+10·6
0·01	+0·565	+0·670	+0·745	+0·830	+0·895	+0·940	0·975	0·995
0·03	+0·180	0·290	0·390	0·515	0·615	0·700	0·775	0·835
0·08	−0·110	+0·015	+0·105	0·225	0·330	0·420	0·515	0·590
0·15	−0·260	−0·155	−0·075	+0·040	0·140	0·225	0·320	0·400
0·225	−0·335	−0·240	−0·170	−0·060	+0·035	0·115	0·205	0·275
0·35	−0·375	−0·295	−0·240	−0·150	−0·070	+0·005	0·085	0·150
0·50	−0·350	−0·280	−0·240	−0·165	−0·100	−0·040	0·030	0·090
0·65	−0·270	−0·225	−0·185	−0·125	−0·075	−0·030	0·030	0·075
0·75	−0·200	−0·180	−0·150	−0·100	−0·055	−0·015	0·035	0·075
0·85	—	—	—	−0·065	−0·025	+0·005	0·050	0·085
0·95	−0·060	−0·045	−0·030	−0·005	+0·010	+0·035	0·060	0·085

TABLE 7—*continued*

$y/c = 0 \cdot 13$ $2y/b = 0 \cdot 053$

Upper surface C_p

x/c	α (deg)							
	−4·0	−1·9	−0·1	+2·3	+4·4	+6·4	+8·5	+10·6
0	+0·490	+0·490	+0·435	+0·270	+0·035	−0·275	−0·710	−1·160
0·01	0·220	+0·030	−0·155	−0·450	−0·750	−1·075	−1·455	−1·835
0·03	0·125	−0·035	−0·180	−0·405	−0·625	−0·860	−1·130	−1·280
0·08	+0·015	−0·115	−0·220	−0·375	−0·515	−0·635	−0·780	−0·920
0·15	−0·045	−0·145	−0·235	−0·350	−0·455	−0·550	−0·655	−0·750
0·225	−0·100	−0·195	−0·260	−0·365	−0·425	−0·520	−0·615	−0·695
0·35	−0·145	−0·220	−0·275	−0·350	−0·400	−0·465	−0·540	−0·600
0·50	−0·100	−0·160	—	−0·240	−0·285	−0·335	−0·385	−0·430
0·65	−0·060	−0·085	−0·120	−0·160	−0·195	−0·225	−0·260	−0·290
0·75	+0·015	−0·040	−0·050	−0·080	−0·105	−0·135	−0·165	−0·195
0·85	0·035	—	−0·005	−0·025	−0·040	−0·055	−0·075	−0·100
0·95	+0·055	—	+0·050	+0·045	+0·040	+0·015	+0·020	+0·010

Lower surface C_p

x/c	α (deg)							
	−4·0	−1·9	−0·1	+2·3	+4·4	+6·4	+8·5	+10·6
0·01	+0·005	+0·205	+0·320	+0·450	+0·520	+0·545	0·535	0·495
0·03	−0·180	+0·010	+0·135	0·290	0·405	0·485	0·545	0·585
0·08	−0·350	−0·205	−0·100	+0·045	0·165	0·260	0·360	0·440
0·15	−0·390	−0·270	−0·190	−0·070	+0·035	0·125	0·220	0·300
0·225	−0·410	−0·315	−0·240	−0·140	−0·050	+0·030	0·115	0·195
0·35	−0·380	−0·310	−0·250	−0·170	−0·100	−0·035	0·045	0·110
0·50	−0·305	−0·245	−0·205	−0·145	−0·085	−0·035	0·025	0·075
0·65	−0·195	−0·160	−0·135	−0·095	−0·050	−0·010	0·035	0·075
0·75	−0·120	−0·095	−0·070	−0·045	−0·020	+0·015	0·050	0·080
0·85	−0·045	−0·030	−0·020	+0·005	+0·025	0·045	0·070	0·100
0·95	+0·040	+0·040	+0·040	+0·045	+0·055	+0·055	0·070	0·090

TABLE 7—*continued*

$y/c = 0 \cdot 6$ $2y/b = 0 \cdot 245$

Upper surface C_p

x/c	α (deg) −4·0	−1·9	−0·1	+2·3	+4·4	+6·4	+8·5	+10·6
0	+0·245	+0·445	+0·495	+0·415	+0·190	−0·175	−0·720	−1·320
0·01	0·370	0·180	−0·040	−0·435	−0·850	−1·315	−1·915	−2·485
0·03	0·240	+0·045	−0·135	−0·450	−0·755	−1·095	−1·535	−2·015
0·08	+0·070	−0·085	−0·225	−0·440	−0·635	−0·845	−1·035	−1·255
0·15	−0·035	−0·155	−0·260	−0·420	−0·560	—	−0·820	−0·955
0·225	−0·100	−0·200	−0·285	−0·410	−0·510	−0·605	−0·715	−0·805
0·35	−0·125	−0·195	−0·260	−0·355	−0·400	−0·470	−0·535	−0·585
0·50	−0·080	−0·135	−0·180	−0·200	−0·240	−0·285	−0·320	−0·330
0·65	−0·020	−0·045	−0·075	−0·110	−0·130	−0·150	−0·160	−0·170
0·75	0	−0·015	−0·030	−0·055	−0·060	−0·070	−0·080	−0·095
0·85	+0·035	+0·020	+0·005	−0·005	−0·005	−0·010	−0·020	−0·050
0·95	+0·080	+0·075	+0·065	+0·065	+0·065	+0·045	+0·030	−0·015

Lower surface C_p

x/c	α (deg) −4·0	−1·9	−0·1	+2·3	+4·4	+6·4	+8·5	+10·6
0·01	−0·405	−0·045	+0·165	+0·395	+0·490	+0·505	0·440	0·325
0·03	−0·560	−0·255	−0·055	+0·185	0·340	0·440	0·500	0·520
0·08	−0·540	−0·340	−0·195	−0·015	+0·130	0·240	0·340	0·420
0·15	−0·510	−0·375	−0·265	−0·120	0	0·100	0·200	0·285
0·225	−0·490	−0·380	−0·295	−0·175	−0·075	+0·010	0·100	0·180
0·35	—	−0·325	−0·265	−0·185	−0·115	−0·050	0·025	0·085
0·50	−0·240	−0·185	−0·170	−0·125	−0·070	−0·030	0·025	0·065
0·65	−0·110	−0·085	−0·065	−0·030	−0·005	+0·020	0·050	0·085
0·75	−0·050	−0·040	−0·030	−0·010	+0·005	0·025	0·040	0·065
0·85	+0·005	+0·005	+0·005	+0·020	0·030	0·040	0·050	0·060
0·95	+0·065	+0·060	+0·055	+0·055	+0·055	+0·050	0·045	0·035

TABLE 8

Coefficients of Local Normal Force, Tangential Force, Lift, Drag, Pitching Moment and Aerodynamic Centre Position

Wing C with twisted and cambered centre section

$\varphi = 45$ deg $\qquad A = 5 \cdot 0$

C_N

α (deg)	2y/b		
	0	0·053	0·245
−4·0	−0·199	−0·205	−0·241
−1·9	−0·075	−0·078	−0·109
−0·1	+0·029	+0·025	+0·007
+2·3	0·167	0·161	0·157
4·4	0·284	0·280	0·281
6·5	0·401	0·397	0·403
8·6	0·520	0·516	0·522
+10·7	+0·631	+0·630	+0·639

C_T

α (deg)	2y/b		
	0	0·053	0·245
−4·0	0·0316	+0·0007	−0·0124
−1·9	0·0393	0·0076	−0·0018
−0·1	0·0456	0·0088	−0·0005
+2·3	0·0521	0·0091	−0·0033
4·4	0·0559	+0·0054	−0·0122
6·5	0·0613	−0·0012	−0·0268
8·6	0·0632	−0·0123	−0·0459
+10·7	0·0655	−0·0220	−0·0690

C_L

α (deg)	2y/b		
	0	0·053	0·245
−4·0	−0·196	−0·205	−0·242
−1·9	−0·074	−0·078	−0·109
−0·1	+0·029	+0·025	+0·007
+2·3	0·165	0·161	0·157
4·4	0·279	0·280	0·281
6·5	0·391	0·394	0·403
8·6	0·504	0·512	0·523
+10·7	+0·607	+0·623	+0·641

C_D

α (deg)	2y/b		
	0	0·053	0·245
−4·0	0·046	0·015	0·004
−1·9	0·042	0·010	0·002
−0·1	0·046	0·009	0
+2·3	0·059	0·016	0·003
4·4	0·078	0·028	0·010
6·5	0·107	0·045	0·020
8·6	0·142	0·066	0·034
+10·7	0·182	0·096	0·050

C_m

α (deg)	2y/b		
	0	0·053	0·245
−4·0	+0·044	+0·025	0·002
−1·9	0·031	0·018	0·003
−0·1	0·019	0·011	0·002
+2·3	+0·003	+0·004	0·002
4·4	−0·010	−0·004	0·003
6·5	−0·024	−0·012	0·003
8·6	−0·041	−0·021	0·005
+10·7	−0·052	−0·032	0·002

h/c

α (deg)	2y/b		
	0	0·053	0·245
2·3	0·232	0·225	0·239
4·4	0·286	0·264	0·240
6·5	0·310	0·280	0·242
8·6	0·328	0·290	0·241
10·7	0·333	0·300	0·247

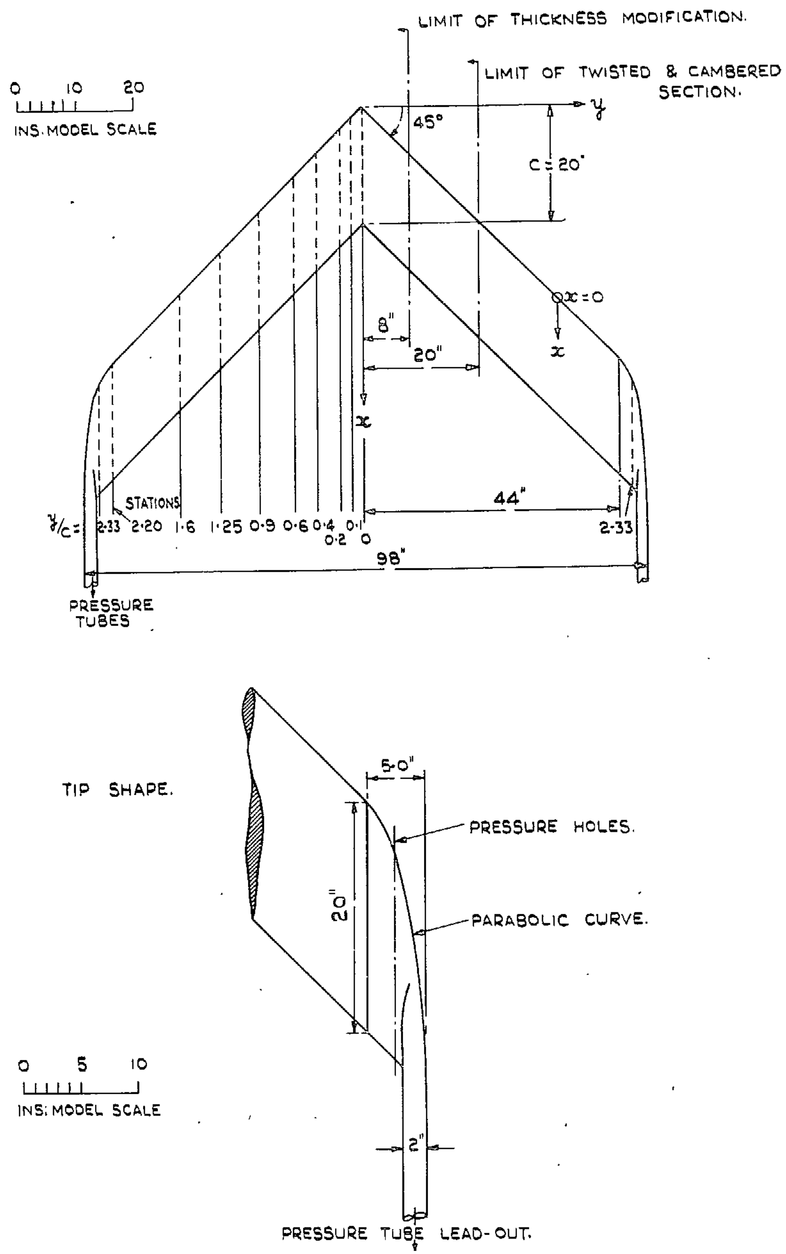

FIG. 1. View of models and dimensions.

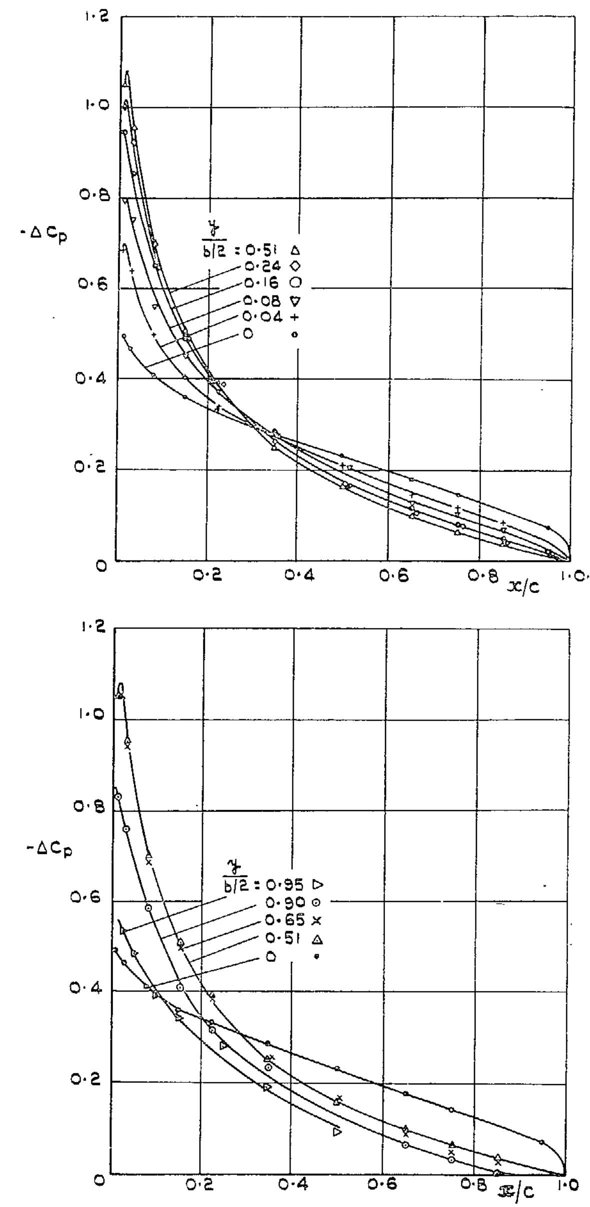

FIG. 2. Wing A. Chordwise lift distribution at various spanwise sections for $\alpha = 4 \cdot 2$ deg.

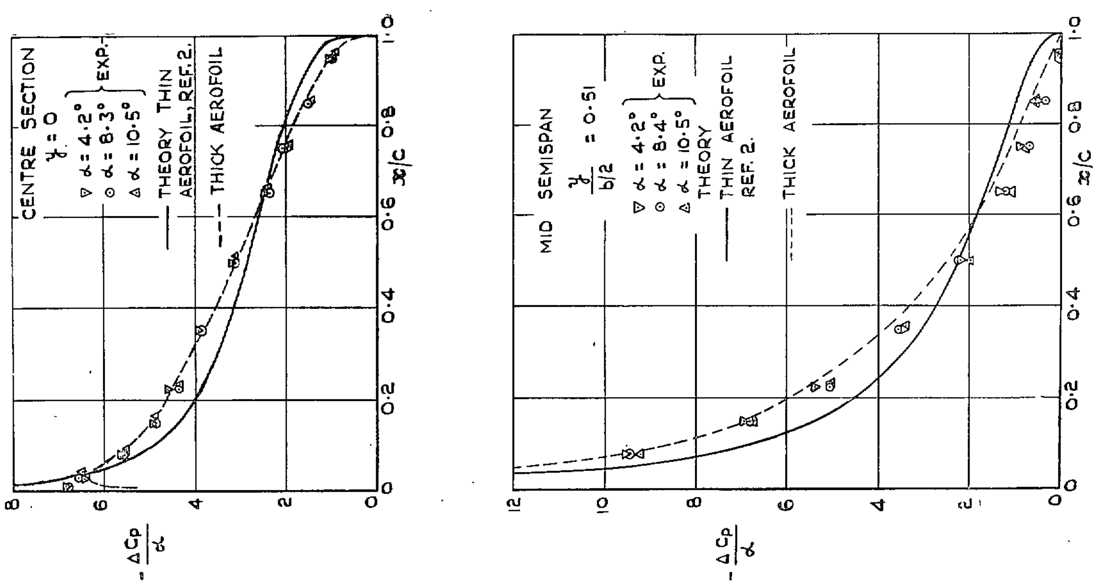

FIG. 3. Wing A. Chordwise lift distributions. Comparison of experiment with theory.

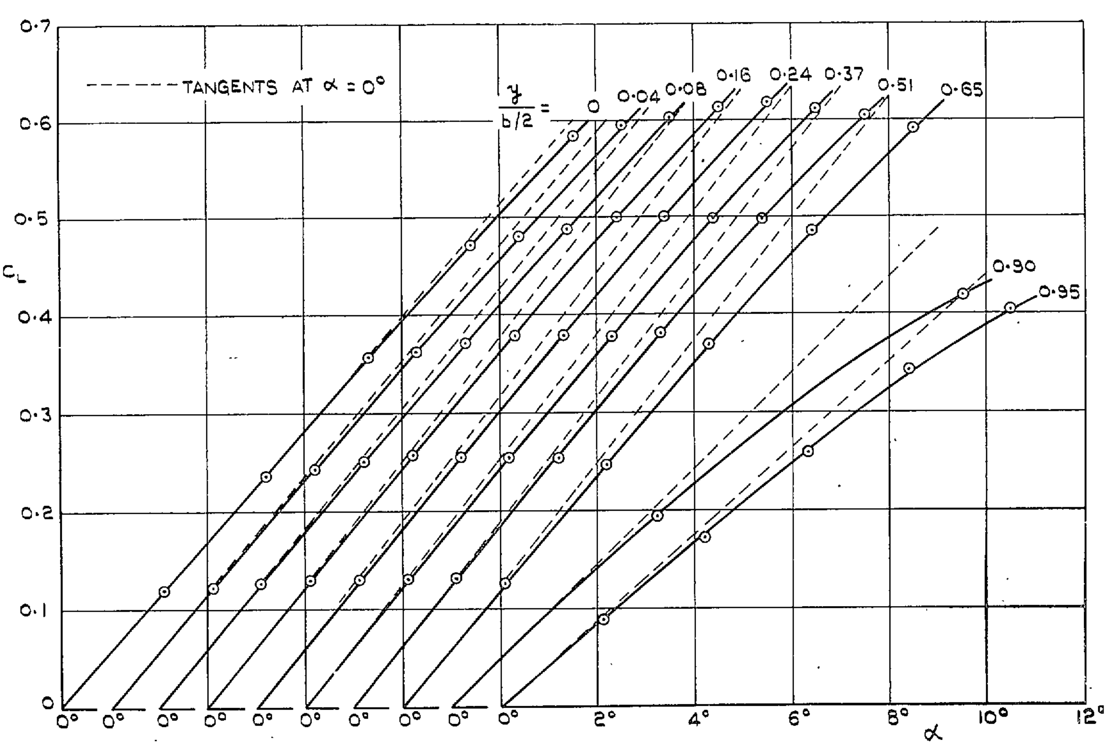

FIG. 4. Wing A. Local lift coefficients.

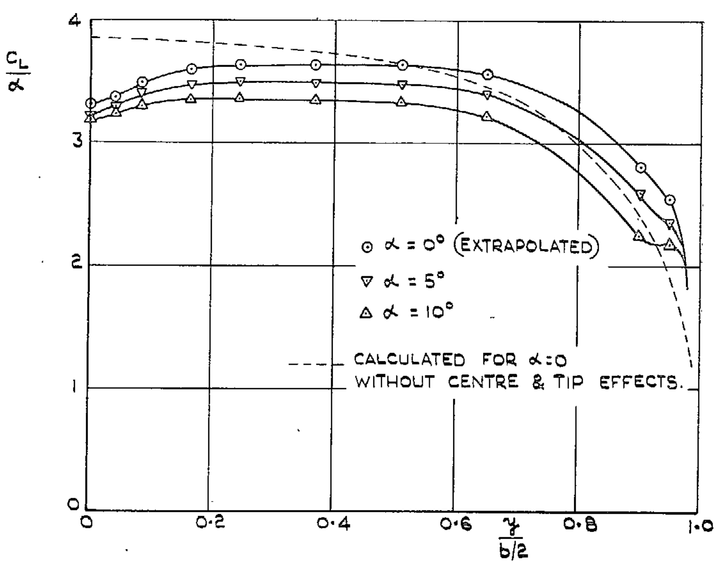

FIG. 5. Wing A. Spanwise lift distribution.

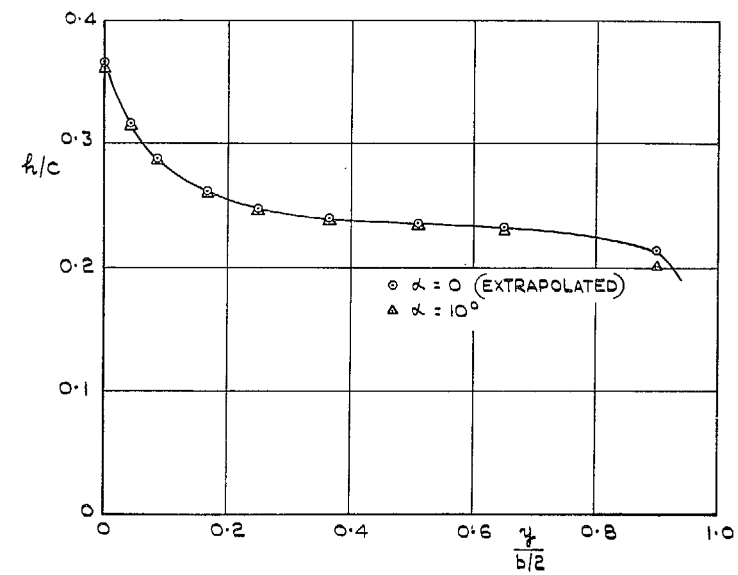

FIG. 6. Wing A. Chordwise position of aerodynamic centre.

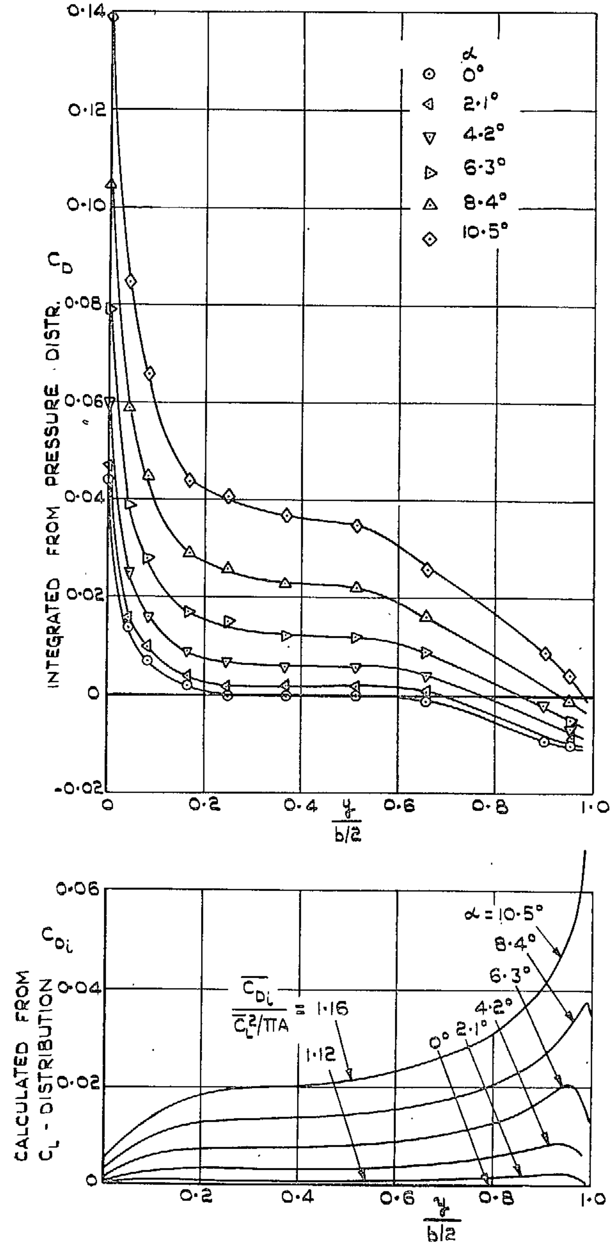

FIG. 7. Wing A. Local drag coefficients.

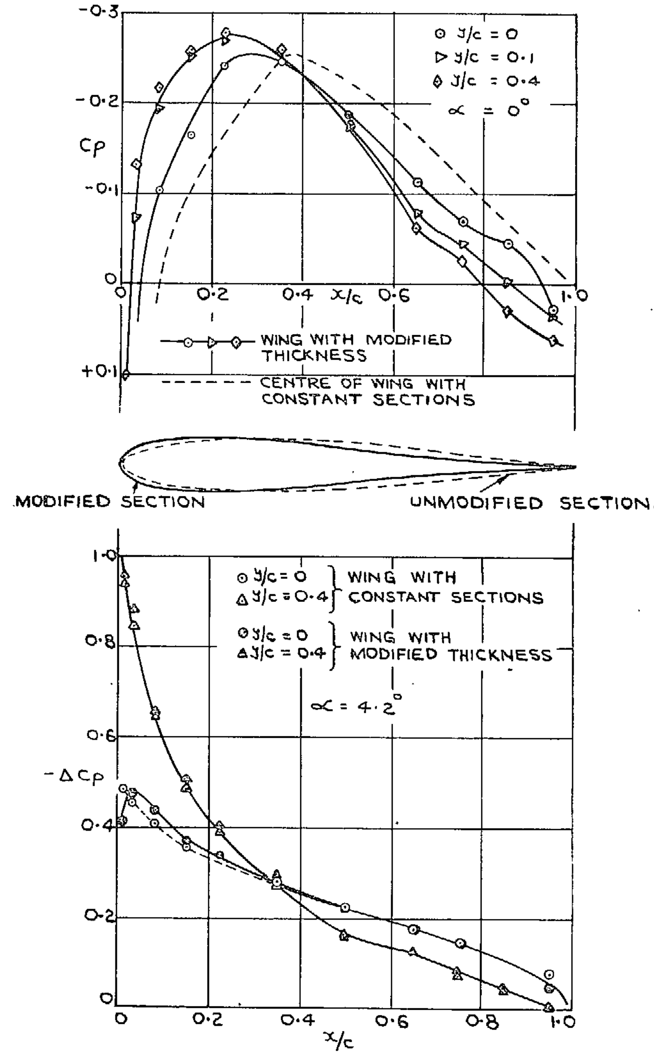

FIG. 8. Chordwise pressure and lift distributions. Comparison between wings A and B.

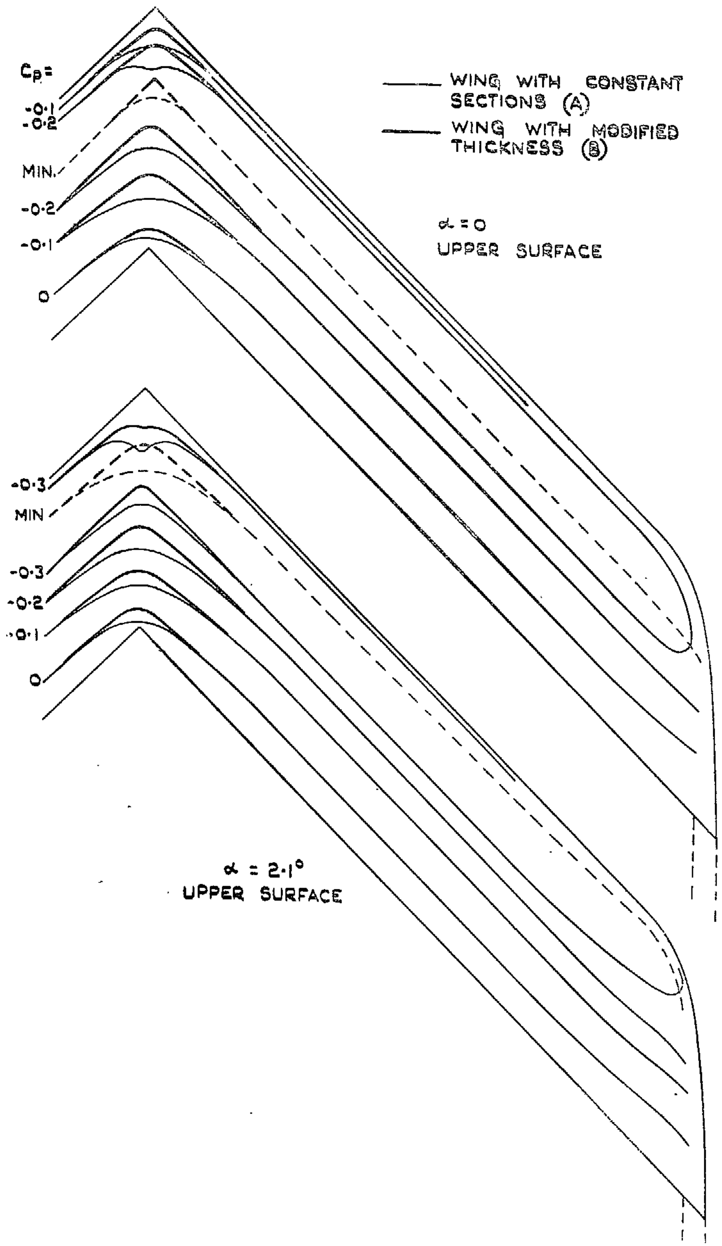

FIG. 9. Wings A and B. Isobars on upper surface.
$\alpha = 0$ deg and $2 \cdot 1$ deg.

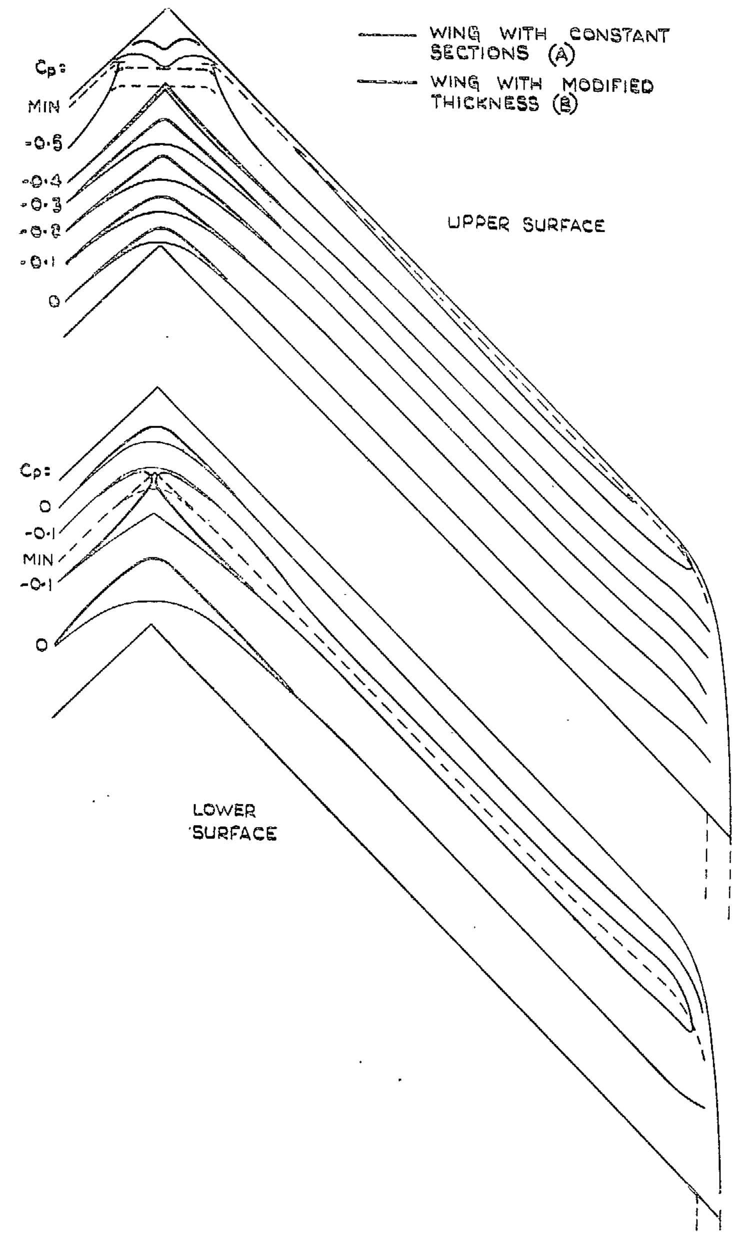

FIG. 10. Wings A and B. Isobars on upper and lower surfaces.
$\alpha = 4 \cdot 2$ deg.

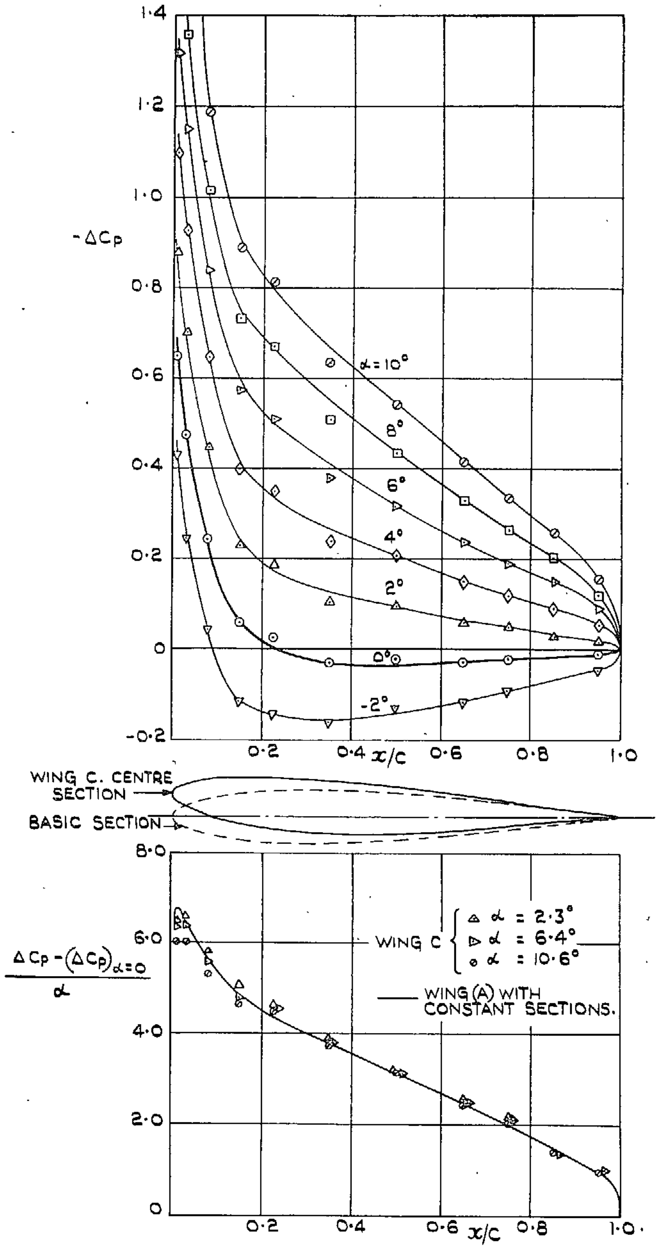

FIG. 11. Wing C. Chordwise lift distributions at the centre section.

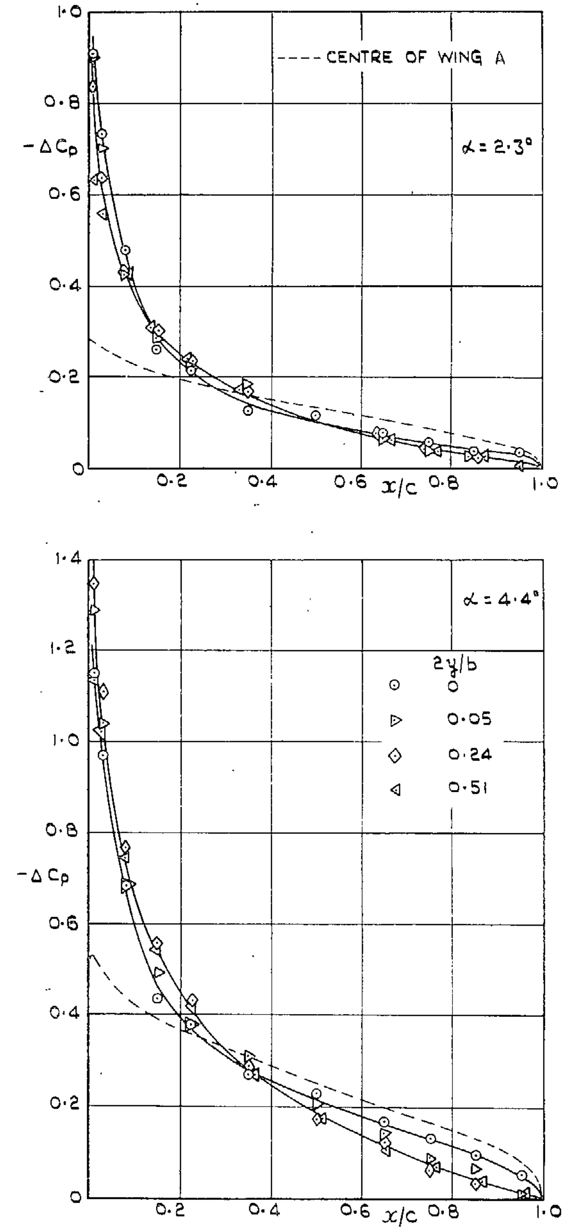

FIG. 12. Wing C. Chordwise lift distributions near the centre for two incidences.

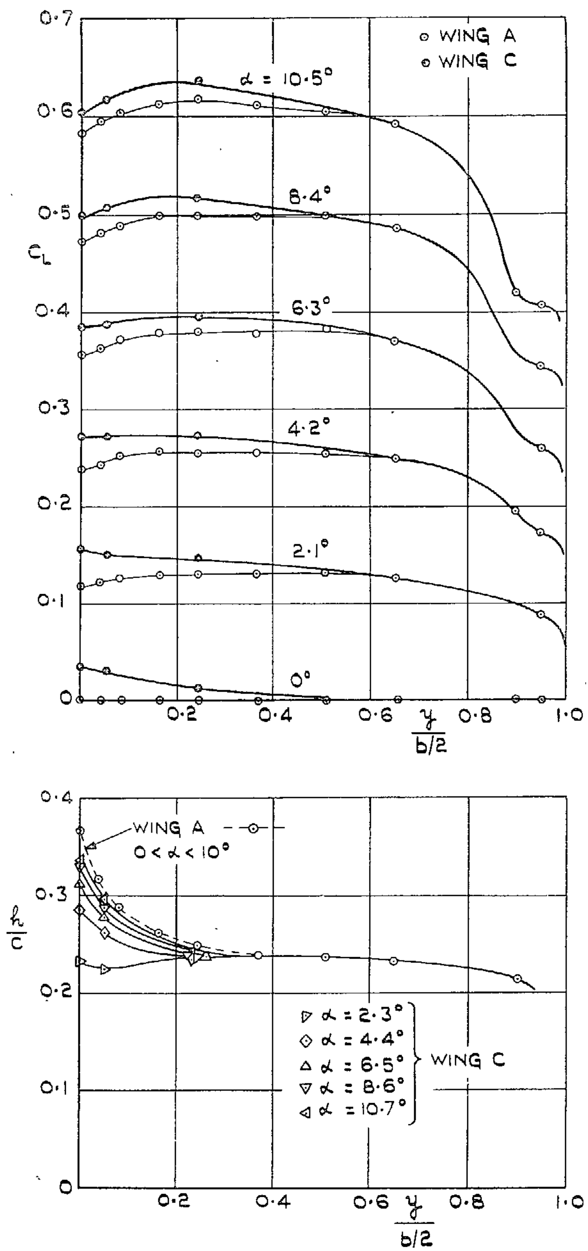

FIG. 13. Wings A and C. Spanwise lift distributions and position of aerodynamic centre.

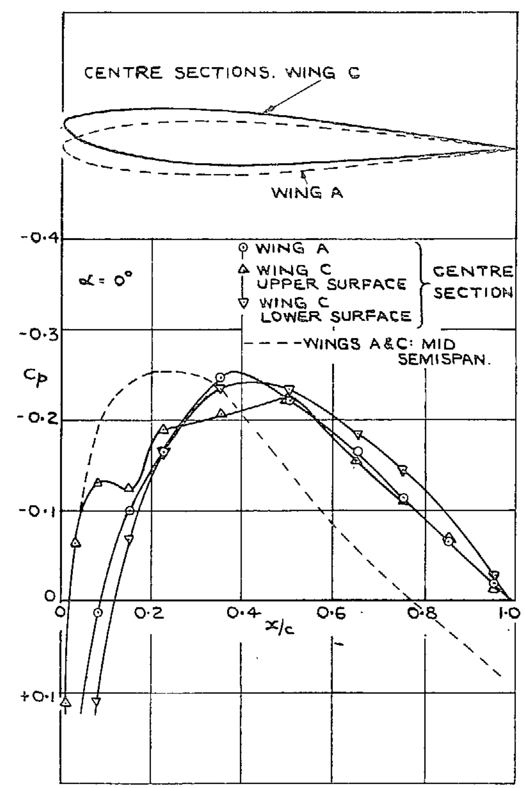

FIG. 14. Wings A and C. Chordwise pressure distributions at zero incidence.

PART II

Balance and Pressure Measurements on Wings of Different Aspect Ratios

By

D. KÜCHEMANN, Dr.rer.nat.,

J. WEBER, Dr.rer.nat.

and

G. G. BREBNER, M.A.

Summary.—This Part contains the results of balance and pressure measurements on constant-chord wings of 45-deg sweepback. Together with wing A of Part I they provide data for aspect ratios 2, 3, 5 and infinity.

The results at low $\bar{C}_L$ are analysed and used to verify assumptions made in the calculation method of Refs. 2 and 3. The growth of the boundary layer and its influence on the lift, drag and pitching moment are discussed. The effect of tip vortices on lift and drag is also discussed. The stall is investigated on the wing of aspect ratio 3.

---

1. *Introduction.*—This report deals with part of the work done in an investigation of the chordwise and spanwise pressure distribution of swept-back wings and the associated variations of lift, drag and pitching moment. It gives the results of pressure measurements on two wings of aspect ratios 2 and 3 and on a third wing spanning the tunnel, with balance measurements on the wing of aspect ratio 3 only. The results supplement those in Part I where the tests on the wing of aspect ratio 5 of this series have been described (Wing A of Part I).

The wings have constant chord and symmetrical wing section, and differ only in aspect ratio. Thus the complications introduced by taper, twist, camber, dihedral and varying thickness are avoided. Refs. 2 and 3 present a calculation method for the loading and pressure distributions on swept wings. This method is based on non-viscous flow but a constant is introduced into the lift slope of the two-dimensional unswept wing to represent the effect of viscosity. Calculations made on this basis are compared with the experimental results as C_L tends to zero, and the additional effects of boundary-layer thickness on the swept wing can then be separated. For a 12 per cent infinite sheared wing in non-viscous flow, the theoretical value of the lift slope is $1 \cdot 14 \times 2\pi \cos \varphi$. Measurements of $\partial C_L/\partial \alpha$ on a two-dimensional unswept wing of the same section and at the same Reynolds number as used in this report gave an experimental value equal to $0 \cdot 92 \times$ theoretical value, the difference being attributed to the effect of the boundary layer. In this report, the same factor $0 \cdot 92$ to the two-dimensional lift slope is used in the calculation of the swept wing local lift coefficients. A further report will be written explaining in detail the method of application of Refs. 2 and 3.

In section 3.1 the comparison of the low C_L results with the calculation method is discussed. The additional influence of the boundary layer, whose development is greater on the swept wing than in two-dimensional flow, is described in section 3.2, but the boundary-layer effects are sensitive to changes in Reynolds number and may be much smaller at full-scale Reynolds numbers. A later report will give results of experimental investigation of the boundary layer. Some earlier boundary-layer tests on a 59-deg swept wing are given in Ref. 4. The effect of the vortex configuration at the tip, which is formed before the actual stall is reached, is dealt with in section 3.3. Its influence becomes more apparent as aspect ratio decreases. Section 3.4 describes the stalling characteristics of the wing of aspect ratio 3. Some estimates of the local critical Mach numbers along the span, based on the measured isobar patterns are made in section 3.5.

2. *Details of Models and Tests*.—The tests described in this report were made in the No. 2 $11\frac{1}{2}$-ft × $8\frac{1}{2}$-ft Wind Tunnel at the R.A.E. between March 1949 and August 1950. They consisted mainly of pressure measurements on a constant-chord wing of 45-deg sweep which originally spanned the tunnel, with its centre at the middle of the tunnel: it was successively cut down to aspect ratios 5, 3* and 2, being then rigged horizontally. Balance measurements of lift, drag and pitching moment were also made on the pressure-plotting wing of aspect ratio 3 and on a solid wing of identical dimensions (but without the tip distortion necessary to fair the pressure tubes).

The pressure-plotting model is shown in Fig. 1. The chord was 20 inches and the wing had the same symmetrical section throughout the span. Pressure measurements were made using rows of flush holes in the wing surface at different spanwise stations, *see* Table 1. The wings of finite aspect ratio were fitted with curved leading edge tips as described in Ref. 6; this shape minimises the forward swing of the isobars at the tip.

The design wing section along wind was RAE 101, 12 per cent thick, the co-ordinates of which are given in Part I.

All pressure measurements were made at a speed of 163 ft/sec giving a Reynolds number of $1 \cdot 71 \times 10^6$ based on the wing chord. Total pitching-moment coefficients were calculated about the mean quarter-chord line for each finite wing. Balance measurements on the pressure plotting wing of aspect ratio 3 were also made at a Reynolds number of $1 \cdot 71 \times 10^6$, the model being rigged on wires. The balance measurements on the solid wing of aspect ratio 3 were made at Reynolds numbers of $1 \cdot 05 \times 10^6$, $1 \cdot 71 \times 10^6$, and $2 \cdot 95 \times 10^6$, the model being mounted on struts. These struts introduce a very bad asymmetry of flow, and their redesign is being considered. The corrections applied, though large, are checked by the agreement at the Reynolds number $1 \cdot 71 \times 10^6$ with the results for the pressure-plotting wing on wires.

It was necessary to make special corrections to the results of the tests on the swept wing spanning the tunnel in order to represent the effect of infinite aspect ratio. Near the tunnel walls the lift and induced drag obtained from the pressure measurements are different from those on an infinite swept wing, and must be corrected for the reflection plate effect of the walls. These corrections were estimated by considering the loading of a wing alternately swept back and swept forward at intervals of half the tunnel width, and using the calculation of Ref. 2. The corrections are given in Table 11.

3. *Results and Discussion*.—The measured values of C_p are given in Tables 2, 5 and 9. Coefficients of total lift, drag and pitching moment obtained from pressure measurements on the wings of aspect ratio 3 and 2 are given in Tables 4 and 7, and Table 8 contains the lift, drag and pitching-moment coefficients obtained from balance measurements on the wings of aspect ratio 3.

The illustrations are arranged in the following order: Figs. 2 to 9 show pressure distributions, in Figs. 10 to 20 lift coefficients and the positions of the aerodynamic centre are plotted, with pitching-moment coefficients in Figs. 21 and 22. Drag coefficients are shown in Figs. 23 to 30, and isobar patterns and critical Mach numbers in Figs. 31 to 33.

3.1. *Comparison of Calculations*[2,3] *with Results at Small Values of* C_L.—3.1.1. *Chordwise pressure and lift distributions* (*Figs.* 2 *to* 6).—Experimental results show that, near the centre and tip, the chordwise pressure distributions deviate from the sheared wing distribution in the same way and by almost the same amount for all aspect ratios (Figs. 2 and 6). This is true with and without lift. The chordwise pressure and lift distributions for the different aspect ratios are

* Actually 3·04.

compared at the same local C_N value and not at the same C_L or geometric incidence, (Figs. 2, 5 and 6). The measured distributions at the same α are, of course, not the same for different aspect ratios because of the different downwash induced by the trailing vortices. Figs. 2, 5 and 6 thus imply that the induced incidence α_i does not vary along the chord. This forms an experimental verification of this assumption, which is used in Refs. 2 and 3.

Fig. 6 shows that for aspect ratio 2 the centre effect on the chordwise loading is slightly less than for the higher aspect ratios. Thus aspect ratio 2 seems to be the lower limit for the application to untapered wings of 45 deg sweepback of the assumption that the chordwise lift distribution at the centre is independent of aspect ratio at the same effective incidence α_e. The centre effect due to thickness, however, is independent of aspect ratio down to $A = 1 \cdot 0$ for untapered wings as shown in Ref. 6. On the present series of wings the distortion of the pressure distribution near the tip, where the leading edge is curved, is less than it would be with a square tip, since this modification of the plan-form was designed to counteract the tip effect.

The centre effects due to lift and thickness decrease at different rates along the span, the former being zero at about $y/c = 1 \cdot 0$ and the latter at about $y/c = 0 \cdot 5$, for all aspect ratios. Figs. 3 and 4 show how the pressure distribution changes from the central type to the sheared wing type. This again is part of the data on which Refs. 2 and 3 are based.

3.1.2. *Lift* (*Figs.* 10 *to* 13, 19, 20).—Local lift coefficients for the wings of aspect ratio 2, 3 and infinity are plotted against incidence in Figs. 10 to 12. The corresponding figure for the wing of aspect ratio 5 is Fig. 4 of Part I. The local lift slopes and the position of the aerodynamic centre at zero incidence are plotted against span in Figs. 13 and 14. On all wings with $A \geqslant 3$ the local lift slopes at small incidences agree with calculated values (Fig. 13), which implies that α_i induced by the trailing vortices is constant along the chord and equal to half the induced angle at infinity downstream. This is no longer true for the wing of aspect ratio 2 where the induced downwash is greater and the measured lift smaller than the calculated values.

Total lift coefficients obtained from pressure measurements are plotted against incidence in Fig. 19, together with the balance measurements on the wing of aspect ratio 3. Comparison between the balance and pressure measurements shows good agreement to within 3 deg or 4 deg of the stall. This indicates that the effect of leading the pressure tubes out of the wing tip (Fig. 1) is not noticeable. There is, however, a discrepancy at incidences above about 19 deg where the flow has broken down on the outer part of the wing (Fig. 9). Total lift slopes are plotted against aspect ratio in Fig. 20.

The spanwise loadings in Fig. 13 show the loss of lift at the centre and the gain near the tips which are characteristic of swept-back wings. Both become less pronounced with decreasing aspect ratio. The loss of lift near the centre causes trailing vortices of opposite sense to those arising from the outer part of the wing. An upwash is thus produced at the centre.

3.1.3. *Drag* (*Figs.* 23, 24, 28).—The nature of the spanwise lift distribution causes the drag induced by the trailing vortices to vary considerably along the span ; in particular it is small at the centre section and large near the tips, (Figs. 24 and 25). The large spanwise variation of the induced angle explains why the total induced drag, $\bar{C}_{Di}$, and the K_i factor

$$K_i = \frac{\bar{C}_{Di}}{\bar{C}_L^2/\pi A}$$

are both greater than for the corresponding unswept wings, (Fig. 28). This is only true for constant-chord wings, and a highly-tapered swept-back wing might have a lower induced drag than the corresponding unswept wing ; *see* Ref. 2, section 6.1.

The spanwise distribution of the drag coefficient obtained from pressure measurements is quite different from that of the drag induced by the trailing vortices, being very large at the centre and perhaps even negative at the tips, (Figs. 23 and 24). The existence at zero incidence of drag forces near the centre and thrust forces near the tips in non-viscous flow has already been noted in Ref. 6. These drag and thrust coefficients are proportional to $(t/c)^2$ and will thus be smaller with thinner wings. Fig. 24 shows that there is a similar effect when $C_L \neq 0$, resulting from the distorted chordwise load distributions at the centre and the tips. The additional local drag or thrust, ΔC_D, is proportional to $\bar{C}_L^2$. The actual values of ΔC_D are considerable. For instance, at $y = 0$ $\Delta C_D/\bar{C}_L^2 = 0{\cdot}28$, so that $\Delta C_D = 0{\cdot}07$ for $\bar{C}_L = 0{\cdot}5$, that is about ten times the ordinary profile drag. ΔC_D integrated over the span is zero as long as the high suction peaks near the tips, which give the main contribution to the thrust force, still exist. The loss of a fraction of this thrust force means a big increase in drag. This explains why the drag rise is large as soon as there is any breakdown in the forward peak suctions near the tip. This may occur while the overall lift is still rising. There are thus two 'induced drags', the usual one due to the trailing vortices which has a total value $\bar{C}_{Di} \neq 0$, and another one due to the bound vortices whose integral over the span is zero in ideal flow.

3.1.4. *Pitching moment* (*Figs.* 14 *and* 22).—The local position of the aerodynamic centre is behind the sheared wing value (24 per cent) at the centre of the wing and ahead of it at the tips, (Fig. 14). The measured values of h/c agree with the calculated values, except those for aspect ratio 2 which are smaller (*i.e.*, centre of pressure further forward than expected) by about 1 per cent to 2 per cent chord. The calculated values in Fig. 14 are for wings having constant chord everywhere, and the effect of the curved-leading edge at the tip is very marked[5]. There is a total nose-up pitching moment at small $\bar{C}_L$ values, as calculated (Fig. 22).

3.2. *Additional Influence of the Boundary Layer*.—3.2.1. *Lift and pitching moment* (*Figs.* 5, 7, 10 *to* 12, 15, 17, 19).—As is well known, the thickness of the boundary layer increases with incidence more on the upper surface of wings than on the lower surface. This is even more pronounced on swept wings, as the results of Ref. 4 and of boundary-layer investigations on the present series of wings (to be published) have shown. This causes a loss of lift and the curve of C_L against α is not a straight line, a higher incidence $\alpha + \alpha_B$ being needed to produce a certain C_L value, (Figs. 10 to 12, 19). α_B increases towards the tips, which alters the shape of the spanwise loading curve (Fig. 15), and thus alters the downwash behind the wing. Above incidences of about 12 deg this loss of lift is masked by other influences which tend to increase the lift, (*see* section 3.3). The effect of the boundary layer is apparent in the chordwise lift distributions, particularly at stations well outboard such as $2y/b = 0{\cdot}61$, (Fig. 7). Fig. 5 shows that for all aspect ratios the influence of the boundary layer on the lift distribution is roughly the same, for a particular y/c position and C_N. The calculated curves in Figs. 2 to 7 are based on potential flow, the two-dimensional lift-slope correction being included in the calculation of the effective incidence. The differences between the calculated and measured values may be taken as the additional boundary-layer effect for swept wings. The loss of lift is greatest in the rear part of the section, as is to be expected since the boundary-layer thickness increases towards the trailing edge.

The position of the local aerodynamic centre is not much affected up to $\alpha = 12$ deg (Fig. 17). In a spanwise direction the loss of lift is largest near the tips and therefore the total pitching moment increases more rapidly with C_L, *see* Fig. 21.

3.2.2. *Drag* (*Figs.* 25 *to* 30).—There is an appreciable influence of the boundary layer on the drag, even at small incidences. α_B may be regarded as an induced angle of incidence due to the boundary layer, just as α_i is due to the trailing vortices, and it thus gives rise to a drag coefficient $\alpha_B \times C_L$. The magnitude of this drag for the wing of aspect ratio 5 at $\alpha = 10$ deg is shown in Fig. 25. Curve A represents the drag induced by the trailing vortices as calculated from the measured spanwise loading. To this was added the drag term $\alpha_B \times C_L$ from the boundary layer (curve B). The value of α_B used was obtained as the difference in α, for the given C_L, between the measured curve and the calculated tangent at $\alpha = 0$ deg in Fig. 4 of Part I. Curve C was obtained by adding to curve B the drag forces arising from the distortion of the pressure distributions at the centre and tip due to the thickness, derived from the measurements at $C_L = 0$. The measured curve, D, includes the drag and thrust induced by the bound vortices. Integrating $\alpha_B \times C_L$ along the span to give $\bar{C}_{DB}$, it can be seen from the values given in Fig. 25 that $\bar{C}_{Di} + \bar{C}_{DB} = \bar{C}_D$, the total drag coefficient obtained from the pressure measurements. This confirms that the sum of the additional local drag and thrust which is induced by the bound vortices on the wing in potential flow (*see* section 3.1) is zero. The values of $\bar{C}_{DB}$ are quite large compared with $\bar{C}_{Di}$ (Fig. 25). Therefore the total K values in Figs. 28 and 30 are much larger than K_i.

The drag coefficients calculated from the measured pressure distributions do not include the skin friction and are therefore smaller than those from the balance measurements, (Fig. 26). The difference decreases with increasing lift; this decrease may be partly due to an increased outflow in the boundary layer and a consequent reduction in the component of the shear stresses in the free stream direction. The drag factor K derived from the balance measurements is therefore less than that derived from the pressure measurements, and is constant for small $\bar{C}_L$. This should be kept in mind when studying Fig. 30, especially since the difference will depend on aspect ratio, A being a factor of K. Fig. 26 shows how much the drag due to skin friction and boundary layer is dependent on Reynolds number; it may be much smaller at full-scale Reynolds numbers.

3.3. *Effect of the Tip Vortex.*—Tuft observations indicate that at some $\bar{C}_L$ value well below $\bar{C}_{L\max}$ the air flowing round the tip from the lower surface to the upper surface breaks away at the extreme tip and re-attaches a short distance inboard on the upper surface, thus forming a particular kind of trailing vortex. This begins at the trailing edge and extends gradually along the whole of the tip chord and a vertical sheet of trailing vortices is formed*. The 'height' of this sheet is thus connected with the incidence, (*see* also Mangler[7] (1939) and Küchemann and Kettle[1] (1951)). The vortex occurs on unswept wings but may be more noticeable on swept wings, for several reasons. Due to the different spanwise loading, more vorticity is shed near the tip on a swept-back wing than on an unswept wing; again, for a given $\bar{C}_L$, a higher incidence is required on a swept wing than on an unswept wing, and the height of the vortex sheet increases with α. The sharp suction peaks near the tips of swept-back wings may also intensify the flow around the tip and thus the strength of the vortex. Since the tip vortex probably arises because of a breakaway in the flow, it is dependent on Reynolds number, but it is not associated with any general breakdown of the flow over the wing surface.

3.3.1. *Lift* (*Figs.* 7, 10, 11, 15, 18 *to* 20).—The effect of the vortex sheet is to increase the local lift coefficients near the tip by restricting the flow round the edge, (Figs. 10 and 11). With increasing incidence and height of the vortex sheet, the slope of the $\bar{C}_L$ against α curve increases, the effect being more pronounced as aspect ratio decreases (Figs. 19 and 20). The ratio of the height of the vortex sheet to the wing span is the parameter which determines the magnitude of the tip vortex effect, and this ratio obviously increases as aspect ratio decreases.

Fig. 15 shows how much the spanwise lift distribution is affected and how far inboard the influence of the tip vortex is felt. The effect on the chordwise lift distribution is illustrated in Fig. 7; at the front of the section, where there may be no separation or where the height of the vortex sheet is zero or small, there is little change, but at the rear, where the height is greater, there is a marked increase in lift.

* The effect is described in Ref. 5 where the influence of various tip shapes was investigated.

3.3.2. *Pitching moment* (*Figs.* 17, 21, 22).—Since the lift is increased mostly at the rear of the sections, there is a considerable rearward shift of the local aerodynamic centre positions, (Fig. 17), and since those sections where the lift is increased are near the tips there is a very marked nose-down pitching moment, due to the long moment-arm of the tip sections on swept wings, *see* Figs. 21 and 22*. Again this is not connected with a general breakdown of the flow over the wing surface. The turning point of the curve of $\bar{C}_m$ against $\bar{C}_L$ occurs at that $\bar{C}_L$ at which the flow round the tip first breaks down, (Fig. 22). The turning point is also affected by the Reynolds number, (Fig. 21). A detailed explanation of the tip vortex sheet and its effect on the pitching moment is given in Ref. 1.

3.3.3. *Drag* (*Figs.* 24 *and* 26).—At about the same $\bar{C}_L$ as the turning point mentioned above there is a fairly sudden increase in the slope† of the curve of the drag due to skin friction and boundary layer against $\bar{C}_L$, (Fig. 26). There is an increase in the local drag coefficient, C_D, (Fig. 24) because the increase in the suction forces is mainly found at the rear part of the sections near the tip where the suction force has a drag component. This is again connected with the fact that the height of the vortex sheet is greatest near the trailing edge, and is also influenced by the geometry of the swept wing.

3.4. *Stalling Characteristics* (*Figs.* 7 *to* 9, 11, 16, 18, 19).—The stall was investigated only in the case of the wing of aspect ratio 3. At $\alpha = 18 \cdot 5$ deg there is no sign of a stall over any part of the wing, but at $\alpha = 20 \cdot 6$ deg the flow has broken down over the outer half of the wing, as shown in Fig. 9‡. The breakdown is brought about not by the thick boundary layer in the rear part of the section but by the high suction peaks near the leading edge, (Fig. 7). The effect of this breakdown on the curve of C_L against α is shown in Figs. 11, 16 and 18. Tuft observations indicated that the separation of the flow took place first at about mid-semispan where the highest suction peaks have been found, (Fig. 9). This spread rapidly outwards but slowly inwards. A 'part-span vortex sheet' is formed, which separates the inner region with attached flow from the outer region with broken-down flow.

The maximum value of $-C_p$ measured is between 7 and 8. This value is smaller than on straight wings where a peak suction coefficient greater than 10 has been measured on sections between 9 per cent and 12 per cent thickness/chord ratio (McCullough and Gault[8,9,10] (1948-49)). This fact may be explained by the assumption that the magnitude of the adverse pressure gradient is responsible for the breakdown. For the same local C_L (and therefore the same peak suction) on the straight and sheared wings, the gradient is higher on the sheared wing. This is because the streamlines are curved and, in the extreme case, cross the peak suction line at right-angles, thus introducing a factor of $1/\cos\varphi$ to the pressure gradient.

3.5. *Estimated Critical Mach numbers* (*Figs.* 31 *to* 33).—An estimate of the effect of compressibility has been made using the experimental isobar patterns on the wings of finite aspect ratio, (Figs. 32, 33, and Figs. 9, 10, of Part I), and applying equation (27) of Ref. 11:—

$$\frac{C_{pc}}{C_{pi}} = \frac{1}{\sqrt{[1 - M_0^2(\cos^2\varphi - C_{pi})]}}$$

where C_{pc} is the pressure coefficient in compressible flow,

C_{pi} ,, ,, ,, ,, in incompressible flow.

---

* The accuracy of the $\bar{C}_m$ values integrated from the pressure measurements is about $\pm 0 \cdot 004$ for the wing of aspect ratio 3 at a $\bar{C}_L$ of $0 \cdot 6$, due to the small number of measuring stations near the tips.

† This can be more easily seen from the values of K shown in Fig. 27.

‡ Fig. 19 shows that the slope of the lift curve at this incidence is different on the pressure-plotting model due to interference from the holes and the tubes, and that the reduction in slope is less from the balance measurements when this interference is absent.

This is strictly applicable only to the sheared part of the wing but has been used for the whole wing.

The main difference between the different aspect ratios appears at $\bar{C}_L = 0$, when the peak suction line on the wings of lower aspect ratio never attains a sweep of 45 deg. The estimated critical Mach number is lowest at the centre, (Fig. 33), except for higher $\bar{C}_L$ values where high suction peaks on the sheared part of the wing (Figs. 8 and 9) reduce M_{crit} below that at the centre. The beneficial effect of the curved leading-edge tip is apparent.

4. *Conclusions.*—(*a*) Assumptions made in the calculation method of Refs. 2 and 3 are verified by the present tests. For example, it was assumed that the only effect of the trailing vortices is a change in the effective incidence at any spanwise position. This implies that, at the same C_N, the chordwise pressure distributions at the centre and tip are independent of aspect ratio. This is shown to be true, except for some small deviation at aspect ratio 2. The empirical curve for the rate of decrease of the centre and tip effects is confirmed (section 3.1.1.), as is the correction to the lift slope for two-dimensional boundary-layer effects.

(*b*) At low $\bar{C}_L$, where viscosity effects are of little importance, the experimental results show that the aerodynamic characteristics of a given wing can be calculated satisfactorily by the method of Refs. 2 and 3 if the characteristics of the aerofoil section, including the two-dimensional lift slope at the required Reynolds number, are known.

Due to distorted pressure distributions there is a considerable drag at the centre of a swept-back wing, which is almost exactly compensated by a thrust near the tips each consisting of a term proportional to $(t/c)^2$ and another proportional to $\bar{C}_L^2$.

(*c*) As the incidence increases, the loss of lift due to the boundary-layer becomes appreciable. This effect is greater on swept-back wings than on unswept wings because of the outflow in the boundary-layer near the trailing edge; this causes the air in the boundary-layer to follow a longer path along the wing surface, and the thickness of the layer is thereby increased. Associated with the loss of lift is an increase in drag (*see* section 3.2).

As the incidence increases still further, the effect of a tip vortex becomes noticeable. This causes an increase of lift at the rear of sections near the tips, spreading forwards and inwards as the incidence increases, and also an increase in the total lift slope. This is accompanied by another drag increment and also by a nose-down pitching moment. The effect is more apparent on swept-back wings than on straight wings, (*see* section 3.3).

The stall begins with a breakdown of the suction peaks near the leading edge. The spanwise position where the breakdown first occurs depends on the spanwise variation of the peak suction and therefore on the geometry of the wing. Even on constant-chord wings the central region remains unstalled after the flow has broken down over the outer part. The leading-edge separation vortex which is formed at this stage causes a rapid reversal of the pitching moment and a decrease of the total lift slope. Since the large drag at the centre induced by the bound vortices is normally balanced by the thrust induced near the tip, the loss of the peak suctions near the tip means a large increase in drag (*see* section 3.4).

Acknowledgement.—The authors wish to acknowledge the assistance given by Mr. F. W. Dee who helped with the model tests and Miss M. Patterson who did most of the computing.

NOTATION

x, y, z		Rectangular co-ordinates; x-axis in direction of main flow, y-axis spanwise, z-axis upwards, origin at leading edge
$c(y)$		Local wing chord
$\bar{c}$		Mean chord
b		Span
A		Aspect ratio
φ		Angle of sweep
α		Geometric angle of incidence
α_i		Induced angle of incidence due to trailing vortices
α_e		Effective angle of incidence $= \alpha - \alpha_i$
α_B		Induced angle of incidence due to boundary layer
C_p	$=$	$(p - p_0)/q_0$, pressure coefficient
ΔC_p		Difference of pressure coefficients on upper and lower surface
$C_N(y)$		Coefficient of local normal force $= -\int_0^1 \Delta C_p(x,y)\, d\left(\frac{x}{c(y)}\right)$
$C_T(y)$		Coefficient of local tangential force $= \int_{\substack{\text{around}\\\text{profile}}} C_p(x,y)\, d\left(\frac{z(x)}{c(y)}\right)$
$C_L(y)$		Local lift coefficient $= C_N \cos \alpha - C_T \sin \alpha$
$C_{L\infty}$		Lift coefficient on an infinite sheared wing
$C_D(y)$		Local drag coefficient $= C_N \sin \alpha + C_T \cos \alpha$
$\bar{C}_L$		Coefficient of total lift $= \int_0^1 C_L(y) \frac{c(y)}{\bar{c}}\, d\left(\frac{y}{b/2}\right)$
$\bar{C}_D$		Coefficient of total drag, either from balance measurements or from pressure measurements $= \int_0^1 C_D(y) \frac{c(y)}{\bar{c}}\, d\left(\frac{y}{b/2}\right)$
$\bar{C}_{Di}$		Coefficient of total induced drag
$\bar{C}_{D\min}$		Minimum value of $\bar{C}_D$
ΔC_D		Local drag coefficient or thrust coefficient due to distorted chordwise pressure distribution
$\bar{C}_{DB}$		Total drag coefficient due to boundary layer
K	$=$	$\dfrac{\bar{C}_D - \bar{C}_{D\min}}{\bar{C}_L^2/\pi A}$

$K_i \quad = \quad \dfrac{\bar{C}_{Di}}{\bar{C}_L^2/\pi A}$

$K_B \quad = \quad \dfrac{\bar{C}_{DB}}{\bar{C}_L^2/\pi A}$

$C_m(y)$ Coefficient of local pitching moment with respect to the local quarter-chord point

$$= \int_0^1 \Delta C_p(x,y)\left(\frac{x}{c(y)} - 0\cdot 25\right) d\left(\frac{x}{c(y)}\right)$$

$$+ \int_{\substack{\text{around}\\\text{profile}}} C_p(x,y)\frac{z(x)}{c(y)}\, d\left(\frac{z(x)}{c(y)}\right)$$

$\bar{C}_m$ Total pitching-moment coefficient with respect to the mean quarter-chord point ; measured positive when 'nose-up'

h x co-ordinate of local aerodynamic centre

$$= \left(0\cdot 25 - \frac{C_m(y)}{C_N(y)}\right)c(y)$$

$\delta \quad = \quad t/c$, thickness/chord ratio in wind direction

M_0 Free-stream Mach number

M_{crit} Critical Mach number, the free-stream Mach number at which the local Mach number first becomes unity somewhere on the wing

R Reynolds number

REFERENCES

No.	*Author*	*Title, etc.*
1	D. Küchemann and D. J. Kettle	The effect of endplates on swept wings. C.P. 104. June, 1951.
2	D. Küchemann	A simple method for calculating the span and chordwise loadings on thin swept wings. R.A.E. Report Aero. 2392. A.R.C. 13,758. 1950.
3	J. Weber	A simple method for calculating the chordwise pressure distribution on two-dimensional and swept wings for aerofoil sections of finite thickness. R.A.E. Report Aero. 2391. A.R.C. 13,757. 1950.
4	G. G. Brebner	Boundary layer measurements on a 59 deg sweptback wing at low speed. C.P. 86. August, 1950.
5	J. Weber	Low speed measurements of the pressure distributions and overall forces on wings of small aspect ratio and 53 deg sweepback. R.A.E. Tech. Note Aero. 2017. A.R.C. 12,878. 1949.
6	J. Weber	Low speed measurements of the pressure distribution near the tips of swept back wings at no lift. R.A.E. Report Aero. 2318. A.R.C. 12,421. 1949.

REFERENCES—*continued*

No.	Author	Title, etc.
7	W. Mangler	Der kleinste induzierte Widerstand eines Tragflügels mit kleinem Seitenverhältnis. *Jahrbuch* 1939 *der deutschen Luftfahrtforschung*. I, p. 139.
8	G. B. McCullough and D. E. Gault ..	Boundary layer and stalling characteristics of the NACA 64A006 airfoil section. N.A.C.A. Tech. Note 1923. A.R.C. 12,781. August, 1949.
9	D. E. Gault	Boundary layer and stalling characteristics of the NACA 63-009 airfoil section. N.A.C.A. Tech. Note 1894. A.R.C. 12,780. June, 1949.
10	G. B. McCullough and D. E. Gault ..	An experimental investigation of a NACA 63_1-012 airfoil section with leading-edge suction slots. N.A.C.A. Tech. Note No. 1683. August, 1948.
11	J. Weber	Some remarks on the application of the theory of incompressible flow around a swept wing at zero incidence to the flow at high subsonic Mach numbers. R.A.E. Report Aero. 2274. A.R.C. 11,774. 1948.
12	V. W. Falkner	Calculated loadings due to incidence of a number of straight and swept back wings. R. & M. 2596. June, 1948.

TABLE 1

Details of Models

The main dimensions of the models are given in Fig. 1. The RAE 101 wing section was maintained on the curved tip, except where the pressure-tube guides made this impossible. The co-ordinates of the tip plan-form are given below, referred to an origin at point 0 in Fig. 1.

x (in.)	y (in.)
0	0
1·0	0·80
2·0	1·43
3·0	2·00
4·0	2·40
5·0	2·78
6·0	3·08
7·0	3·35
8·0	3·60
9·0	3·80
10·0	4·00
11·0	4·12
12·0	4·28

x (in.)	y (in.)
13·0	4·40
14·0	4·50
15·0	4·60
16·0	4·68
17·0	4·75
18·0	4·80
19·0	4·86
20·0	4·92
21·0	4·95
22·0	4·98
23·0	5·00
24·0	5·00
25·0	5·00

TABLE 1—*continued*

Arrangement of pressure holes:—

Aspect ratio	Spanwise stations of rows of pressure holes, y/c										y/c at tip
∞	0	0·10	0·20	0·40	0·60	0·90	1·25	1·60			
5	0	0·10	0·20	0·40	0·60	0·90	1·25	1·60	2·2	2·33	2·45
3	0	0·10	0·20	0·40	0·60	0·90			1·23	1·35	1·47
2	0	0·10	0·20	0·40	0·60					0·83	0·95

Checks of the model wing section at two spanwise stations ($y/c = 0 \cdot 10$ and $0 \cdot 20$) showed discrepancies between the model and the design sections: the model section was too thick all over, the discrepancy increasing from about 0·1 per cent chord at maximum thickness to about 0·4 per cent chord near the trailing edge. The actual maximum thickness was 12·1 per cent. This discrepancy was not the same on both surfaces, so that the section had a slight camber. This asymmetry has been allowed for in analysing the results by subtracting from ΔC_p* at any incidence α the value of ΔC_p at $\alpha = 0$ deg: *i.e.*, the ΔC_p plotted in Figs. 5, 6 and 7 is really $(\Delta C_{p\alpha} - \Delta C_{p0})$. The values of C_p given in Tables 2, 5 and 9 are those actually measured. The calculated distributions of C_p for sections in the central region of the wing, (Figs. 2, 3 and 4), are based on the true thickness profile of the model at stations $y/c = 0 \cdot 10$ and $0 \cdot 20$. Distributions calculated for the tip region are based on the design section. This may account for some difference between experimental and theoretical results (*see* Fig. 2) for the station near the tip.

The total pitching-moment coefficients were calculated about the mean quarter-chord line for each finite wing:—

Aspect ratio:	5	3	2
Distance of mean quarter-chord line behind apex of wing:	29·30 in.	19·70 in.	14·60 in.

* ΔC_p is the difference between the pressure coefficients on the upper and lower surfaces of the wing.

TABLE 2

Pressure Coefficients on Wing of Aspect Ratio 2·0

$y = 0$

Upper surface C_p

x/c	α (deg)												
	0	2·0	4·1	6·1	8·1	10·2	12·2	14·2	16·3	17·3	18·3	19·3	20·3
0	+1·005	+1·000	+0·950	+0·940	+0·905	+0·845	+0·760	+0·655	+0·520	+0·480	+0·410	+0·310	+0·255
0·01	0·470	0·335	+0·200	+0·060	−0·090	−0·255	−0·430	−0·615	−0·830	−0·895	−1·000	−1·140	−1·225
0·03	0·210	+0·090	−0·025	−0·140	−0·245	−0·375	−0·510	−0·650	−0·765	−0·845	−0·915	−1·005	−1·065
0·08	+0·020	−0·080	−0·175	−0·260	−0·340	−0·435	−0·530	−0·635	−0·735	−0·755	−0·800	−0·870	−0·920
0·15	−0·105	−0·190	−0·270	−0·345	−0·410	−0·485	−0·565	−0·650	−0·735	−0·760	−0·790	−0·855	−0·865
0·225	−0·175	−0·250	−0·325	−0·390	−0·445	−0·505	−0·575	−0·650	−0·725	−0·735	−0·760	−0·815	−0·825
0·35	−0·260	−0·330	−0·390	−0·440	−0·480	−0·530	−0·590	−0·655	−0·705	−0·715	−0·735	−0·780	−0·785
0·50	−0·215	−0·265	−0·305	−0·340	−0·370	−0·405	−0·440	−0·480	−0·520	−0·530	−0·545	−0·575	−0·590
0·65	−0·160	−0·195	−0·225	−0·245	−0·265	−0·285	−0·315	−0·340	−0·365	−0·370	−0·380	−0·405	−0·410
0·75	−0·095	−0·125	−0·145	−0·165	−0·175	−0·200	−0·205	−0·225	−0·240	−0·240	−0·260	−0·265	−0·265
0·85	−0·065	−0·080	−0·100	−0·110	−0·115	−0·140	−0·135	−0·150	−0·160	−0·160	−0·180	−0·175	−0·180
0·95	—	—	—	—	−0·025	−0·040	−0·035	−0·035	−0·040	−0·035	−0·060	−0·045	−0·040

Lower surface C_p

x/c	α (deg)												
	0	2·0	4·1	6·1	8·1	10·2	12·2	14·2	16·3	17·3	18·3	19·3	20·3
0·01	+0·520	+0·625	+0·720	+0·790	+0·870	0·925	0·960	0·985	0·995	1·005	1·000	0·985	0·985
0·03	+0·230	0·335	0·435	0·530	0·630	0·700	0·770	0·825	0·885	0·905	0·925	0·940	0·960
0·08	−0·005	+0·085	0·180	0·260	0·350	0·435	0·510	0·580	0·655	0·685	0·715	0·740	0·775
0·15	−0·105	−0·025	+0·060	0·135	0·220	0·295	0·370	0·430	0·510	0·540	0·575	0·600	0·635
0·225	−0·175	−0·105	−0·030	+0·045	0·120	0·195	0·260	0·320	0·400	0·430	0·460	0·495	0·525
0·35	−0·255	−0·195	−0·130	−0·070	+0·005	0·070	0·130	0·190	0·260	0·290	0·315	0·350	0·380
0·50	−0·235	−0·185	−0·135	−0·085	−0·025	0·025	0·080	0·130	0·190	0·220	0·245	0·265	0·295
0·65	−0·170	−0·140	−0·100	−0·060	−0·010	0·030	0·075	0·110	0·160	0·185	0·205	0·225	0·255
0·75	−0·110	−0·090	−0·060	−0·035	−0·010	0·025	0·060	0·095	0·135	0·155	0·160	0·185	0·210
0·85	−0·065	−0·050	−0·035	−0·010	+0·025	0·035	0·075	0·100	0·130	0·150	0·150	0·175	0·195
0·95	−0·020	−0·005	+0·005	+0·020	+0·045	0·050	0·080	0·095	0·120	0·135	0·130	0·150	0·170

TABLE 2—*continued*

$y/c = 0 \cdot 1$ $\qquad$ $2y/b = 0 \cdot 105$

Upper surface

C_p

x/c	α (deg)										
	0	2·0	4·1	6·1	8·1	10·2	12·2	14·2	16·3	18·3	20·3
0	+0·540	+0·520	+0·430	+0·300	+0·125	−0·120	−0·415	−0·790	−1·290	−1·700	−2·245
0·01	+0·205	+0·025	−0·180	−0·400	−0·650	−0·940	−1·245	−1·595	−2·005	−2·310	−2·715
0·03	−0·015	−0·180	−0·345	−0·520	−0·705	−0·910	−1·130	−1·390	−1·620	−1·840	−2·010
0·08	−0·125	−0·240	−0·360	−0·470	−0·585	−0·715	−0·805	−0·930	−1·080	−1·180	−1·315
0·15	−0·200	−0·290	−0·385	−0·470	−0·550	−0·610	−0·685	−0·785	−0·885	−0·940	−1·030
0·225	−0·250	−0·325	−0·395	−0·475	−0·530	−0·605	−0·670	−0·730	−0·805	−0·860	−0·940
0·35	−0·250	−0·315	−0·370	−0·410	−0·450	−0·500	−0·540	−0·590	−0·645	−0·680	−0·740
0·50	−0·195	—	−0·260	−0·290	−0·325	−0·360	−0·385	−0·420	−0·455	−0·480	−0·535
0·65	−0·115	−0·145	−0·175	−0·195	−0·200	−0·230	−0·240	−0·260	−0·290	−0·315	−0·330
0·75	−0·060	−0·080	−0·100	−0·110	−0·115	−0·140	−0·145	−0·160	−0·175	−0·195	−0·200
0·85	−0·005	−0·020	−0·030	−0·035	−0·040	−0·055	−0·055	−0·060	−0·070	−0·080	−0·070
0·95	+0·055	+0·050	+0·050	+0·050	+0·055	+0·040	+0·050	+0·050	+0·050	+0·025	+0·070

Lower surface

C_p

x/c	α (deg)										
	0	2·0	4·1	6·1	8·1	10·2	12·2	14·2	16·3	18·3	20·3
0·01	+0·205	+0·345	+0·450	+0·515	+0·570	0·555	0·520	0·445	0·320	0·205	0·015
0·03	+0·025	+0·165	0·275	0·375	0·465	0·530	0·580	0·605	0·615	0·610	0·585
0·08	−0·115	−0·005	+0·100	0·195	0·280	0·365	0·440	0·505	0·570	0·615	0·660
0·15	−0·215	−0·125	−0·040	+0·045	0·130	0·210	0·280	0·350	0·430	0·490	0·550
0·225	−0·240	−0·170	−0·090	−0·020	+0·060	0·130	0·200	0·260	0·335	0·400	0·460
0·35	−0·260	−0·210	−0·150	−0·090	−0·025	0·040	0·100	0·155	0·220	0·275	0·340
0·50	−0·210	−0·170	−0·125	−0·080	−0·030	0·020	0·070	0·115	0·190	0·235	0·265
0·65	−0·120	—	−0·080	−0·045	0	0·035	0·070	0·100	0·145	0·185	0·230
0·75	−0·060	—	−0·040	−0·015	+0·030	0·045	0·080	0·105	0·135	0·155	0·200
0·85	−0·020	−0·010	+0·010	+0·020	0·035	0·050	0·085	0·100	0·125	0·135	0·175
0·95	+0·050	+0·050	+0·055	+0·065	+0·075	0·075	0·095	0·110	0·125	0·130	0·155

TABLE 2—*continued*

$y/c = 0 \cdot 2$ $\qquad$ $2y/b = 0 \cdot 21$

Upper surface $\qquad$ C_p

x/c	α (deg)										
	0	2·0	4·1	6·1	8·1	10·2	12·2	14·2	16·3	18·3	20·3
0	+0·485	+0·440	+0·310	+0·110	−0·170	−0·550	−1·005	−1·590	−2·335	−2·950	−3·755
0·01	+0·160	−0·050	−0·300	−0·575	−0·870	−1·230	−1·620	−2·080	−2·625	−3·040	−3·595
0·03	−0·055	−0·240	−0·450	−0·650	−0·855	−1·120	−1·390	−1·735	−2·015	−2·230	−2·445
0·08	−0·170	−0·300	−0·435	−0·560	−0·685	−0·825	−0·925	−1·110	−1·290	−1·410	−1·575
0·15	−0·240	−0·345	−0·445	−0·540	−0·615	−0·680	−0·760	−0·875	−0·985	−1·080	−1·190
0·225	−0·255	−0·345	−0·425	−0·495	−0·555	−0·590	−0·645	−0·730	−0·805	−0·880	−0·960
0·35	−0·255	−0·320	−0·375	−0·405	−0·445	−0·500	−0·530	−0·590	−0·640	−0·675	−0·735
0·50	−0·190	—	−0·235	−0·270	−0·290	−0·325	−0·335	−0·375	−0·405	−0·440	−0·495
0·65	−0·085	−0·120	−0·140	−0·155	−0·165	−0·190	−0·190	−0·215	−0·235	−0·260	−0·295
0·75	−0·030	−0·055	−0·070	−0·075	−0·080	−0·100	−0·105	−0·115	−0·125	−0·145	−0·160
0·85	+0·020	0	−0·005	−0·010	−0·020	−0·025	−0·020	−0·025	−0·025	−0·035	−0·035
0·95	+0·075	+0·065	+0·065	+0·065	+0·070	+0·055	+0·060	+0·060	+0·070	+0·075	+0·080

Lower surface $\qquad$ C_p

x/c	α (deg)										
	0	2·0	4·1	6·1	8·1	10·2	12·2	14·2	16·3	18·3	20·3
0·01	+0·190	+0·350	+0·450	+0·505	+0·530	0·505	0·470	0·355	0·210	0·040	−0·195
0·03	−0·015	+0·145	0·270	0·375	0·455	0·505	0·565	0·555	0·550	0·500	0·435
0·08	−0·180	−0·065	+0·050	+0·150	0·245	0·315	0·415	0·465	0·540	0·570	0·610
0·15	−0·245	−0·160	−0·065	−0·020	0·110	0·180	0·270	0·330	0·415	0·465	0·520
0·225	−0·265	−0·195	−0·120	−0·045	+0·035	0·095	0·185	0·240	0·320	0·365	0·430
0·35	−0·265	−0·220	−0·160	−0·100	−0·035	0·015	0·100	0·135	0·210	0·250	0·310
0·50	−0·205	−0·165	−0·125	−0·080	−0·030	0·005	0·065	0·095	0·160	0·195	0·245
0·65	−0·080	−0·080	−0·070	−0·020	+0·015	0·035	0·095	0·105	0·145	0·170	0·210
0·75	−0·050	−0·040	−0·020	−0·010	0·015	0·030	0·060	0·085	0·130	0·145	0·175
0·85	−0·005	+0·005	+0·015	0·020	0·045	0·050	0·070	0·090	0·125	0·140	0·160
0·95	+0·060	+0·055	+0·055	0·060	+0·075	0·070	0·080	0·080	0·115	0·125	0·140

TABLE 2—*continued*

$y/c = 0 \cdot 4$ $2y/b = 0 \cdot 42$

Upper surface C_p

x/c	α (deg)								
	−1·0	1·0	3·1	7·1	11·2	13·2	15·2	17·3	19·3
0	+0·455	+0·490	+0·380	−0·085	−0·950	−1·610	−2·355	−3·145	−4·190
0·01	+0·200	+0·030	−0·230	−0·890	−1·805	−2·380	−2·975	−3·575	−4·370
0·03	0	−0·140	−0·340	−0·835	−1·425	−1·760	−2·000	−2·315	−2·705
0·08	−0·150	−0·245	−0·405	−0·705	−0·950	−1·170	−1·335	−1·505	−1·715
0·15	−0·240	−0·295	−0·410	−0·625	−0·835	−0·935	−1·035	−1·140	−1·245
0·225	−0·245	−0·280	−0·375	−0·480	−0·645	−0·735	−0·800	−0·860	−0·955
0·35	−0·250	−0·260	−0·315	−0·390	−0·480	−0·530	−0·555	−0·590	−0·645
0·50	—	−0·145	−0·185	−0·240	−0·255	−0·300	−0·315	−0·345	−0·415
0·65	−0·060	−0·080	−0·095	−0·110	−0·130	−0·140	−0·165	−0·200	−0·280
0·75	−0·025	−0·030	−0·030	−0·040	−0·040	−0·065	−0·080	−0·120	−0·190
0·85	+0·015	+0·005	+0·010	+0·015	+0·010	−0·005	−0·025	−0·060	−0·090
0·95	+0·065	+0·060	+0·070	+0·075	+0·065	+0·040	+0·025	+0·015	+0·015

Lower surface C_p

x/c	α (deg)								
	−1·0	1·0	3·1	7·1	11·2	13·2	15·2	17·3	19·3
0·01	−0·025	+0·230	+0·365	+0·500	0·425	0·300	0·140	−0·070	−0·370
0·03	−0·220	+0·015	+0·165	0·395	0·515	0·520	0·515	0·475	0·395
0·08	−0·320	−0·140	−0·030	0·195	0·360	0·425	0·495	0·535	0·570
0·15	−0·355	−0·210	−0·130	+0·055	0·220	0·280	0·360	0·415	0·475
0·225	−0·350	−0·230	−0·165	−0·015	0·125	0·185	0·260	0·315	0·370
0·35	−0·320	−0·225	−0·185	−0·080	0·030	0·075	0·145	0·195	0·245
0·50	−0·195	−0·150	−0·115	−0·035	0·025	0·055	0·105	0·145	0·185
0·65	−0·085	—	−0·020	+0·015	0·060	0·075	0·110	0·135	0·160
0·75	−0·050	−0·050	−0·030	0	0·025	0·040	0·070	0·095	0·110
0·85	−0·010	−0·010	+0·005	0·020	0·030	0·035	0·060	0·075	0·090
0·95	+0·070	+0·060	+0·070	+0·080	0·075	0·065	—	0·090	0·100

TABLE 2—*continued*

$y/c = 0 \cdot 6$ $\qquad$ $2y/b = 0 \cdot 63$

Upper surface $\qquad$ C_p

x/c	α (deg)								
	−1·0	1·0	3·1	7·1	11·2	13·2	15·2	17·3	19·3
0	+0·485	+0·465	+0·360	−0·170	−1·135	−1·825	−2·620	−3·430	−4·465
0·01	0·235	+0·030	−0·210	−0·820	−1·695	−2·240	−2·915	−3·585	−4·380
0·03	+0·025	−0·165	−0·370	−0·840	−1·435	−1·745	−2·035	−2·320	−2·690
0·08	−0·130	−0·265	−0·395	−0·710	−0·975	−1·170	−1·355	−1·530	−1·735
0·15	−0·220	−0·310	−0·405	−0·600	−0·780	−0·890	−0·995	−1·095	−1·215
0·225	−0·245	−0·305	−0·375	−0·515	−0·660	−0·730	−0·785	−0·840	−0·900
0·35	−0·180	−0·250	−0·300	−0·330	−0·415	−0·455	−0·490	−0·485	−0·500
0·50	−0·100	−0·120	−0·150	−0·185	−0·220	−0·240	−0·260	−0·255	−0·305
0·65	−0·060	−0·075	−0·085	−0·090	−0·100	−0·105	−0·135	−0·135	−0·215
0·75	−0·005	−0·010	−0·020	−0·020	−0·025	−0·040	−0·075	−0·090	−0·200
0·85	+0·025	+0·020	+0·025	+0·030	+0·025	+0·015	−0·010	−0·070	−0·175
0·95	+0·075	+0·070	+0·075	+0·080	+0·070	+0·045	0	−0·045	−0·095

Lower surface $\qquad$ C_p

x/c	α (deg)								
	−1·0	1·0	3·1	7·1	11·2	13·2	15·2	17·3	19·3
0·01	−0·045	+0·175	+0·330	+0·480	0·400	0·275	0·095	−0·110	−0·395
0·03	−0·195	−0·005	+0·155	0·385	0·490	0·500	0·480	0·435	0·355
0·08	−0·315	−0·175	−0·050	0·165	0·320	0·390	0·445	0·485	0·510
0·15	−0·330	−0·235	−0·145	+0·030	0·175	0·240	0·300	0·350	0·405
0·225	−0·320	−0·250	−0·185	−0·050	0·070	0·130	0·190	0·245	0·295
0·35	−0·255	−0·210	−0·165	−0·075	0·010	0·050	0·100	0·145	0·190
0·50	−0·120	−0·095	—	−0·040	0·010	0·040	0·065	0·100	0·130
0·65	−0·070	−0·065	−0·050	−0·020	0·010	0·025	0·040	0·065	0·090
0·75	−0·005	−0·010	0	+0·025	0·040	0·045	0·050	0·065	0·085
0·85	+0·045	+0·035	+0·045	+0·055	0·030	0·050	0·055	0·065	0·070
0·95	—	—	—	—	—	—	—	—	—

TABLE 2—*continued*

$y/c = 0 \cdot 83$ $\qquad$ $2y/b = 0 \cdot 87$

Upper surface $\qquad$ C_p

$x/c(y)$	α (deg)												
	0	2·0	4·1	6·1	8·1	10·2	12·2	14·2	16·3	17·3	18·3	19·3	20·3
0	+0·005	−0·050	−0·160	−0·275	−0·410	−0·680	−0·965	−1·340	−1·800	−1·965	−2·190	−2·440	−2·670
0·025	−0·055	−0·190	−0·370	−0·560	−0·790	−1·055	−1·405	−1·735	−2·175	−2·350	−2·515	−2·765	−2·865
0·05	−0·110	−0·235	−0·385	−0·540	−0·730	−0·940	−1·200	−1·475	−1·790	−1·890	−2·110	−2·095	−2·220
0·10	−0·155	−0·260	−0·370	−0·495	−0·640	−0·790	−0·965	−1·125	−1·345	−1·350	−1·470	−1·420	−1·545
0·15	−0·185	−0·270	−0·370	−0·465	−0·575	−0·685	−0·815	−0·940	−1·085	−1·120	−1·170	−1·070	−1·230
0·25	−0·170	−0·240	−0·310	−0·380	−0·440	−0·525	−0·620	−0·695	−0·785	−0·800	−0·845	−0·865	−0·895
0·35	−0·150	−0·205	−0·250	−0·285	−0·340	−0·395	−0·455	−0·515	−0·610	−0·655	−0·745	−0·825	−0·815
0·50	−0·085	−0·125	−0·155	−0·175	−0·210	−0·240	−0·285	−0·335	−0·355	—	−0·435	−0·655	−0·735
0·70	+0·020	−0·015	−0·030	−0·045	−0·060	−0·080	−0·095	−0·160	−0·270	−0·335	−0·435	−0·665	−0·745

Lower surface $\qquad$ C_p

$x/c(y)$	α (deg)												
	0	2·0	4·1	6·1	8·1	10·2	12·2	14·2	16·3	17·3	18·3	19·3	20·3
0·025	−0·075	+0·020	+0·075	+0·080	+0·065	−0·030	−0·110	−0·255	−0·510	−0·545	−0·655	−0·785	−0·895
0·05	−0·100	−0·015	+0·040	0·075	0·085	0·020	+0·005	−0·060	−0·180	−0·225	−0·285	−0·365	−0·430
0·10	−0·170	−0·080	−0·035	+0·020	0·030	0·030	0·030	+0·015	−0·025	−0·040	−0·065	−0·100	−0·130
0·15	−0·180	−0·120	−0·070	−0·020	+0·010	0·020	0·035	0·035	+0·025	+0·015	−0·005	−0·025	−0·040
0·25	−0·185	−0·135	−0·095	−0·050	−0·015	−0·005	+0·025	0·040	0·055	0·055	+0·050	+0·050	+0·050
0·35	−0·175	−0·145	−0·110	−0·080	−0·050	−0·040	−0·010	0·010	0·025	0·025	0·035	0·035	0·045
0·50	−0·080	−0·060	−0·040	−0·020	−0·005	+0·005	+0·030	0·040	0·055	0·055	0·060	0·070	0·080
0·70	+0·010	+0·005	+0·020	+0·030	+0·035	+0·025	+0·035	+0·055	+0·060	+0·055	+0·070	+0·075	+0·090

TABLE 3

Coefficients of Local Normal Force, Tangential Force, Lift, Drag and Aerodynamic Centre Position

Wing of aspect ratio 2

C_N

α (deg)	$2y/b$					
	0	0·105	0·210	0·420	0·630	0·870
1·0	0·048	—	—	0·047	0·043	0·037
2·0	0·097	0·096	0·097	—	—	0·073
3·1	0·144	—	—	0·141	0·130	0·108
4·1	0·197	0·191	0·196	—	—	0·145
6·1	0·293	0·285	0·288	—	—	0·213
7·1	0·338	—	—	0·322	0·291	0·248
8·1	0·386	0·376	0·378	—	—	0·283
10·2	0·478	0·471	0·468	—	—	0·347
11·2	0·525	—	—	0·497	0·450	0·388
12·2	0·568	0·561	0·562	—	—	0·416
13·2	0·623	—	—	0·595	0·528	0·458
14·2	0·662	0·652	0·653	—	—	0·505
15·2	0·719	—	—	0·693	0·620	0·545
16·3	0·759	0·752	0·752	—	—	0·608
17·3	0·803	—	—	0·790	0·699	0·675
18·3	0·849	0·843	0·842	—	—	0·747
19·3	0·901	—	—	0·909	0·817	0·844
20·3	0·943	0·931	0·942	—	—	0·942

C_T

α (deg)	$2y/b$					
	0	0·105	0·210	0·420	0·630	0·870
0	+0·044	+0·013	+0·006	—	—	−0·014
1·0	0·043	—	—	+0·001	−0·004	−0·014
2·0	0·042	0·012	+0·004	—	—	−0·013
3·1	0·041	—	—	−0·004	−0·006	−0·016
4·1	0·041	0·008	−0·001	—	—	−0·018
6·1	0·039	+0·002	−0·008	—	—	−0·026
7·1	0·037	—	—	−0·024	−0·026	−0·032
8·1	0·036	−0·006	−0·019	—	—	−0·037
10·2	0·032	−0·014	−0·031	—	—	−0·053
11·2	0·029	—	—	−0·055	−0·057	−0·061
12·2	0·027	−0·027	−0·047	—	—	−0·071
13·2	0·023	—	—	−0·080	−0·081	−0·081
14·2	0·020	−0·042	−0·069	—	—	−0·093
15·2	0·016	—	—	−0·104	−0·108	−0·102
16·3	0·013	−0·061	−0·094	—	—	−0·117
17·3	0·011	—	—	−0·134	−0·135	−0·124
18·3	0·007	−0·074	−0·116	—	—	−0·132
19·3	+0·002	—	—	−0·172	−0·178	−0·132
20·3	−0·002	−0·097	−0·141	—	—	−0·142

TABLE 3—*continued*

C_L

α (deg)	2y/b: 0	0·105	0·210	0·420	0·630	0·870
1·0	0·048	—	—	0·047	0·043	0·037
2·0	0·096	0·096	0·097	—	—	0·073
3·1	0·142	—	—	0·141	0·130	0·109
4·1	0·194	0·190	0·196	—	—	0·146
6·1	0·287	0·283	0·287	—	—	0·215
7·1	0·330	—	—	0·322	0·292	0·249
8·1	0·377	0·373	0·378	—	—	0·285
10·2	0·465	0·466	0·466	—	—	0·350
11·2	0·509	—	—	0·498	0·453	0·393
12·2	0·550	0·554	0·559	—	—	0·422
13·2	0·602	—	—	0·598	0·533	0·465
14·2	0·638	0·643	0·650	—	—	0·512
15·2	0·689	—	—	0·696	0·627	0·552
16·3	0·726	0·740	0·748	—	—	0·616
17·3	0·763	—	—	0·794	0·708	0·681
18·3	0·804	0·823	0·837	—	—	0·751
19·3	0·849	—	—	0·915	0·830	0·841
20·3	0·886	0·907	0·933	—	—	0·933

C_D

α (deg)	2y/b: 0	0·105	0·210	0·420	0·630	0·870
0	0·044	0·013	0·006	0·001	—0·004	—0·014
1·0	0·044	—	—	0·002	—0·003	—0·013
2·0	0·046	0·016	0·007	—	—	—0·011
3·1	0·049	—	—	0·005	+0·001	—0·009
4·1	0·054	0·022	0·013	—	—	—0·008
6·1	0·069	0·033	0·023	—	—	—0·003
7·1	0·078	—	—	0·017	0·011	—0·001
8·1	0·089	0·048	0·035	—	—	+0·004
10·2	0·116	0·070	0·052	—	—	0·009
11·2	0·131	—	—	0·042	0·031	0·014
12·2	0·146	0·093	0·073	—	—	0·019
13·2	0·164	—	—	0·058	0·042	0·026
14·2	0·182	0·120	0·094	—	—	0·034
15·2	0·204	—	—	0·082	0·058	0·044
16·3	0·226	0·151	0·121	—	—	0·058
17·3	0·248	—	—	0·107	0·079	0·082
18·3	0·273	0·194	0·154	—	—	0·110
19·3	0·300	—	—	0·138	+0·102	0·155
20·3	0·326	0·232	0·196	—	—	+0·194

TABLE 3—*continued*

$$\frac{h}{c(y)}$$

α (deg)	2y/b: 0	0·105	0·21	0·42	0·63	0·87
0	0·336	0·291	0·266	0·230	0·208	0·258
2·0	0·335	0·292	0·266	—	—	0·258
3·1	0·337	—	—	0·230	0·211	0·258
4·1	0·337	0·291	0·267	—	—	0·260
6·1	0·338	0·290	0·265	—	—	0·258
7·1	0·339	—	—	—	0·207	0·258
8·1	0·340	0·291	0·267	—	—	0·257
10·2	0·342	0·297	0·269	—	—	0·256
11·2	0·342	—	—	0·234	0·210	0·256
12·2	0·342	0·300	0·270	—	—	0·256
13·2	0·343	—	—	0·237	0·214	0·264
14·2	0·342	0·298	0·270	—	—	0·275
15·2	0·344	—	—	0·244	0·219	0·283
16·3	0·346	0·301	0·275	—	—	0·298
17·3	0·346	—	—	0·254	0·230	0·315
18·3	0·346	0·307	0·281	—	—	0·332
19·3	0·348	0·307	0·283	0·266	0·251	0·353
20·3	0·349	0·308	0·284	—	—	0·386

TABLE 4

Coefficients of Total Lift, Drag and Pitching Moment from Pressure Measurements

Wing of aspect ratio 2·0

α (deg)	$\bar{C}_L$	$\bar{C}_D$	$\bar{C}_m$
2·0	0·088	0·0025	0·003
4·1	0·176	0·0062	0·006
6·1	0·258	0·0136	0·009
8·1	0·345	0·0239	0·012
10·2	0·428	0·0367	0·016
12·2	0·513	0·0523	0·017
14·2	0·605	0·0717	0·016
16·3	0·702	0·0963	0·006
17·3	0·751	0·112	−0·002
18·3	0·810	0·132	−0·014
19·3	0·885	0·156	−0·029

TABLE 5

Pressure Coefficients on Wing of Aspect Ratio 3

$y = 0$

Upper surface

C_p

x/c	α (deg)											
	0	2·1	4·1	6·2	8·2	10·3	12·3	14·4	16·4	18·5	20·6	22·6
0	+1·000	—	+0·980	+0·935	+0·875	+0·805	+0·700	+0·600	+0·465	+0·320	+0·155	0
0·01	0·460	+0·330	+0·205	+0·035	−0·135	−0·295	−0·495	−0·685	−0·885	−1·105	−1·240	−1·485
0·03	0·195	+0·075	−0·035	−0·175	−0·300	−0·430	−0·585	−0·725	−0·845	−1·005	−1·105	−1·270
0·08	+0·015	−0·095	−0·175	−0·280	−0·385	−0·475	−0·585	−0·680	−0·780	−0·900	−1·010	−1·080
0·15	−0·115	−0·200	−0·270	−0·370	−0·455	−0·530	−0·620	−0·710	−0·795	−0·890	−0·975	−1·020
0·225	−0·180	−0·255	−0·320	−0·410	−0·480	−0·545	−0·630	−0·705	−0·770	−0·845	−0·930	−0·960
0·35	−0·255	−0·310	−0·380	−0·455	−0·510	−0·570	−0·635	−0·695	−0·750	−0·815	−0·885	−0·925
0·50	−0·220	−0·270	−0·310	−0·360	−0·410	−0·450	−0·495	−0·540	−0·580	−0·635	−0·690	−0·755
0·65	−0·175	−0·210	−0·235	−0·275	−0·310	−0·340	−0·370	−0·400	−0·430	−0·470	−0·525	−0·625
0·75	−0·115	−0·145	−0·165	−0·200	−0·225	−0·245	−0·265	−0·285	−0·310	−0·335	−0·395	−0·500
0·85	−0·080	−0·100	−0·115	−0·140	−0·160	−0·175	−0·190	−0·205	−0·220	−0·235	−0·280	−0·385
0·95	−0·025	−0·025	−0·035	−0·055	−0·060	−0·065	−0·070	−0·075	−0·075	−0·075	−0·120	−0·190

Lower surface

C_p

x/c	α (deg)											
	0	2·1	4·1	6·2	8·2	10·3	12·3	14·4	16·4	18·5	20·6	22·6
0·01	+0·540	+0·630	+0·735	+0·805	+0·870	0·925	0·965	0·990	1·005	1·000	0·990	0·985
0·03	+0·225	0·340	0·450	0·545	0·630	0·710	0·785	0·850	0·905	0·940	0·990	1·045
0·08	−0·010	+0·095	0·200	0·280	0·370	0·450	0·540	0·615	0·685	0·745	0·815	0·900
0·15	−0·105	−0·020	+0·075	0·155	0·235	0·310	0·395	0·470	0·540	0·590	0·680	0·760
0·225	−0·175	−0·100	−0·010	+0·065	0·145	0·215	0·295	0·365	0·440	0·510	0·585	0·675
0·35	−0·250	−0·185	−0·105	−0·045	+0·030	0·095	0·170	0·240	0·310	0·370	0·445	0·530
0·50	−0·240	−0·180	−0·115	−0·060	−0·005	0·055	0·125	0·180	0·245	0·295	0·360	0·430
0·65	−0·180	−0·135	−0·080	−0·040	+0·005	0·055	0·110	0·155	0·215	0·260	0·310	0·370
0·75	−0·130	−0·095	−0·065	−0·020	0·020	0·060	0·110	0·155	0·205	0·245	0·280	0·325
0·85	−0·070	−0·050	−0·015	+0·010	0·040	0·070	0·105	0·140	0·180	0·230	0·255	0·285
0·95	−0·035	−0·005	+0·025	+0·030	+0·055	0·075	0·105	0·130	0·160	0·190	0·205	0·225

TABLE 5—*continued*

$y/c = 0 \cdot 1$ $\qquad$ $2y/b = 0 \cdot 068$

Upper surface $\qquad$ C_p

x/c	α (deg)											
	0	2·1	4·1	6·2	8·2	10·3	12·3	14·4	16·4	18·5	20·6	22·6
0	+0·540	+0·505	+0·430	+0·265	+0·055	−0·220	−0·605	−1·005	−1·460	−1·980	−2·635	−3·140
0·01	+0·200	+0·010	−0·185	−0·455	−0·735	−1·060	−1·410	−1·765	−2·195	−2·610	−3·105	−3·480
0·03	−0·020	−0·190	−0·350	−0·565	−0·770	−1·010	−1·265	−1·540	−1·810	−2·030	−2·220	−2·335
0·08	−0·125	−0·240	−0·350	−0·495	−0·630	−0·765	−0·850	−0·980	−1·135	−1·290	−1·465	—
0·15	−0·205	−0·310	−0·390	−0·505	−0·600	−0·655	−0·755	−0·855	−0·955	−1·070	−1·180	−1·245
0·225	−0·255	−0·335	−0·415	−0·505	−0·580	−0·655	−0·735	−0·810	−0·885	−0·970	−1·065	−1·125
0·35	−0·260	−0·330	−0·375	−0·435	−0·500	−0·550	−0·610	−0·665	−0·720	−0·785	−0·870	−0·965
0·50	−0·200	−0·245	−0·270	−0·320	−0·365	−0·405	−0·445	−0·490	−0·530	−0·585	−0·665	−0·785
0·65	−0·130	−0·160	−0·185	−0·220	−0·245	−0·270	−0·295	−0·320	−0·345	−0·385	−0·450	−0·565
0·75	−0·075	−0·095	−0·110	−0·140	−0·160	−0·180	−0·195	−0·215	−0·235	−0·250	−0·305	−0·400
0·85	−0·015	−0·030	−0·035	−0·055	−0·065	−0·075	−0·085	−0·095	−0·100	−0·110	−0·150	−0·230
0·95	+0·035	+0·045	+0·045	+0·035	+0·035	+0·030	+0·030	+0·035	+0·035	+0·050	+0·025	−0·025

Lower surface $\qquad$ C_p

x/c	α (deg)											
	0	2·1	4·1	6·2	8·2	10·3	12·3	14·4	16·4	18·5	20·6	22·6
0·01	+0·210	+0·360	+0·475	+0·535	+0·560	0·540	0·475	0·390	0·260	0·100	−0·100	−0·325
0·03	+0·025	0·180	0·305	0·400	0·490	0·540	0·585	0·605	0·610	0·595	+0·575	+0·525
0·08	−0·115	+0·005	+0·125	0·220	0·310	0·380	0·465	0·530	0·590	0·640	0·700	0·740
0·15	−0·215	−0·115	−0·010	0·075	0·165	0·235	0·320	0·390	0·465	0·530	0·605	0·670
0·225	−0·240	−0·155	−0·065	+0·010	0·090	0·150	0·235	0·300	0·375	0·440	0·520	0·585
0·35	−0·265	−0·195	−0·120	−0·060	+0·005	0·060	0·140	0·205	0·270	0·330	0·405	0·460
0·50	−0·215	−0·165	−0·105	−0·055	−0·005	0·040	0·105	0·155	0·215	0·270	0·330	0·370
0·65	−0·125	−0·100	−0·055	−0·020	+0·025	0·055	0·100	0·145	0·190	0·235	0·280	0·300
0·75	−0·065	−0·030	−0·020	+0·020	0·055	0·080	0·120	0·145	0·185	0·225	0·255	0·270
0·85	−0·025	−0·010	+0·030	0·040	0·060	0·075	0·110	0·140	0·165	0·185	0·220	0·220
0·95	+0·045	+0·055	+0·070	+0·070	+0·085	0·085	0·105	0·125	0·150	0·170	+0·170	+0·145

TABLE 5—*continued*

$y/c = 0 \cdot 2$ $\qquad$ $2y/b = 0 \cdot 135$

Upper surface $\qquad C_p$

x/c	α (deg)											
	0	2·1	4·1	6·2	8·2	10·3	12·3	14·4	16·4	18·5	20·6	22·6
0	+0·480	+0·425	+0·290	+0·030	−0·315	−0·755	−1·365	−1·970	−2·795	−3·620	−4·600	−5·485
0·01	+0·155	−0·070	−0·305	−0·650	−0·995	−1·375	−1·865	−2·350	−2·905	−3·490	−4·165	−4·685
0·03	−0·055	−0·255	−0·455	−0·700	−0·960	−1·245	−1·595	−1·915	−2·110	−2·430	−2·785	−3·025
0·08	−0·170	−0·310	−0·440	−0·605	−0·740	−0·890	−1·050	−1·230	−1·410	−1·600	−1·810	−1·875
0·15	−0·240	−0·355	−0·450	−0·575	—	−0·755	−0·860	−0·975	−1·100	−1·230	−1·365	−1·235
0·225	−0·270	−0·360	−0·435	−0·540	−0·590	−0·690	−0·750	−0·835	−0·930	−1·050	−1·145	−1·185
0·35	−0·265	−0·330	−0·390	−0·430	−0·495	−0·560	−0·615	−0·670	−0·735	−0·795	−0·890	−1·115
0·50	−0·195	−0·230	−0·245	−0·300	−0·335	−0·375	−0·415	−0·450	−0·495	−0·550	−0·650	−0·885
0·65	−0·095	−0·130	−0·145	−0·180	−0·200	−0·230	−0·250	−0·280	−0·310	−0·345	−0·435	−0·600
0·75	−0·040	−0·065	−0·070	−0·100	−0·115	−0·135	−0·150	−0·170	−0·195	−0·210	−0·280	−0·415
0·85	+0·010	−0·005	0	−0·020	−0·025	−0·045	−0·050	−0·060	−0·070	−0·075	−0·125	−0·235
0·95	+0·060	+0·060	+0·070	+0·055	+0·055	+0·045	+0·045	+0·040	+0·045	+0·050	+0·015	−0·065

Lower surface $\qquad C_p$

x/c	α (deg)											
	0	2·1	4·1	6·2	8·2	10·3	12·3	14·4	16·4	18·5	20·6	22·6
0·01	+0·195	+0·365	+0·480	+0·530	+0·540	0·495	0·405	0·280	0·105	−0·110	−0·365	−0·635
0·03	−0·015	+0·160	0·300	0·405	0·490	0·525	0·550	0·550	0·520	+0·460	+0·390	+0·305
0·08	−0·180	−0·045	+0·080	0·170	0·280	0·350	0·435	0·500	0·555	0·600	0·645	0·685
0·15	−0·250	−0·145	−0·035	+0·055	0·145	0·220	0·300	0·375	0·450	0·510	0·590	0·645
0·225	−0·270	−0·180	−0·090	−0·015	+0·070	0·140	0·220	0·285	0·360	0·430	0·505	0·570
0·35	−0·270	−0·205	−0·135	−0·070	−0·005	0·050	0·125	0·190	0·255	0·320	0·390	0·440
0·50	−0·210	−0·155	−0·095	−0·050	+0·005	0·040	0·105	0·145	0·205	0·260	0·310	0·340
0·65	−0·090	−0·075	−0·025	+0·005	0·045	0·065	0·115	0·150	0·185	0·230	0·260	0·275
0·75	−0·055	−0·030	0	0·015	0·040	0·055	0·090	0·120	0·150	0·180	0·210	0·205
0·85	0	+0·015	+0·035	0·045	0·070	0·075	0·105	0·130	0·165	0·190	0·200	+0·185
0·95	+0·045	+0·060	+0·075	+0·075	+0·085	0·075	0·090	0·110	0·130	+0·155	+0·145	−0·025

TABLE 5—*continued*

$y/c = 0{\cdot}4$ $2y/b = 0{\cdot}271$

Upper surface C_p

x/c	α (deg)											
	0	2·1	4·1	6·2	8·2	10·3	12·3	14·4	16·4	18·5	20·6	22·6
0	+0·485	+0·410	+0·245	−0·005	−0·430	−0·950	−1·605	−2·410	−3·335	−4·450	−5·770	−6·140
0·01	+0·115	−0·130	−0·440	−0·775	−1·275	−1·780	−2·340	−2·965	−3·725	−4·610	−5·520	−5·600
0·03	−0·075	−0·270	−0·520	−0·770	−1·100	−1·435	−1·755	−2·075	−2·455	−2·780	−3·225	−3·035
0·08	−0·205	−0·335	−0·520	−0·680	−0·810	−0·965	−1·175	−1·355	−1·610	−1·860	−2·125	−2·760
0·15	−0·270	−0·375	−0·505	−0·620	−0·725	−0·850	−0·975	−1·105	−1·230	−1·390	−1·535	—
0·225	−0·270	−0·350	−0·445	−0·510	−0·585	−0·670	−0·755	−0·845	−0·930	−1·050	−1·075	—
0·35	−0·265	−0·320	−0·385	−0·430	−0·490	−0·540	−0·590	−0·635	−0·690	−0·755	−0·935	−1·125
0·50	−0·180	−0·185	−0·215	−0·255	−0·290	−0·315	−0·345	−0·370	−0·420	−0·500	−0·715	−0·860
0·65	−0·075	−0·100	−0·115	−0·140	−0·150	−0·165	−0·185	−0·200	−0·250	−0·330	−0·490	−0·630
0·75	−0·035	−0·045	−0·060	−0·065	−0·070	−0·075	−0·090	−0·115	−0·160	−0·210	−0·310	−0·440
0·85	+0·015	+0·010	0	+0·005	+0·005	−0·005	−0·015	−0·035	−0·065	−0·075	−0·155	−0·270
0·95	+0·060	+0·060	+0·060	+0·065	+0·060	+0·050	+0·035	+0·025	+0·020	+0·035	−0·035	−0·145

Lower surface C_p

x/c	α (deg)											
	0	2·1	4·1	6·2	8·2	10·3	12·3	14·4	16·4	18·5	20·6	22·6
0·01	+0·140	+0·315	+0·435	+0·495	0·495	0·430	0·310	0·140	−0·125	−0·435	−0·810	−0·860
0·03	−0·075	+0·110	0·260	0·375	0·470	0·510	0·535	0·525	+0·470	+0·380	+0·280	+0·310
0·08	−0·215	−0·075	+0·060	0·175	0·290	0·370	0·445	0·520	0·550	0·580	0·620	0·670
0·15	−0·265	−0·160	−0·060	+0·045	0·150	0·235	0·305	0·390	0·440	0·505	0·575	0·620
0·225	−0·280	−0·195	−0·105	−0·010	0·075	0·145	0·225	0·295	0·355	0·420	0·495	0·530
0·35	−0·265	−0·205	−0·140	−0·075	0·005	0·060	0·125	0·195	0·250	0·305	0·365	0·390
0·50	−0·190	−0·145	−0·085	−0·040	0·015	0·055	0·100	0·155	0·200	0·245	0·280	0·295
0·65	−0·070	−0·035	−0·020	+0·010	0·045	0·075	0·110	0·155	0·180	0·220	0·240	0·240
0·75	−0·025	−0·005	+0·010	0·030	0·055	0·075	0·105	0·140	0·165	0·195	0·205	0·195
0·85	+0·010	+0·025	0·035	0·045	0·065	0·075	0·095	0·125	0·145	0·170	0·155	0·135
0·95	+0·070	+0·070	+0·070	+0·080	0·085	0·085	0·090	0·115	+0·125	+0·145	+0·115	+0·065

TABLE 5—*continued*

$y/c = 0{\cdot}6$ $\qquad$ $2y/b = 0{\cdot}406$

Upper surface $\qquad$ C_p

x/c	α (deg)											
	0	2·1	4·1	6·2	8·2	10·3	12·3	14·4	16·4	18·5	20·6	22·6
0	+0·500	+0·430	+0·225	−0·085	−0·615	−1·230	−1·960	−2·835	−3·905	−5·170	−6·225	−2·610
0·01	+0·120	−0·140	−0·490	−0·860	−1·355	−1·870	−2·480	−3·200	−4·070	−5·080	−5·760	−2·020
0·03	−0·070	−0·285	−0·555	−0·830	−1·195	−1·575	−1·920	−2·200	−2·610	−3·120	−3·370	−2·175
0·08	−0·185	−0·340	−0·520	−0·690	—	—	−1·220	−1·430	−1·700	−1·970	−2·135	−2·090
0·15	−0·260	−0·375	−0·510	−0·630	−0·730	−0·855	−0·985	−1·120	−1·245	−1·345	−2·150	−1·655
0·225	−0·275	−0·360	−0·465	−0·530	−0·630	−0·720	−0·800	−0·890	−0·975	−1·085	−1·650	—
0·35	−0·255	−0·305	−0·355	−0·395	−0·440	−0·490	−0·540	−0·585	−0·630	−0·710	−1·085	−1·445
0·50	−0·150	−0·180	−0·210	−0·240	−0·260	−0·285	−0·300	−0·320	−0·380	−0·515	−0·735	−1·105
0·65	−0·060	−0·075	−0·100	−0·115	−0·120	−0·125	−0·140	−0·170	−0·245	−0·365	−0·490	−0·835
0·75	−0·025	−0·035	−0·050	−0·055	−0·055	−0·060	−0·075	−0·115	−0·195	−0·240	−0·355	−0·680
0·85	+0·015	+0·005	+0·005	+0·005	+0·010	+0·005	−0·020	−0·070	−0·115	—	−0·220	−0·505
0·95	+0·060	+0·060	+0·065	+0·065	+0·065	+0·045	+0·020	−0·015	−0·020	−0·065	−0·110	−0·350

Lower surface $\qquad$ C_p

x/c	α (deg)											
	0	2·1	4·1	6·2	8·2	10·3	12·3	14·4	16·4	18·5	20·6	22·6
0·01	+0·100	+0·295	+0·435	+0·495	0·495	0·405	0·270	0·070	−0·195	−0·560	−0·795	−0·360
0·03	−0·065	+0·125	0·280	0·395	0·490	0·520	0·525	0·505	+0·435	+0·320	+0·295	+0·395
0·08	−0·220	−0·075	+0·075	0·180	0·300	0·375	0·450	0·515	0·550	0·640	0·640	0·595
0·15	−0·265	−0·155	−0·045	+0·055	0·165	0·240	0·315	0·395	0·450	0·505	0·580	0·600
0·225	−0·265	−0·180	−0·090	−0·010	0·085	0·155	0·230	0·300	0·360	0·420	0·485	0·505
0·35	−0·245	−0·190	−0·125	−0·060	0·010	0·060	0·125	0·190	0·245	0·300	0·345	0·360
0·50	−0·170	−0·130	−0·080	−0·030	0·025	0·055	0·090	0·155	0·195	0·240	0·260	0·265
0·65	−0·055	−0·030	−0·015	+0·015	0·045	0·065	0·100	0·135	0·165	0·205	0·210	0·205
0·75	−0·015	+0·005	+0·020	0·035	0·060	0·070	0·095	0·125	0·155	0·185	0·175	0·155
0·85	+0·005	0·015	0·025	0·040	0·055	0·055	0·070	0·095	0·120	0·145	0·120	+0·075
0·95	+0·060	+0·065	+0·065	+0·070	0·070	0·060	0·060	0·075	+0·095	+0·115	+0·055	−0·045

TABLE 5—*continued*

$y/c = 0 \cdot 9$ $\qquad$ $2y/b = 0 \cdot 610$

Upper surface $\qquad C_p$

x/c	α (deg) 0	2·1	4·1	6·2	8·2	10·3	12·3	14·4	16·4	18·5	20·6	22·6
0	+0·490	+0·455	+0·260	+0·010	−0·455	−1·025	−1·640	−2·415	−3·490	−4·635	−1·755	−1·435
0·01	+0·100	−0·175	−0·545	−0·910	−1·460	−2·015	−2·645	−3·330	−4·110	−4·935	−1·380	−1·085
0·03	—	—	—	—	−1·230	−1·585	−1·835	−2·190	−2·710	−3·245	−1·410	−1·085
0·08	−0·195	−0·350	−0·535	−0·710	−0·905	−1·080	−1·280	−1·470	−1·745	−1·990	−1·385	−1·075
0·15	−0·245	−0·370	−0·500	−0·620	−0·720	−0·850	−0·975	−1·090	−1·205	−1·305	−1·320	−1·035
0·225	−0·260	−0·350	−0·445	−0·490	−0·595	−0·685	−0·760	−0·825	−0·885	−0·910	−1·280	−0·995
0·35	−0·240	−0·300	−0·335	−0·370	−0·420	−0·470	−0·505	−0·510	−0·525	−0·615	−1·210	−0·980
0·50	−0·115	−0·135	−0·180	−0·205	−0·230	−0·250	−0·265	−0·275	−0·370	−0·615	−1·010	−0·900
0·65	−0·055	−0·075	−0·090	−0·100	−0·100	−0·115	−0·135	−0·185	−0·375	−0·645	−0·780	−0·775
0·75	−0·005	−0·015	−0·025	−0·025	−0·025	−0·040	−0·075	−0·150	−0·295	−0·430	−0·645	−0·685
0·85	+0·020	+0·015	+0·015	+0·020	+0·025	+0·005	−0·040	−0·085	−0·115	—	−0·505	−0·615
0·95	+0·070	+0·070	+0·070	+0·075	+0·080	+0·060	+0·045	+0·005	+0·030	—	−0·350	−0·540

Lower surface $\qquad C_p$

x/c	α (deg) 0	2·1	4·1	6·2	8·2	10·3	12·3	14·4	16·4	18·5	20·6	22·6
0·01	+0·090	+0·295	+0·430	+0·495	+0·495	0·400	0·260	0·055	−0·220	−0·600	−0·025	+0·035
0·03	−0·090	+0·100	0·260	0·375	0·480	0·510	0·520	0·510	+0·445	+0·340	+0·510	0·530
0·08	−0·210	−0·060	+0·075	0·185	0·300	0·370	0·440	0·505	0·530	0·550	0·600	0·615
0·15	−0·260	−0·155	−0·045	+0·050	0·160	0·230	0·300	0·375	0·430	0·485	0·510	0·535
0·225	−0·260	−0·180	−0·095	−0·020	+0·075	0·140	0·210	0·280	0·335	0·395	0·415	0·430
0·35	−0·240	−0·180	−0·125	−0·070	−0·005	0·045	0·100	0·165	0·215	0·265	0·275	0·290
0·50	−0·125	−0·115	−0·075	−0·040	−0·005	0·020	0·065	0·105	0·150	0·185	0·175	0·180
0·65	−0·060	−0·045	−0·030	−0·010	+0·020	0·035	0·055	0·085	0·115	0·150	0·120	0·100
0·75	−0·010	−0·005	+0·005	+0·015	0·045	0·045	0·065	0·075	0·105	0·130	0·070	+0·035
0·85	+0·040	+0·040	0·045	0·055	0·075	0·070	0·085	0·085	0·110	+0·130	+0·025	−0·040
0·95	+0·075	+0·070	+0·070	+0·075	+0·085	0·075	0·085	0·055	+0·080	−0·035	−0·110	−0·240

TABLE 5—*continued*

$y/c = 1\cdot228$ $\qquad$ $2y/b = 0\cdot831$

Upper surface $\qquad$ C_p

x/c	α (deg)						
	0	4·1	8·2	12·3	16·4	20·6	22·6
0	+0·460	+0·375	−0·155	−1·130	−3·595	−5·720	−2·485
0·01	−0·065	−0·650	−1·435	−2·420	−3·285	−4·445	−4·120
0·03	−0·105	−0·515	−1·015	−1·610	−2·175	−2·645	−1·800
0·08	−0·195	−0·475	−0·765	−1·135	−1·340	−1·330	−1·355
0·15	−0·245	−0·425	−0·625	−0·860	−1·065	−0·845	−1·055
0·225	−0·230	−0·370	−0·520	−0·665	−0·740	−0·735	−1·035
0·35	−0·215	−0·295	−0·385	−0·450	−0·420	−0·740	−0·945
0·50	−0·090	−0·125	−0·175	−0·220	−0·335	−0·955	−1·145
0·65	−0·020	−0·040	−0·070	−0·095	−0·315	−1·430	−1·065
0·75	−0·020	−0·030	−0·040	−0·045	−0·275	−1·260	−0·910
0·85	+0·070	+0·065	+0·060	+0·010	−0·160	−0·370	−0·465
0·95	+0·095	+0·100	+0·090	+0·035	−0·170	+0·045	−0·250

Lower surface $\qquad$ C_p

x/c	α (deg)						
	0	4·1	8·2	12·3	16·4	20·6	22·6
0·01	−0·025	+0·330	+0·440	+0·320	−0·010	−0·515	−0·675
0·03	−0·175	+0·135	0·315	0·380	+0·310	+0·025	+0·165
0·08	−0·250	−0·025	0·145	0·260	0·335	0·360	0·385
0·15	−0·230	−0·070	0·065	0·165	0·260	0·325	0·355
0·225	−0·225	−0·110	+0·005	0·105	0·155	0·245	0·295
0·35	−0·210	−0·135	−0·060	+0·015	0·080	0·160	0·200
0·50	−0·135	−0·005	−0·055	−0·015	0·010	0·070	0·095
0·65	−0·040	−0·020	0	+0·025	0·075	0·130	0·130
0·75	0	+0·010	+0·020	0·025	0·045	0·105	0·095
0·85	+0·055	0·065	0·065	+0·065	+0·045	+0·110	+0·060
0·95	+0·055	+0·050	+0·035	−0·005	−0·040	—	−0·100

TABLE 5—*continued*

$y/c = 1 \cdot 352$ $\quad\quad$ $2y/b = 0 \cdot 915$

Upper surface $\quad$ C_p

$x/c(y)$	α (deg)											
	0	2·1	4·1	6·2	8·2	10·3	12·3	14·4	16·4	18·5	20·6	22·6
0	+0·035	−0·025	−0·120	−0·265	−0·510	−0·820	−1·170	−1·525	−1·975	−2·470	−1·330	−1·235
0·025	−0·065	−0·215	−0·405	−0·620	−0·905	−1·240	−1·600	−1·980	−2·415	−2·715	−0·915	−0·780
0·05	−0·115	−0·250	−0·415	−0·595	−0·825	−1·095	−1·355	−1·630	−1·935	−2·045	−0·805	−0·720
0·10	−0·175	−0·280	−0·395	−0·535	−0·700	−0·885	−1·045	−1·230	−1·410	−1·435	−0·740	−0·670
0·15	−0·195	−0·275	−0·390	−0·500	−0·635	−0·785	−0·905	−1·030	−1·145	−1·240	−0·690	−0·610
0·25	−0·180	−0·245	−0·325	−0·410	−0·495	−0·600	−0·685	−0·755	−0·890	−1·530	−0·585	−0·515
0·35	−0·155	−0·210	−0·265	−0·320	−0·380	−0·460	−0·520	−0·650	−1·255	−1·240	−0·485	−0·450
0·50	−0·100	−0·135	−0·170	−0·200	−0·240	−0·305	−0·375	−0·420	−0·305	−0·915	−0·415	−0·395
0·70	+0·005	−0·015	−0·040	−0·055	−0·075	−0·135	−0·200	−0·250	−0·345	−0·490	−0·385	−0·385

Lower surface $\quad$ C_p

$x/c(y)$	α (deg)											
	0	2·1	4·1	6·2	8·2	10·3	12·3	14·4	16·4	18·5	20·6	22·6
0·025	−0·080	+0·030	+0·080	+0·080	+0·050	−0·080	−0·205	−0·380	−0·595	−0·830	−0·480	−0·440
0·05	−0·110	−0·010	+0·050	0·085	0·075	+0·015	−0·045	−0·145	−0·250	−0·385	−0·180	−0·230
0·10	−0·175	−0·095	−0·030	+0·015	0·040	0·020	+0·005	−0·025	−0·075	−0·130	−0·010	+0·005
0·15	−0·185	−0·120	−0·060	−0·015	+0·025	+0·020	0·025	+0·020	−0·005	−0·035	+0·055	0·070
0·25	−0·145	−0·110	−0·070	−0·035	−0·005	−0·005	0·015	0·020	+0·020	+0·030	0·070	0·085
0·35	−0·175	−0·135	−0·100	−0·065	−0·030	−0·020	0	0·010	0·025	0·050	0·080	0·090
0·50	−0·085	−0·060	−0·035	−0·015	0	+0·010	0·025	0·040	0·065	0·090	0·090	0·100
0·70	0	+0·020	+0·030	+0·040	+0·055	+0·045	+0·055	+0·055	+0·075	+0·100	+0·065	+0·070

TABLE 6

Coefficients of Local Normal Force, Tangential Force, Lift, Drag and Aerodynamic Centre Position

Wing of aspect ratio 3

C_N

α (deg)	2y/b = 0	0·068	0·135	0·271	0·406	0·610	0·831	0·915
2·1	0·111	0·111	0·113	0·111	0·111	0·107	—	0·082
4·1	0·223	0·221	0·224	0·224	0·226	0·212	0·166	0·165
6·2	0·333	0·332	0·337	0·331	0·329	0·311	—	0·241
8·2	0·440	0·438	0·441	0·438	0·435	0·416	0·326	0·322
10·3	0·545	0·542	0·547	0·544	0·539	0·515	—	0·406
12·3	0·655	0·647	0·658	0·653	0·639	0·619	0·476	0·492
14·4	0·764	0·747	0·769	0·764	0·762	0·718	—	0·575
16·4	0·873	0·851	0·873	0·884	0·891	0·861	0·717	0·724
18·5	0·978	0·962	0·990	1·020	1·047	1·077	—	0·925
20·6	1·097	1·097	1·141	1·214	1·275	1·178	—	0·483
22·6	1·238	1·222	1·292	1·406	1·418	1·041	—	0·458

C_T

α (deg)	2y/b = 0	0·068	0·135	0·271	0·406	0·610	0·831	0·915
0	+0·044	+0·013	+0·007	+0·001	0	−0·002	−0·011	−0·013
2·1	0·043	0·012	+0·005	−0·001	−0·002	−0·004	—	−0·015
4·1	0·042	0·008	0	−0·009	−0·010	−0·013	−0·019	−0·021
6·2	0·039	+0·001	−0·010	−0·019	−0·022	−0·024	—	−0·031
8·2	0·036	−0·008	−0·023	−0·035	−0·041	−0·042	−0·041	−0·046
10·3	0·031	−0·019	−0·038	−0·054	−0·062	−0·063	—	−0·062
12·3	0·025	−0·034	−0·059	−0·077	−0·088	−0·089	−0·076	−0·081
14·4	0·018	−0·050	−0·083	−0·108	−0·119	−0·111	—	−0·102
16·4	0·011	−0·068	−0·109	−0·144	−0·156	−0·138	−0·125	−0·124
18·5	+0·003	−0·088	−0·137	−0·183	−0·196	−0·145	—	−0·149
20·6	−0·002	−0·110	−0·167	−0·216	−0·224	−0·047	—	−0·090
22·6	−0·005	−0·123	−0·188	−0·204	−0·087	−0·008	—	−0·052

TABLE 6—*continued*

C_L

α (deg)	2y/b: 0	0·068	0·135	0·271	0·406	0·610	0·831	0·915
2·1	0·109	0·111	0·113	0·111	0·111	0·107	—	0·082
4·1	0·218	0·220	0·223	0·224	0·226	0·212	0·167	0·166
6·2	0·327	0·330	0·336	0·331	0·330	0·312	—	0·243
8·2	0·430	0·435	0·440	0·439	0·436	0·418	0·328	0·325
10·3	0·531	0·537	0·545	0·545	0·542	0·518	—	0·411
12·3	0·636	0·640	0·656	0·655	0·643	0·624	0·481	0·498
14·4	0·736	0·737	0·766	0·767	0·768	0·723	—	0·582
16·4	0·835	0·837	0·868	0·889	0·899	0·865	0·723	0·730
18·5	0·927	0·941	0·982	1·026	1·055	1·067	—	0·924
20·6	1·028	1·065	1·128	1·212	1·272	1·119	—	0·484
22·6	1·144	1·175	1·265	1·376	1·342	0·964	—	0·444

C_D

α (deg)	2y/b: 0	0·068	0·135	0·271	0·406	0·610	0·831	0·915
0	0·044	0·013	0·007	0·001	0	−0·002	−0·011	−0·013
2·1	0·047	0·016	0·009	0·003	0·002	0	—	−0·012
4·1	0·057	0·024	0·016	0·007	0·006	+0·002	−0·007	−0·009
6·2	0·074	0·037	0·027	0·017	0·014	0·010	—	−0·005
8·2	0·098	0·054	0·041	0·028	0·022	0·018	+0·006	+0·001
10·3	0·127	0·078	0·061	0·044	0·035	0·030	—	0·011
12·3	0·163	0·105	0·083	0·062	0·050	0·045	0·027	0·025
14·4	0·207	0·138	0·111	0·085	0·074	0·071	—	0·045
16·4	0·257	0·175	0·143	0·112	0·102	0·111	+0·082	0·086
18·5	0·313	0·222	0·184	0·149	0·147	0·205	—	0·152
20·6	0·384	0·283	0·245	0·225	0·240	0·371	—	0·086
22·6	0·471	0·356	0·324	0·352	0·464	+0·393	—	+0·128

TABLE 6—*continued*

$$\frac{h}{c(y)}$$

α (deg)	2y/b 0	0·068	0·135	0·271	0·406	0·610	0·831	0·915
0	0·360	0·310	0·285	0·254	0·238	0·227	0·200	0·279
2·1	0·360	0·311	0·285	0·255	0·239	—	—	0·279
4·1	0·359	0·310	0·285	0·254	0·239	0·227	0·205	0·280
6·2	0·360	0·311	0·286	0·255	0·238	0·226	—	0·281
8·2	0·360	0·311	0·288	0·256	0·240	0·227	0·210	0·278
10·3	0·361	0·313	0·290	0·258	0·240	0·231	—	0·288
12·3	0·362	0·316	0·291	0·261	0·244	0·233	0·217	0·301
14·4	0·362	0·318	0·292	0·268	0·251	0·244	—	0·307
16·4	0·363	0·319	0·298	0·276	0·272	0·270	0·270	0·315
18·5	0·365	0·319	0·300	0·284	0·284	0·320	—	0·353
20·6	0·371	0·326	0·306	0·295	0·294	0·371	—	0·400
22·6	0·383	0·339	0·324	0·319	0·360	0·383	—	0·412

TABLE 7

Coefficients of Total Lift, Drag and Pitching Moment from Pressure Measurements

Wing of aspect ratio 3

α (deg)	$\bar{C}_L$	$\bar{C}_D$	$\bar{C}_m$
2·1	0·105	—	0·005
4·1	0·208	0·0061	0·011
6·2	0·308	0·0137	0·017
8·2	0·409	0·0242	0·021
10·3	0·507	0·0381	0·024
12·3	0·608	0·0553	0·025
14·4	0·711	0·0782	0·019
16·4	0·839	0·113	−0·005
18·5	1·006	0·168	—
20·6	1·035	0·260	—
22·6	1·044	0·332	—

TABLE 8

Coefficients of Total Lift, Drag and Pitching Moment from Balance Measurements

Wing of aspect ratio 3

(*a*) Pressure-plotting wing: $R = 1 \cdot 71 \times 10^6$

α (deg)	$\bar{C}_L$
$-0 \cdot 5$	$-0 \cdot 020$
$+1 \cdot 5$	$+0 \cdot 072$
3·6	0·178
5·7	0·279
7·7	0·378
9·8	0·470
11·8	0·576
13·9	0·677
15·9	0·806
18·0	0·963
20·1	1·059
+22·1	+1·134

(*b*) Solid wing: various Reynolds numbers

α (deg)	$R = 1 \cdot 05 \times 10^6$			$R = 1 \cdot 71 \times 10^6$			$R = 2 \cdot 95 \times 10^6$		
	$\bar{C}_L$	$\bar{C}_D$	$\bar{C}_m$	$\bar{C}_L$	$\bar{C}_D$	$\bar{C}_m$	$\bar{C}_L$	$\bar{C}_D$	$\bar{C}_m$
0	0·004	0·0066	0	0·002	0·0068	0	0·002	0·0068	0
2·1	0·101	0·0090	+0·0042	0·097	0·0086	+0·0041	0·106	0·0084	+0·0042
4·1	0·200	0·0137	0·0079	0·195	0·0125	0·0083	0·208	0·0126	0·0084
6·2	0·298	0·0210	0·0132	0·290	0·0191	0·0131	0·308	0·0194	0·0126
8·2	0·394	0·0309	0·0191	0·388	0·0282	0·0193	0·404	0·0285	0·0167
10·3	0·485	0·0434	0·0231	0·485	0·0404	0·0239	0·503	0·0409	0·0198
12·3	0·579	0·0601	0·0242	0·585	0·0562	0·0241	0·601	0·0560	0·0218
14·4	0·684	0·0845	+0·0123	0·687	0·0777	+0·0144	0·708	0·0767	0·0186
16·4	0·835	0·1274	−0·0163	0·814	0·1105	−0·0115	0·834	0·1083	+0·0017
18·5	0·982	0·1801	−0·0511	0·976	0·1614	−0·0520	0·968	0·1502	−0·0255
20·6	0·976	0·2833	+0·0147	1·067	0·1977	−0·0384	1·078	0·1939	−0·0346
22·6	0·986	0·3543	0·0272	0·990	0·2931	−0·0045	1·064	0·2841	+0·0111
24·5	0·996	0·4186	0·0249	0·988	0·4088	+0·0319			
26·5	0·953	0·4604	+0·0103	0·961	0·4538	+0·0250			
28·5	0·832	0·4533	−0·0184	0·864	0·4556	−0·0024			
30·5				0·818	0·4675	−0·0191			

TABLE 9

Pressure Coefficients on Wing Spanning the Tunnel

$y = 0$

Upper surface C_p

x/c	α (deg)				
	0	2	4	6	8
0	+1·000	+1·000	+0·970	+0·915	+0·800
0·01	0·470	0·325	+0·170	−0·005	−0·230
0·03	0·205	+0·075	−0·065	−0·215	−0·400
0·08	+0·025	−0·085	−0·195	−0·305	−0·455
0·15	−0·100	−0·200	−0·295	−0·395	−0·540
0·225	−0·170	−0·255	−0·350	−0·435	−0·565
0·35	−0·240	−0·315	−0·395	−0·465	−0·570
0·50	−0·225	−0·280	−0·345	−0·400	−0·490
0·65	−0·160	−0·205	−0·245	−0·285	−0·375
0·75	−0·110	−0·145	−0·180	−0·215	−0·285
0·85	−0·070	−0·095	−0·125	−0·150	−0·215
0·95	−0·015	−0·030	−0·040	−0·055	−0·115

Lower surface C_p

x/c	α (deg)				
	0	2	4	6	8
0·01	+0·480	+0·615	+0·725	+0·810	+0·845
0·03	+0·200	0·325	0·445	0·555	0·610
0·08	−0·015	+0·105	0·210	0·310	0·360
0·15	−0·115	−0·010	+0·090	0·185	0·310
0·225	−0·185	−0·090	0	+0·090	0·135
0·35	−0·250	−0·170	−0·090	−0·015	+0·020
0·50	−0·235	−0·165	−0·100	−0·030	−0·005
0·65	−0·170	−0·115	−0·060	−0·010	0
0·75	−0·120	−0·075	−0·035	+0·010	+0·010
0·85	−0·065	−0·035	−0·005	0·030	0·025
0·95	−0·035	−0·005	+0·025	+0·045	+0·025

TABLE 9—*continued*

$y/c = 0 \cdot 1$

Upper surface C_p

x/c	α (deg)				
	0	2	4	6	8
0	+0·535	+0·515	+0·410	+0·230	−0·025
0·01	+0·190	−0·025	−0·260	−0·560	−0·875
0·03	−0·010	−0·200	−0·395	−0·635	−0·855
0·08	−0·110	−0·255	−0·395	−0·550	−0·705
0·15	−0·190	−0·305	−0·415	−0·540	−0·640
0·225	−0·240	−0·335	−0·430	−0·525	−0·605
0·35	−0·250	−0·330	−0·400	−0·465	−0·540
0·50	−0·185	−0·240	−0·290	−0·340	−0·385
0·65	−0·120	−0·160	−0·195	−0·235	−0·265
0·75	−0·075	−0·110	−0·135	−0·160	−0·190
0·85	−0·015	−0·035	−0·050	−0·070	−0·080
0·95	+0·055	+0·050	+0·045	+0·040	+0·035

Lower surface C_p

x/c	α (deg)				
	0	2	4	6	8
0·01	+0·190	+0·360	+0·470	+0·535	0·550
0·03	+0·010	0·180	0·310	0·420	0·500
0·08	−0·120	+0·015	+0·135	0·245	0·335
0·15	−0·215	−0·100	0	0·105	0·200
0·225	−0·235	−0·140	−0·050	+0·045	0·125
0·35	−0·255	−0·180	−0·105	−0·030	0·045
0·50	−0·205	−0·145	−0·085	−0·025	0·035
0·65	−0·115	−0·090	−0·045	+0·005	0·050
0·75	−0·055	−0·015	—	0·045	0·085
0·85	−0·020	+0·010	+0·035	0·055	0·085
0·95	+0·050	+0·060	+0·065	+0·075	0·095

TABLE 9—*continued*

$y/c = 0{\cdot}2$

Upper surface C_p

x/c	α (deg)				
	0	2	4	6	8
0	+0·490	+0·430	+0·255	−0·055	−0·480
0·01	+0·180	−0·080	−0·390	−0·765	−1·195
0·03	−0·040	−0·265	−0·515	−0·785	−1·095
0·08	−0·160	−0·320	−0·485	−0·660	−0·855
0·15	−0·230	−0·360	−0·490	−0·615	−0·690
0·225	−0·255	−0·365	−0·470	−0·570	−0·655
0·35	−0·250	−0·335	−0·415	−0·455	−0·550
0·50	−0·190	−0·245	−0·290	−0·335	−0·380
0·65	−0·080	−0·125	−0·160	−0·190	−0·220
0·75	−0·035	−0·070	−0·090	−0·110	−0·130
0·85	+0·015	−0·005	−0·015	−0·025	−0·050
0·95	+0·070	+0·065	+0·060	+0·060	+0·050

Lower surface C_p

x/c	α (deg)				
	0	2	4	6	8
0·01	+0·180	+0·360	+0·475	+0·520	0·520
0·03	−0·020	+0·170	0·315	0·430	0·510
0·08	−0·180	−0·035	+0·100	0·220	0·310
0·15	−0·240	−0·130	−0·020	0·095	0·185
0·225	−0·260	−0·170	−0·075	+0·025	0·110
0·35	−0·255	−0·190	−0·110	−0·035	0·035
0·50	−0·195	−0·135	−0·075	−0·015	0·025
0·65	−0·075	−0·050	−0·015	+0·030	0·070
0·75	−0·040	−0·015	+0·010	0·040	0·070
0·85	+0·015	+0·030	0·045	0·065	0·075
0·95	+0·070	+0·070	+0·075	+0·080	0·075

TABLE 9—*continued*

$y/c = 0 \cdot 4$

Upper surface C_p

x/c	α (deg)				
	0	2	4	6	8
0	+0·480	+0·370	+0·115	−0·335	−0·915
0·01	+0·125	−0·185	−0·550	−1·045	−1·565
0·03	−0·070	−0·315	−0·600	−0·935	−1·275
0·08	−0·200	−0·380	−0·570	−0·785	−0·975
0·15	−0·260	−0·405	−0·545	−0·700	−0·815
0·225	−0·265	−0·375	−0·480	−0·550	−0·670
0·35	−0·260	−0·340	−0·410	−0·485	−0·550
0·50	−0·165	−0·200	−0·240	−0·290	−0·325
0·65	−0·070	−0·105	−0·130	−0·155	−0·170
0·75	−0·030	−0·050	−0·065	−0·085	−0·090
0·85	−0·005	−0·005	−0·010	−0·015	−0·015
0·95	+0·065	+0·065	+0·060	+0·055	+0·050

Lower surface C_p

x/c	α (deg)				
	0	2	4	6	8
0·01	+0·095	+0·315	+0·440	+0·490	0·460
0·03	−0·070	+0·145	0·305	0·425	0·500
0·08	−0·205	−0·045	+0·105	0·230	0·335
0·15	−0·265	−0·140	−0·020	0·100	0·200
0·225	−0·275	−0·175	−0·070	+0·030	0·120
0·35	−0·260	−0·185	−0·110	−0·035	0·045
0·50	−0·165	−0·125	−0·065	−0·010	0·050
0·65	−0·070	−0·035	−0·005	+0·030	0·070
0·75	−0·025	0	+0·025	0·050	0·075
0·85	+0·010	+0·025	0·035	0·050	0·070
0·95	+0·060	+0·060	+0·060	+0·065	0·070

TABLE 9—*continued*

$y/c = 0{\cdot}6$

Upper surface C_p

x/c	α (deg) 0	2	4	6	8
0	+0·510	+0·400	+0·120	−0·365	−0·975
0·01	+0·120	−0·215	−0·635	−1·115	−1·790
0·03	−0·075	−0·355	−0·680	−1·045	−1·440
0·08	−0·200	−0·400	−0·615	−0·845	−1·015
0·15	−0·265	−0·415	−0·570	−0·710	−0·830
0·225	−0·285	−0·405	−0·520	−0·610	−0·720
0·35	−0·260	−0·345	−0·380	−0·435	−0·505
0·50	−0·165	−0·190	−0·245	−0·285	−0·315
0·65	−0·065	−0·095	−0·125	−0·145	−0·165
0·75	−0·035	−0·055	−0·070	−0·085	−0·090
0·85	+0·015	+0·005	−0·005	−0·010	−0·015
0·95	+0·060	+0·065	+0·060	+0·050	+0·035

Lower surface C_p

x/c	α (deg) 0	2	4	6	8
0·01	+0·080	+0·325	+0·460	+0·495	0·450
0·03	−0·075	+0·160	0·325	0·445	0·510
0·08	−0·240	−0·055	+0·100	0·235	0·335
0·15	−0·275	−0·140	−0·015	0·105	0·200
0·225	−0·280	−0·170	−0·065	+0·035	0·125
0·35	−0·255	−0·185	−0·105	−0·030	0·045
0·50	−0·160	−0·130	−0·070	−0·010	0·045
0·65	−0·075	−0·035	−0·015	+0·015	0·050
0·75	−0·015	+0·010	+0·030	0·050	0·070
0·85	+0·020	+0·035	+0·045	+0·055	0·070
0·95	+0·050	—	—	—	—

TABLE 9—*continued*

$y/c = 0 \cdot 90$

Upper surface C_p

x/c	α (deg)				
	0	2	4	6	8
0	+0·425	+0·375	+0·050	−0·235	−0·740
0·01	+0·085	−0·310	−0·820	−1·385	−2·020
0·03	−0·050	−0·340	−0·700	−1·085	−1·490
0·08	−0·195	−0·405	−0·630	−0·865	−1·070
0·15	−0·255	−0·410	−0·570	−0·690	−0·855
0·225	−0·270	−0·395	−0·515	−0·605	−0·720
0·35	−0·245	−0·330	−0·375	−0·450	−0·515
0·50	−0·125	−0·165	−0·215	−0·250	−0·290
0·65	−0·065	−0·095	−0·120	−0·135	−0·145
0·75	−0·010	−0·025	−0·040	−0·050	−0·075
0·85	+0·020	+0·015	+0·010	−0·005	−0·025
0·95	+0·080	+0·075	+0·075	+0·055	+0·025

Lower surface C_p

x/c	α (deg)				
	0	2	4	6	8
0·01	+0·070	+0·330	+0·475	+0·505	0·435
0·03	−0·095	+0·150	0·325	0·450	0·510
0·08	−0·220	−0·020	0·140	0·270	0·370
0·15	−0·275	−0·130	+0·005	0·130	0·215
0·225	−0·285	−0·170	−0·055	+0·045	0·125
0·35	−0·265	−0·190	−0·105	−0·030	0·035
0·50	−0·150	−0·115	−0·035	+0·010	0·050
0·65	−0·075	−0·040	−0·005	0·025	0·050
0·75	−0·020	+0·005	+0·025	0·045	0·060
0·85	+0·015	0·030	0·045	0·055	0·060
0·95	+0·060	+0·065	+0·065	+0·065	0·050

TABLE 9—*continued*

$y/c = 1 \cdot 25$

Upper surface C_p

x/c	α (deg)				
	0	2	4	6	8
0	+0·485	+0·515	+0·350	−0·035	−0·590
0·01	+0·170	−0·205	−0·665	−1·255	−1·905
0·03	−0·060	−0·385	−0·755	−1·180	−1·595
0·08	−0·200	−0·425	−0·670	−0·935	−1·090
0·15	−0·245	−0·415	−0·585	−0·715	−0·840
0·225	−0·270	−0·405	−0·525	−0·635	−0·705
0·35	−0·255	−0·350	−0·405	−0·485	−0·540
0·50	−0·165	−0·170	−0·235	−0·285	−0·300
0·65	−0·060	−0·090	−0·120	−0·150	−0·140
0·75	−0·025	−0·050	−0·065	−0·085	−0·065
0·85	+0·010	0	−0·005	−0·015	−0·015
0·95	+0·060	+0·065	+0·060	+0·035	+0·020

Lower surface C_p

x/c	α (deg)				
	0	2	4	6	8
0·01	+0·070	+0·335	+0·485	+0·505	0·475
0·03	−0·070	+0·180	0·360	0·465	0·545
0·08	−0·220	−0·020	0·140	0·265	0·400
0·15	−0·275	−0·130	+0·005	0·120	0·240
0·225	−0·285	−0·170	−0·060	+0·030	0·135
0·35	−0·265	−0·185	−0·105	−0·035	0·045
0·50	−0·140	—	−0·040	+0·005	0·060
0·65	−0·065	−0·025	−0·005	0·015	0·060
0·75	−0·020	0	+0·020	0·030	0·060
0·85	+0·025	+0·040	0·045	0·045	0·060
0·95	+0·070	+0·070	+0·065	+0·045	0·045

TABLE 9—*continued*

$y/c = 1 \cdot 6$

Upper surface C_p

x/c	α (deg)				
	0	2	4	6	8
0	+0·505	+0·405	+0·075	−0·495	−1·245
0·01	+0·150	−0·235	−0·740	−1·365	−2·070
0·03	−0·070	−0·405	−0·785	−1·210	−1·660
0·08	−0·220	−0·455	−0·710	−0·970	−1·185
0·15	−0·265	−0·435	−0·605	−0·770	−0·935
0·225	−0·275	−0·410	−0·535	−0·640	−0·740
0·35	−0·255	−0·350	−0·410	−0·495	−0·540
0·50	−0·160	−0·210	−0·255	−0·285	−0·295
0·65	−0·085	−0·120	−0·145	−0·150	−0·135
0·75	−0·020	−0·045	−0·060	−0·070	−0·065
0·85	+0·020	+0·005	0	0	−0·020
0·95	+0·080	+0·080	+0·075	+0·050	0

Lower surface C_p

x/c	α (deg)				
	0	2	4	6	8
0·01	+0·090	+0·355	+0·495	+0·515	0·450
0·03	−0·085	+0·180	0·365	0·485	0·540
0·08	−0·220	−0·025	0·150	0·280	0·390
0·15	−0·265	−0·110	+0·030	0·155	0·250
0·225	−0·280	−0·160	−0·050	0·060	0·140
0·35	−0·260	−0·170	−0·090	0·000	0·060
0·50	−0·160	−0·105	−0·040	+0·010	0·060
0·65	−0·060	−0·025	+0·005	0·030	0·070
0·75	−0·020	+0·005	0·030	0·045	0·070
0·85	+0·020	0·035	0·050	0·050	0·060
0·95	+0·065	+0·070	+0·070	+0·050	0·035

TABLE 10

Coefficients of Local Normal Force, Tangential Force, Lift, Drag and Aerodynamic Centre Position

Wing Spanning the Tunnel

C_N

(uncorrected for tunnel-wall interference)

α (deg)	y/c							
	0	0·1	0·2	0·4	0·6	0·9	1·25	1·6
2	0·134	0·134	0·138	0·141	0·149	0·153	0·162	0·168
4	0·264	0·260	0·267	0·273	0·285	0·295	0·307	0·319
6	0·390	0·391	0·396	0·402	0·417	0·428	0·441	0·453
8	0·510	0·510	0·511	0·520	0·534	0·549	0·553	0·574

C_T

(uncorrected for tunnel-wall interference)

α (deg)	y/c							
	0	0·1	0·2	0·4	0·6	0·9	1·25	1·6
0	0·043	+0·015	+0·006	0	−0·001	0	0	−0·001
2	0·042	0·013	+0·004	−0·003	−0·004	−0·004	−0·005	−0·006
4	0·040	+0·008	−0·004	−0·013	−0·015	−0·017	−0·017	−0·019
6	0·037	−0·001	−0·016	−0·029	−0·031	−0·035	−0·036	−0·039
8	0·033	−0·013	−0·031	−0·048	−0·053	−0·056	−0·056	−0·067

C_L

(corrected for tunnel-wall interference)

α (deg)	y/c							
	0	0·1	0·2	0·4	0·6	0·9	1·25	1·6
2	0·130	0·130	0·135	0·138	0·147	0·149	0·156	0·158
4	0·256	0·254	0·261	0·267	0·279	0·287	0·294	0·298
6	0·377	0·382	0·388	0·394	0·408	0·417	0·423	0·424
8	0·491	0·497	0·500	0·510	0·523	0·536	0·530	0·536

TABLE 10—*continued*

C_D

(corrected for tunnel-wall interference)

α (deg)	y/c							
	0	0·1	0·2	0·4	0·6	0·9	1·25	1·6
0	0·043	0·015	0·006	0	−0·001	0	0	−0·001
2	0·047	0·018	0·009	0·002	+0·001	0·002	0·001	0
4	0·059	0·027	0·016	0·007	0·005	0·004	0·005	+0·004
6	0·078	0·041	0·027	0·015	0·014	0·011	0·012	0·011
8	0·105	0·059	0·042	0·027	+0·023	0·022	0·024	+0·017

h/c

(uncorrected for tunnel-wall interference)

α (deg)	y/c							
	0	0·1	0·2	0·4	0·6	0·9	1·25	1·6
0	0·366	0·316	0·293	0·269	0·258	0·254	—	—
2	0·366	0·315	0·293	0·268	0·257	0·252	0·254	0·260
4	0·367	0·316	0·292	0·266	0·255	0·249	0·247	0·252
6	0·367	0·316	0·292	0·264	0·252	0·246	0·242	0·243
8	0·367	0·317	0·291	0·263	0·252	0·246	0·237	0·236

TABLE 11

Corrections for Tunnel-Wall Interference

Wing Spanning the Tunnel

y/c	$\dfrac{\Delta C_L}{C_{L\infty}}$	$\dfrac{\Delta C_D}{C_{L\infty}^2}$
0	−0·014	0·005
0·1	−0·015	0·004
0·2	−0·015	0·004
0·4	−0·017	0·003
0·6	−0·020	0·003
0·9	−0·025	0·005
1·25	−0·040	0·008
1·6	−0·064	0·013

$C_{L\infty}$ is the C_L-value far away from the centre.

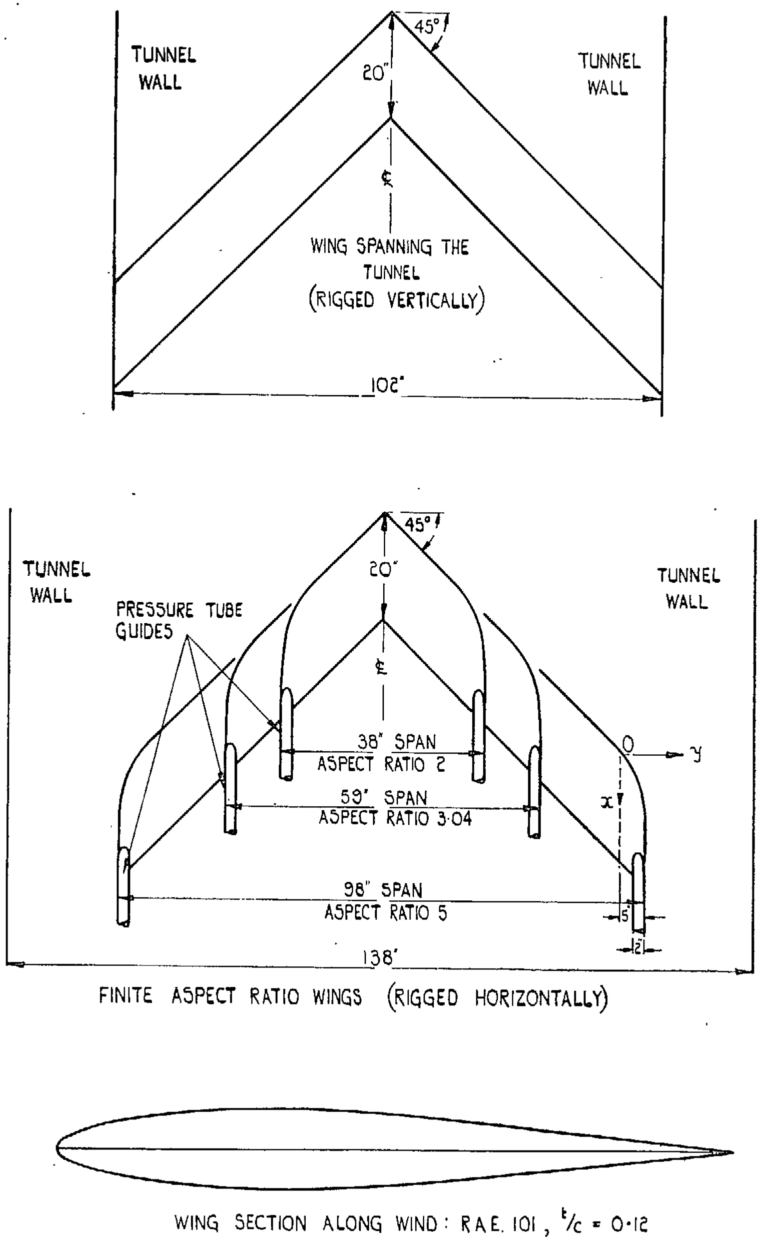

FIG. 1. View of models and dimensions.

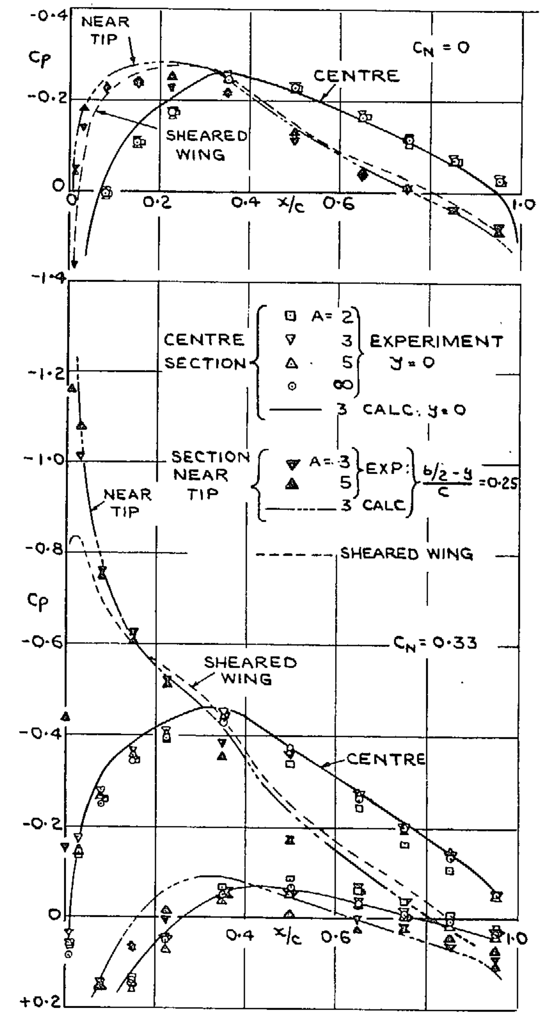

FIG. 2. Pressure distributions at $C_N = 0$ and $C_N = 0{\cdot}33$.

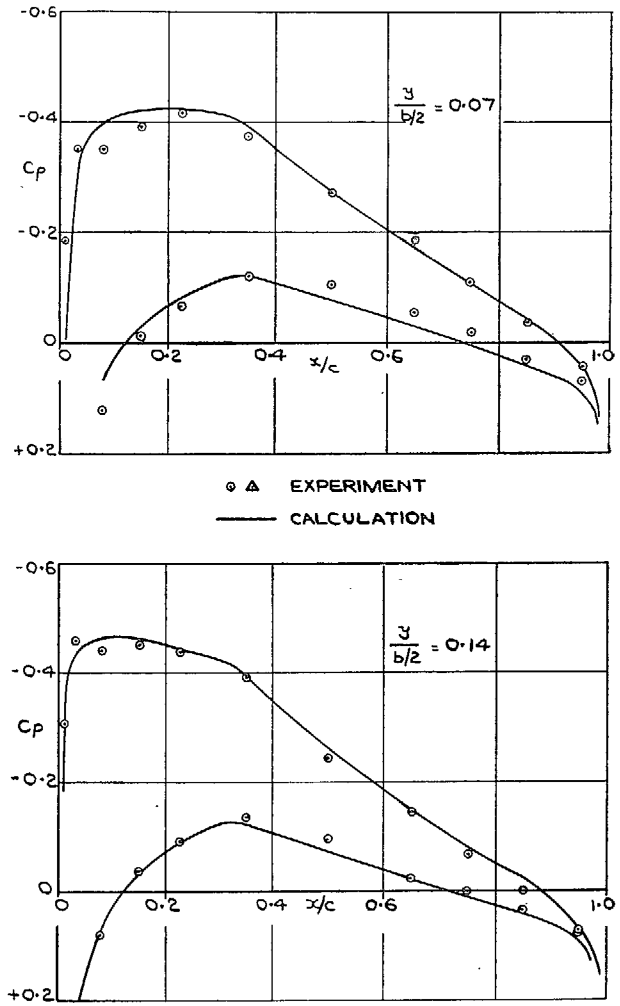

FIG. 3. Pressure distributions at two spanwise stations.

$A = 3. \quad \alpha = 4{\cdot}1$ deg. $\quad \bar{C}_L = 0{\cdot}21.$

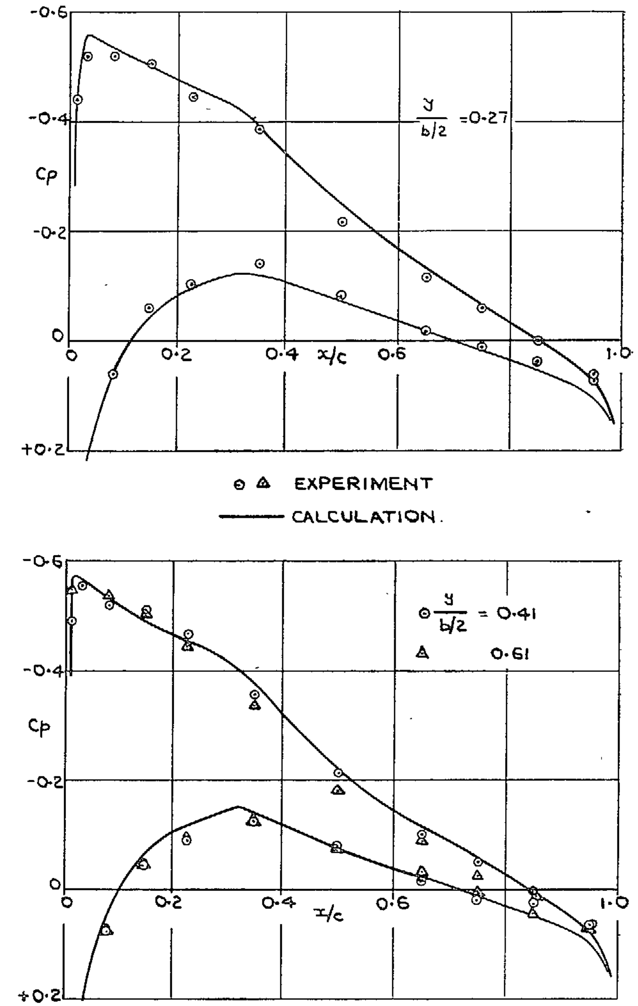

FIG. 4. Pressure distributions at three spanwise stations.

$A = 3. \quad \alpha = 4{\cdot}1$ deg. $\quad \bar{C}_L = 0{\cdot}21.$

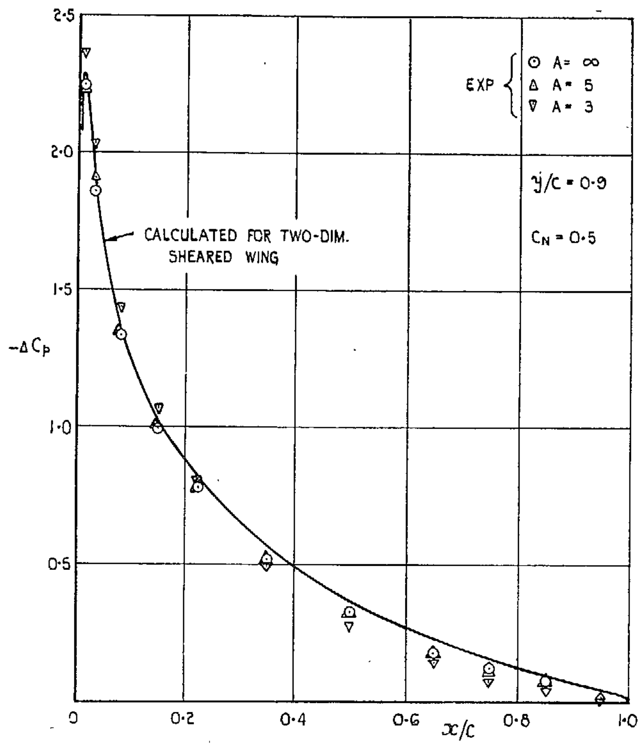

FIG. 5. Chordwise lift distributions for wings of different aspect ratio at $y/c = 0 \cdot 9$ for the same local C_N .

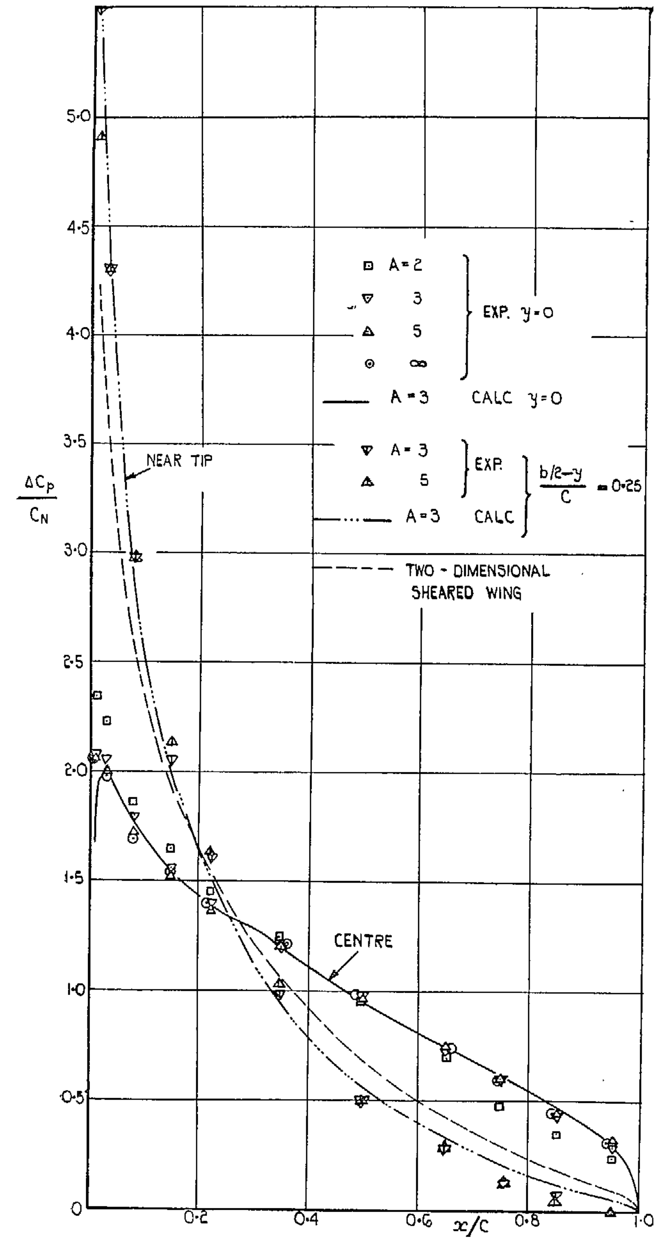

FIG. 6. Chordwise lift distributions. $C_N = 0 \cdot 33$.

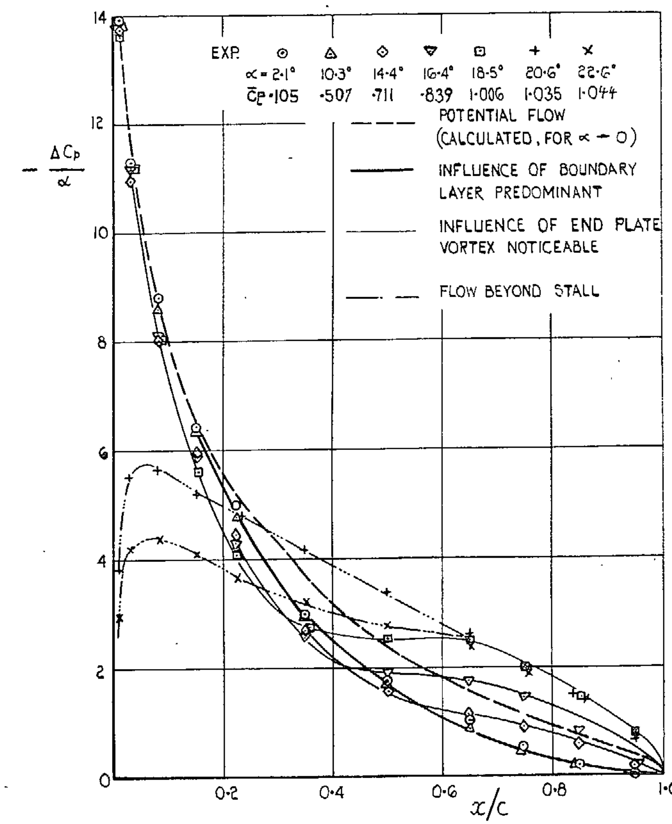

FIG. 7. Chordwise lift distributions.

$y/\frac{1}{2}b = 0\cdot61. \quad A = 3.$

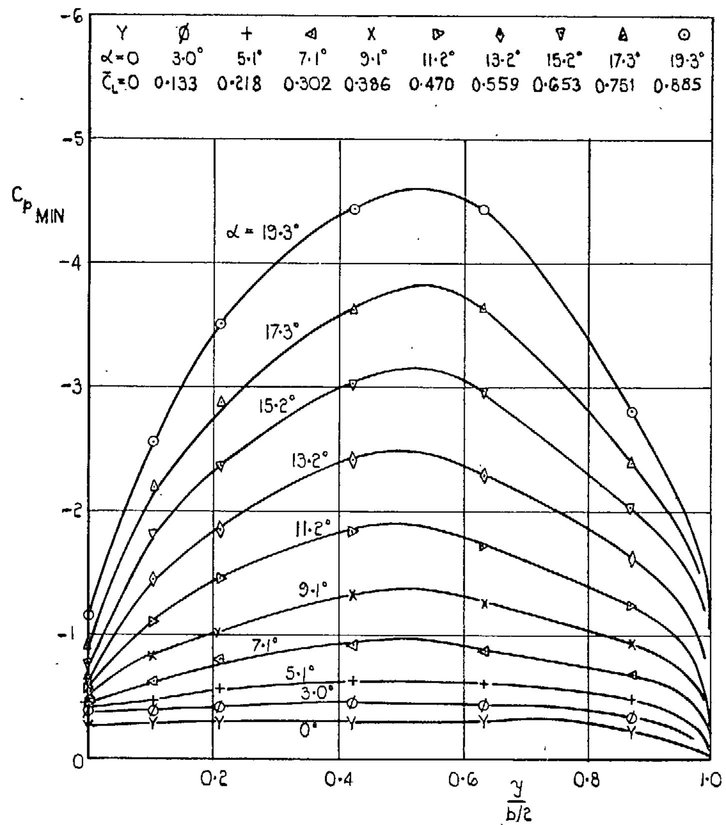

FIG. 8. Spanwise variation of peak suction.

$A = 2$.

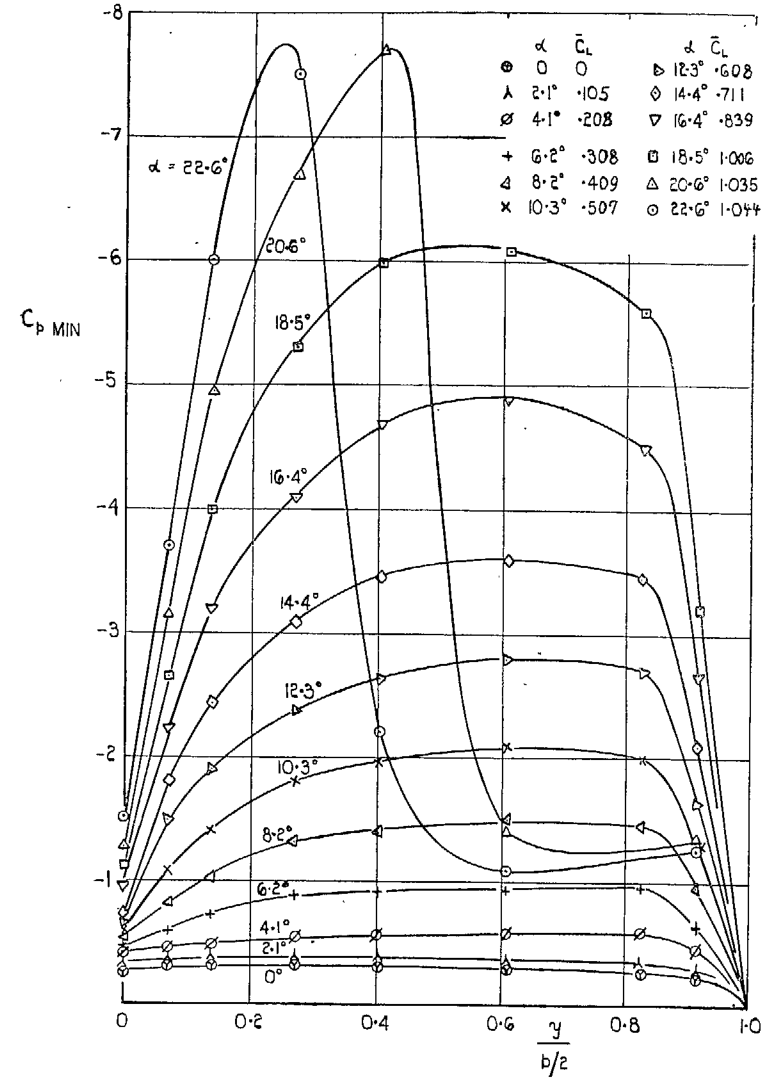

FIG. 9. Spanwise variation of peak suction.

$A = 3$.

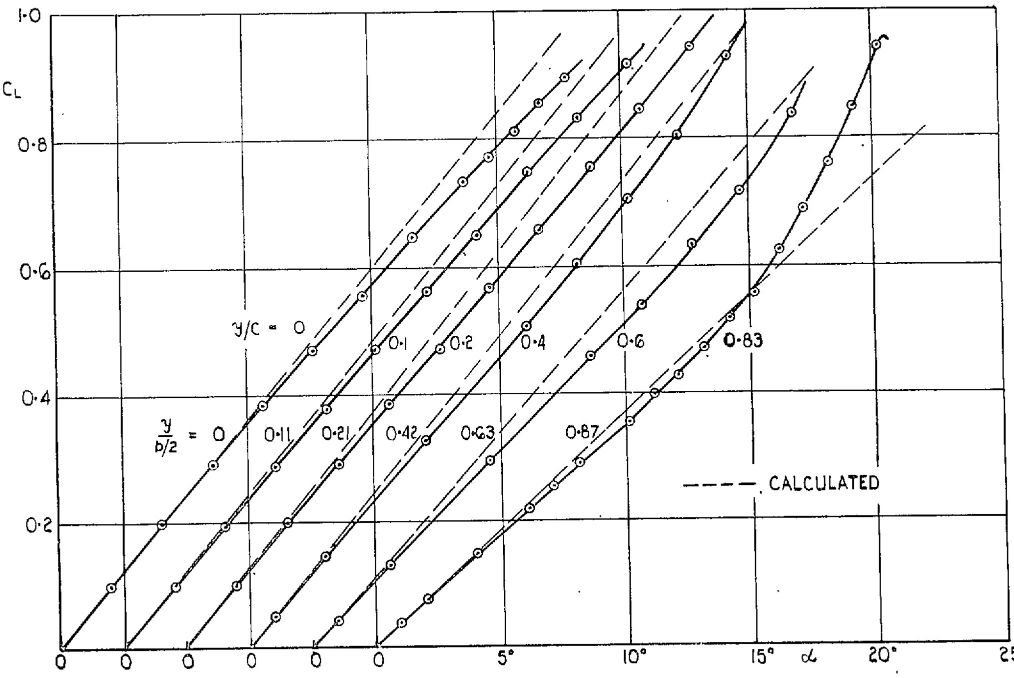

FIG. 10. Local lift coefficients. $A = 2$.

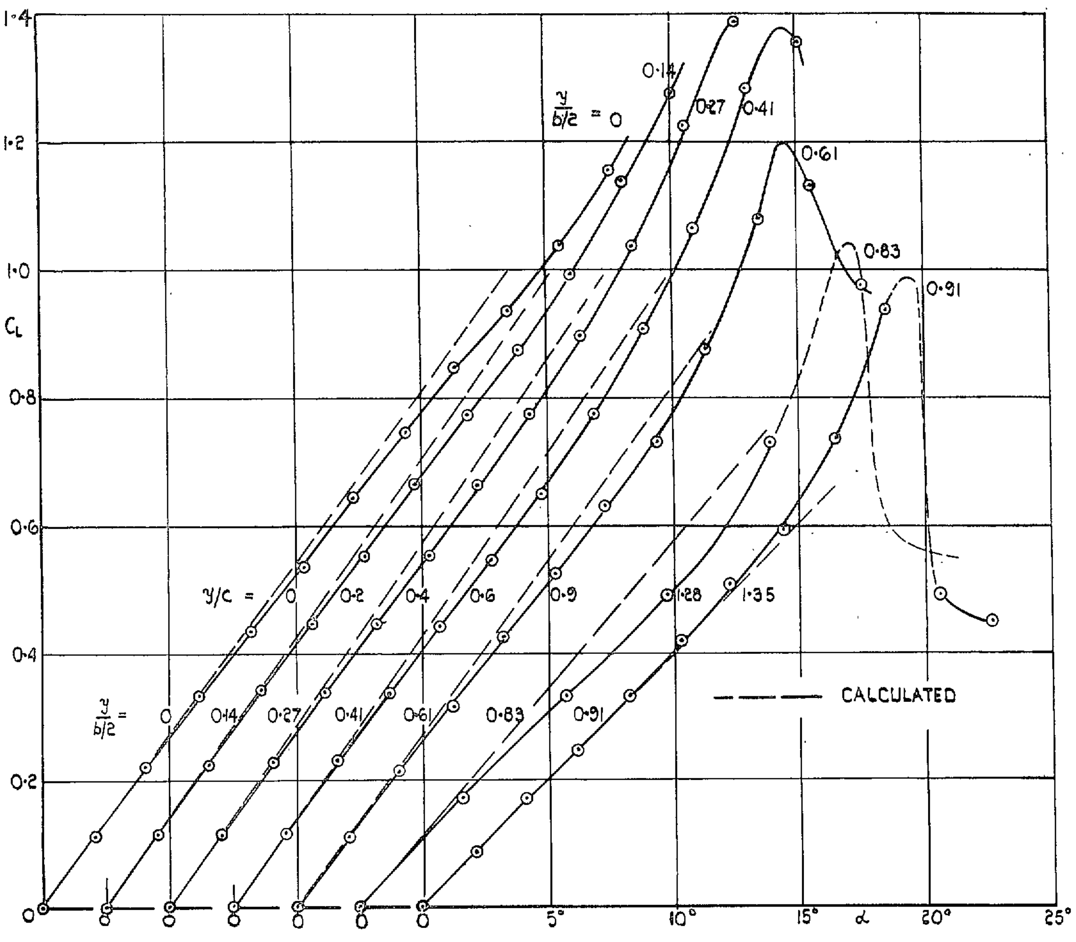

FIG. 11. Local lift coefficients. $A = 3$.

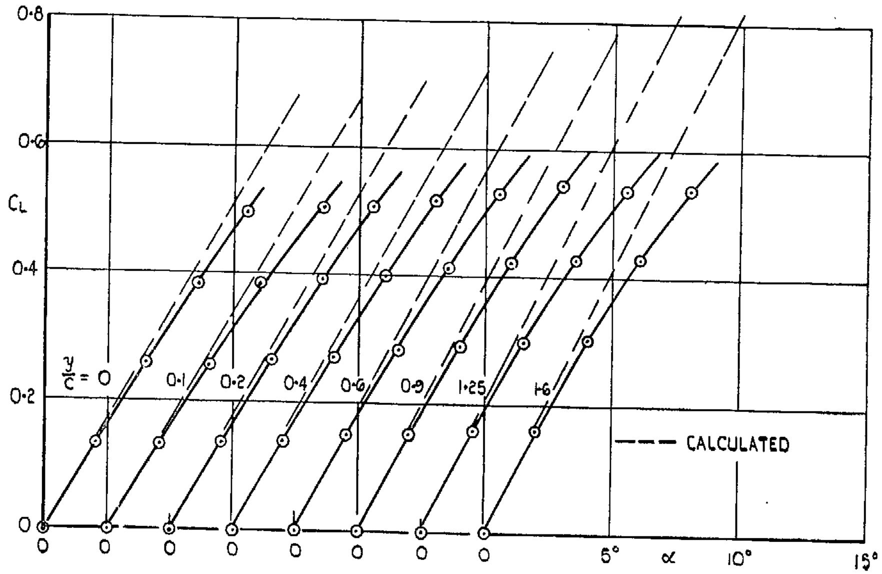

FIG. 12. Local lift coefficients.

$A = \infty$.

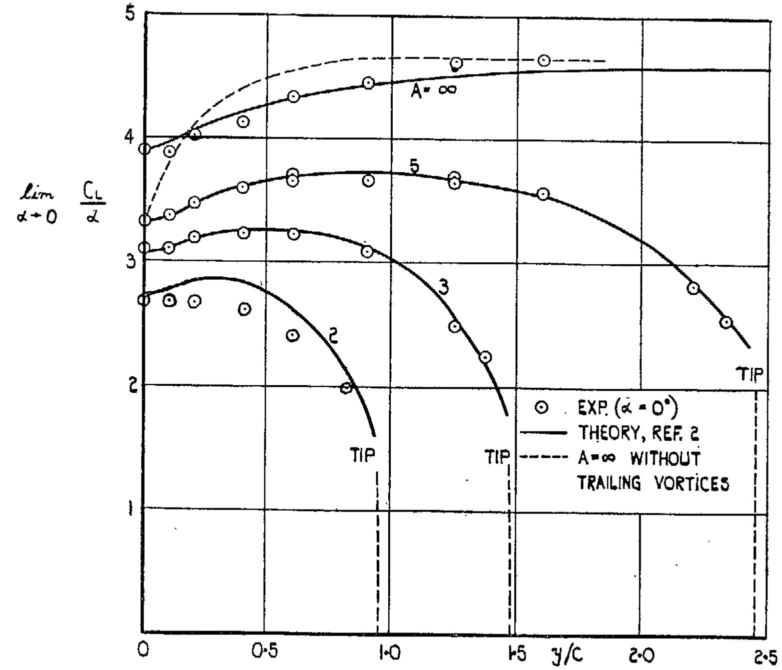

FIG. 13. Spanwise lift distribution.

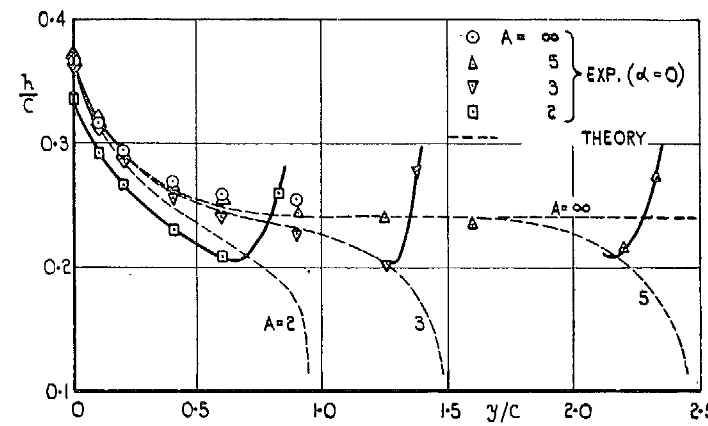

FIG. 14. Position of aerodynamic centre.

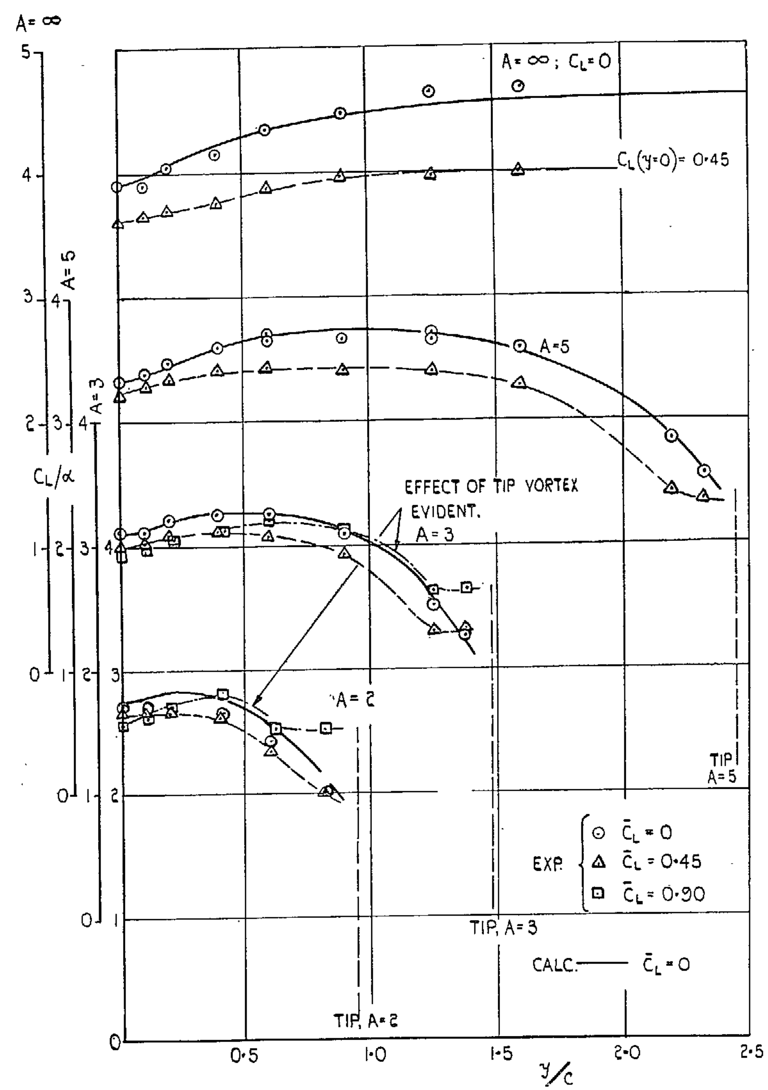

FIG. 15. Spanwise lift distributions.

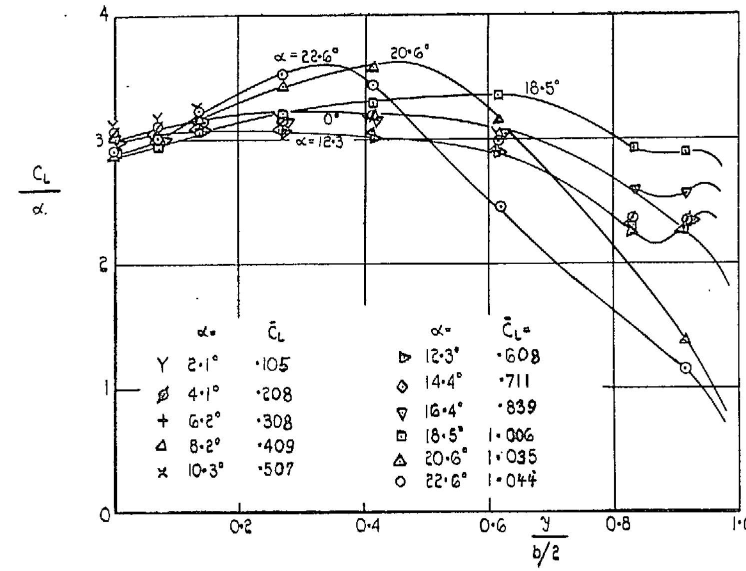

FIG. 16. Spanwise lift distributions.

$A = 3$.

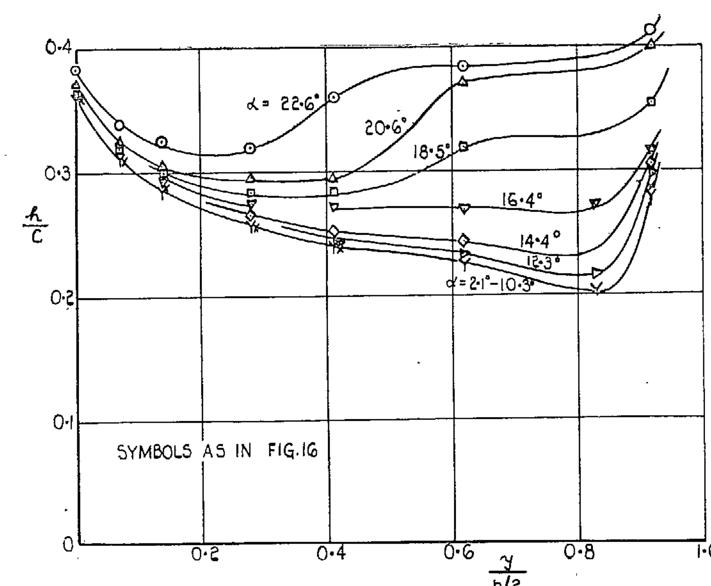

FIG. 17. Position of aerodynamic centre.

$A = 3$.

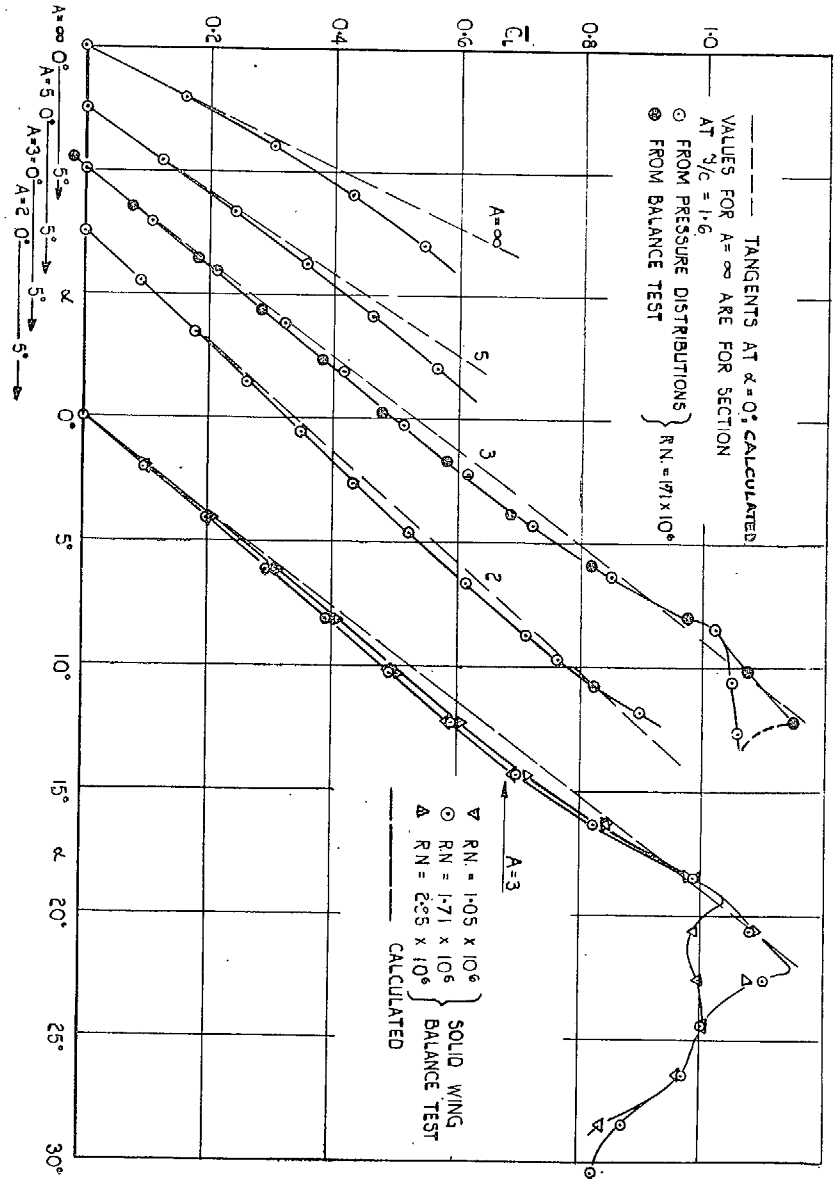

FIG. 19. Total lift coefficients.

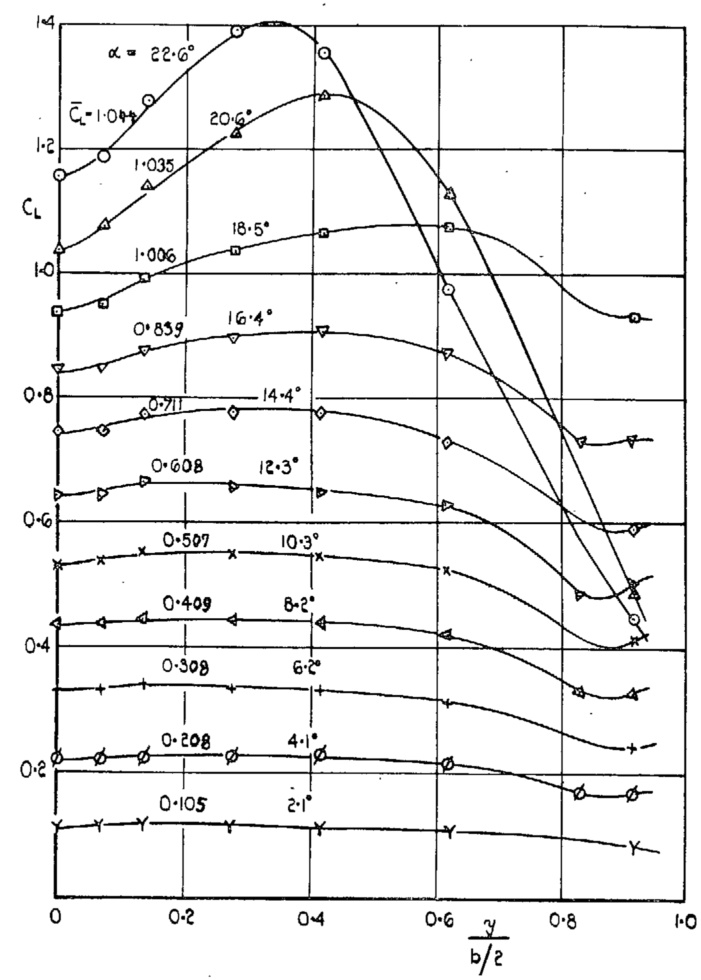

FIG. 18. Spanwise distributions of lift coefficient.

$A = 3$.

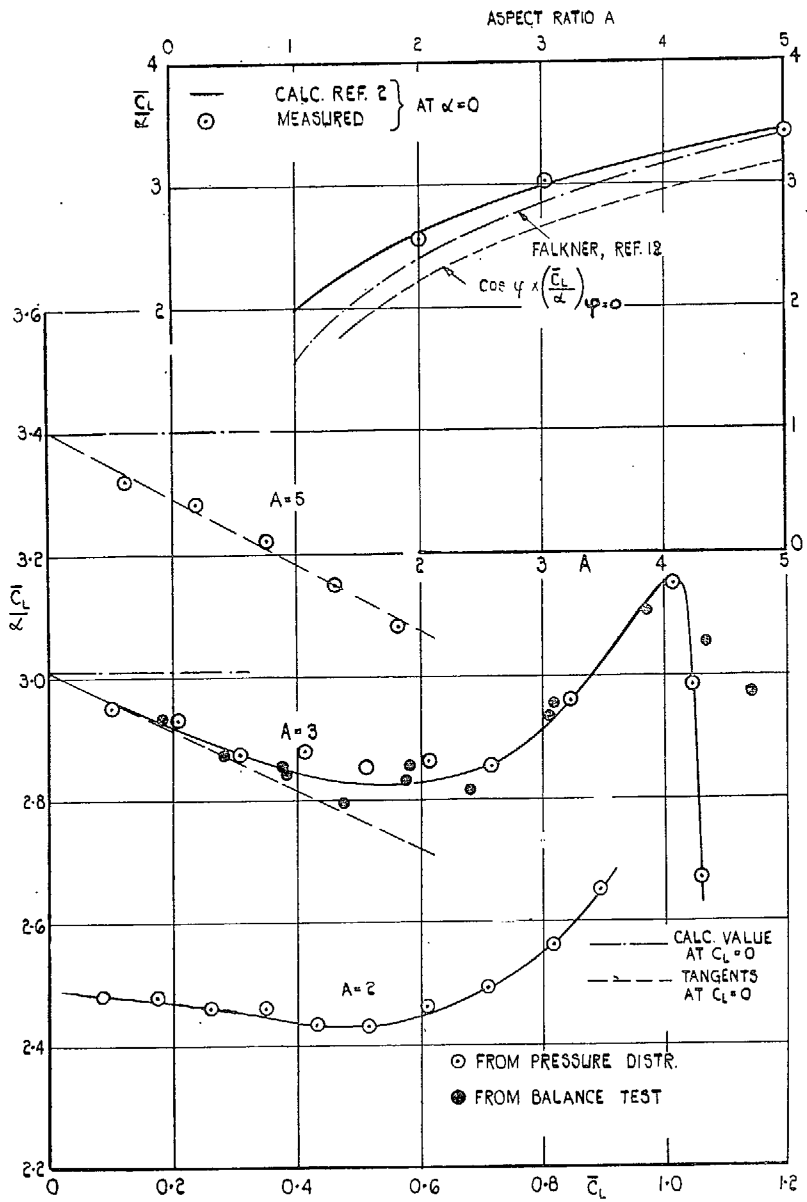

FIG. 20. Total lift slopes.

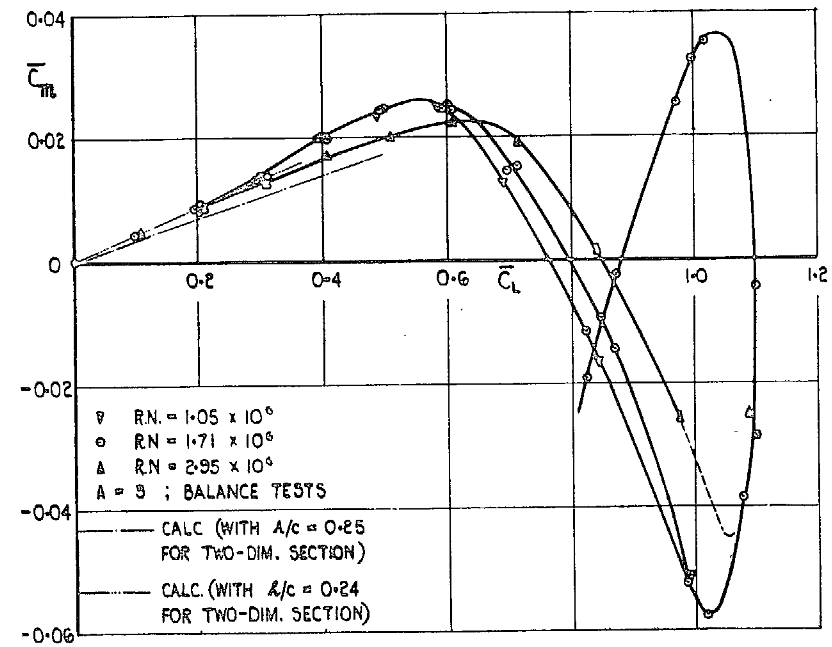

FIG. 21. Total pitching moments about mean quarter-chord point.

$A = 3$.

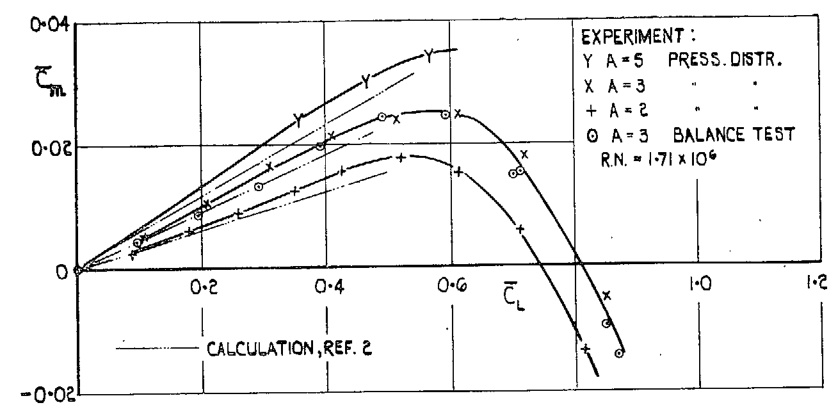

FIG. 22. Total pitching moments about mean quarter-chord point.

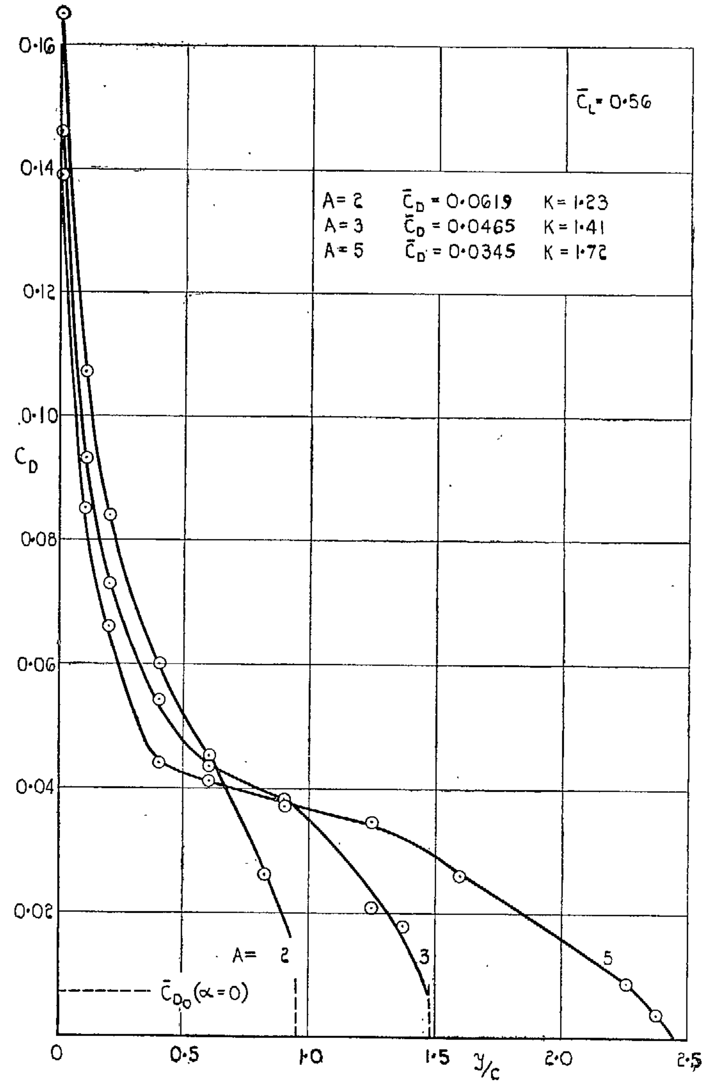

FIG. 23. Local drag coefficients.

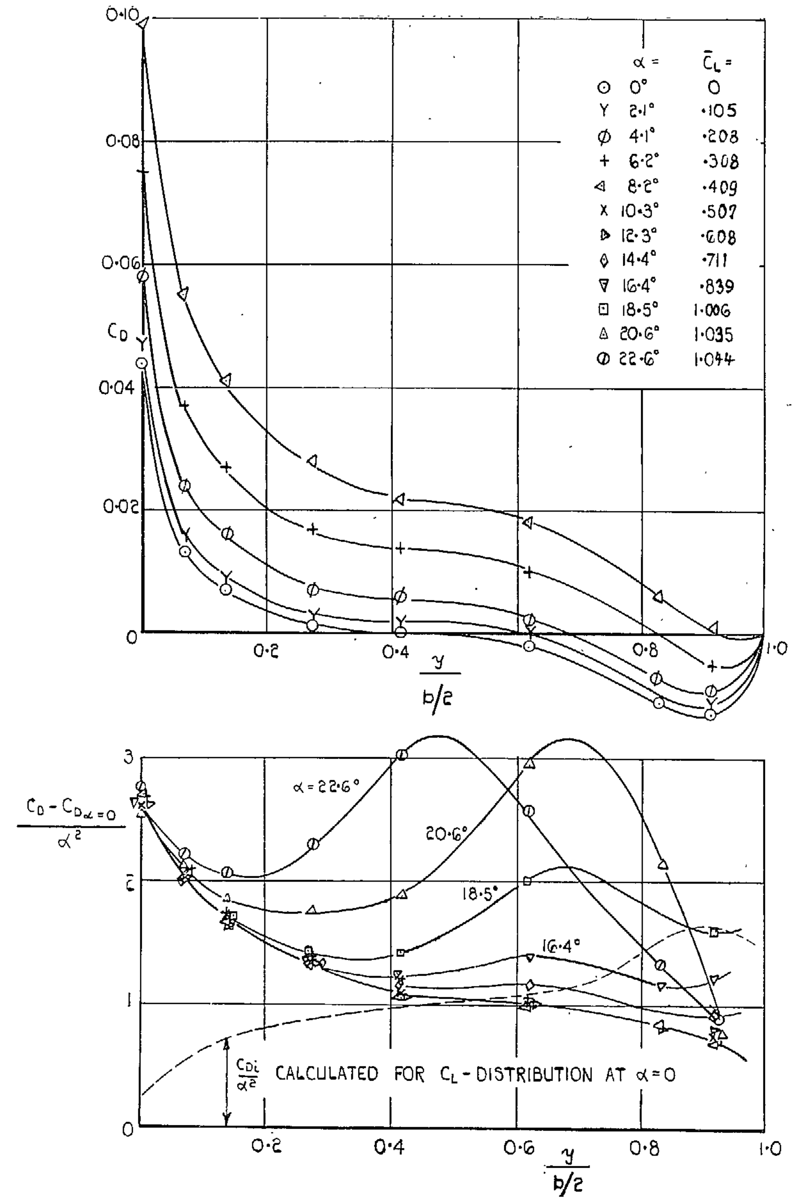

FIG. 24. Local drag coefficients.

$A = 3$.

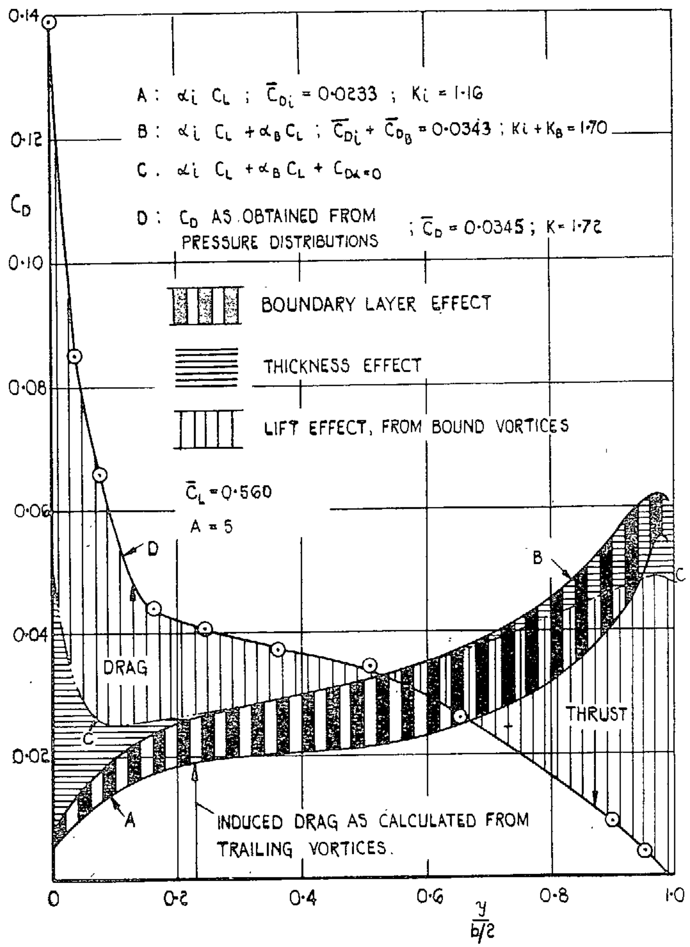

FIG. 25. Analysis of spanwise drag distribution.

$A = 5.$

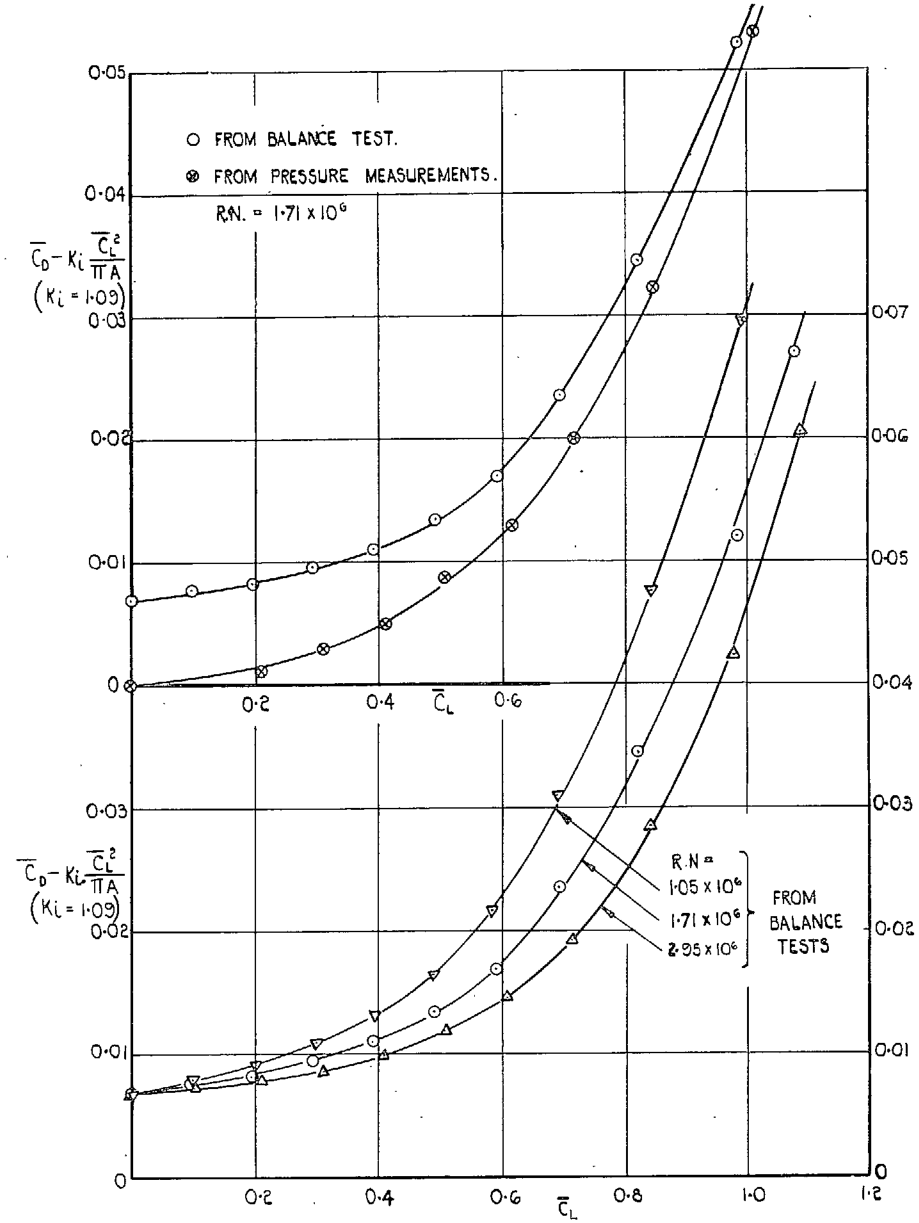

FIG. 26. Total drag minus induced drag due to trailing vortices.

$A = 3.$

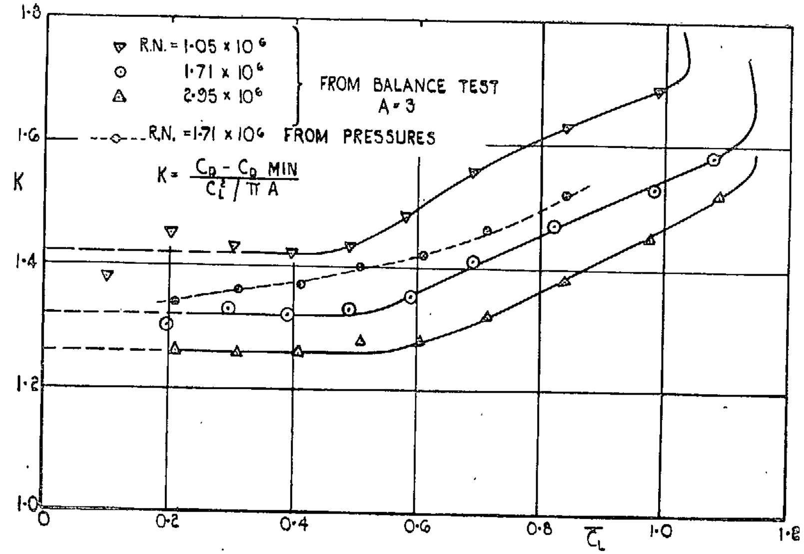

FIG. 27. Total induced drag factor. $A = 3$.

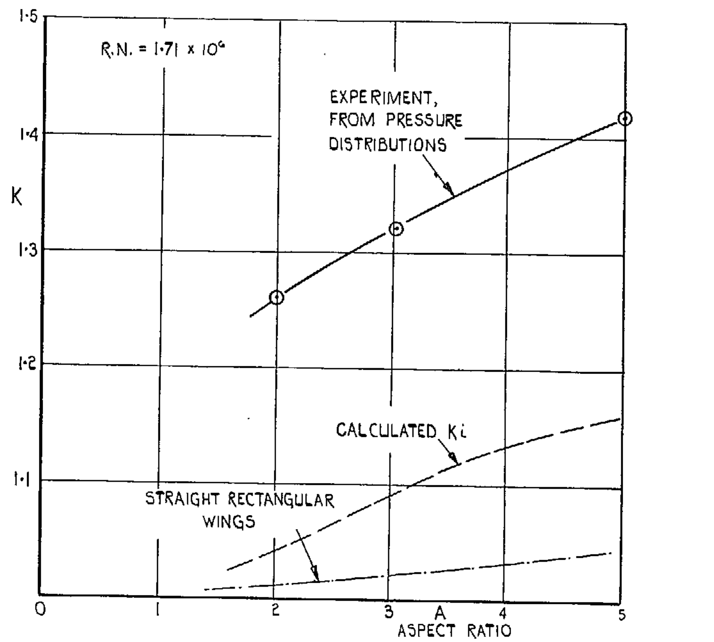

FIG. 28. Total induced drag factors at low C_L ($\simeq 0 \cdot 2$).

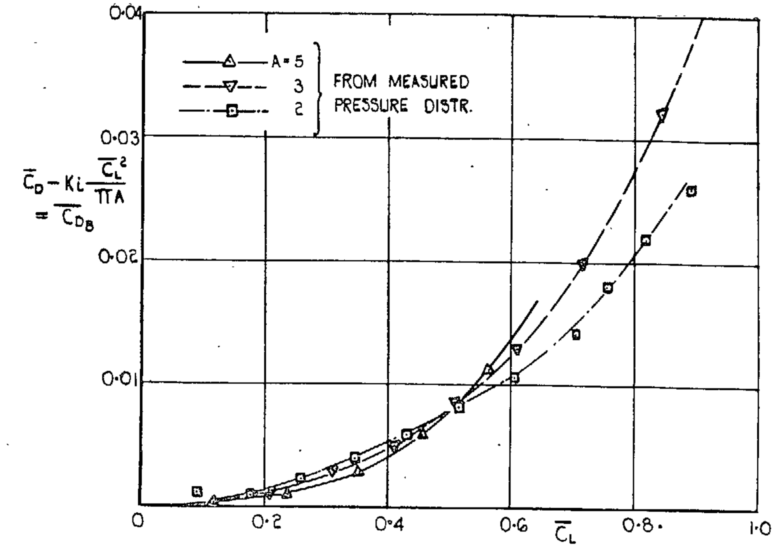

FIG. 29. Boundary-layer drag, from pressure distribution.

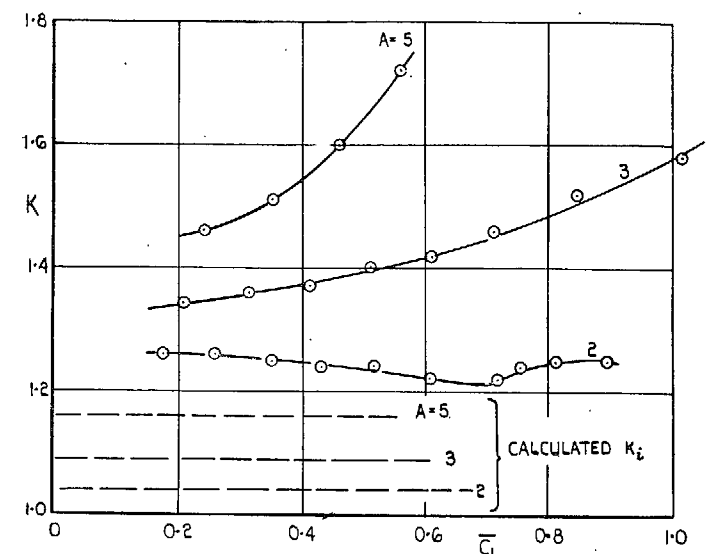

FIG. 30. Total induced drag factor, from pressure distribution.

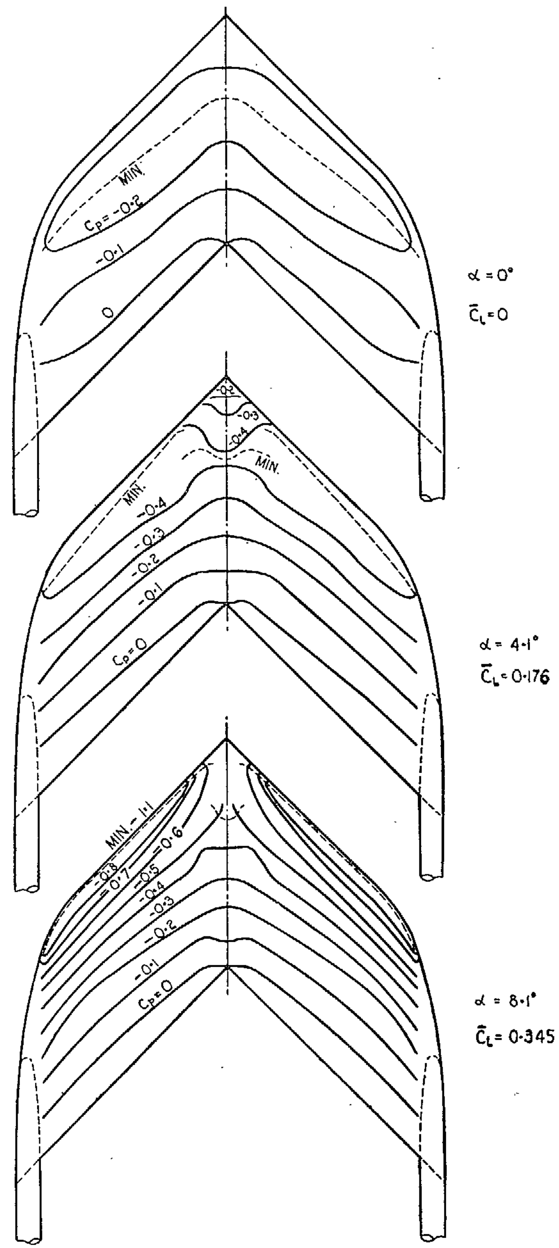

FIG. 31. Isobars on upper surface.
$A = 2.$

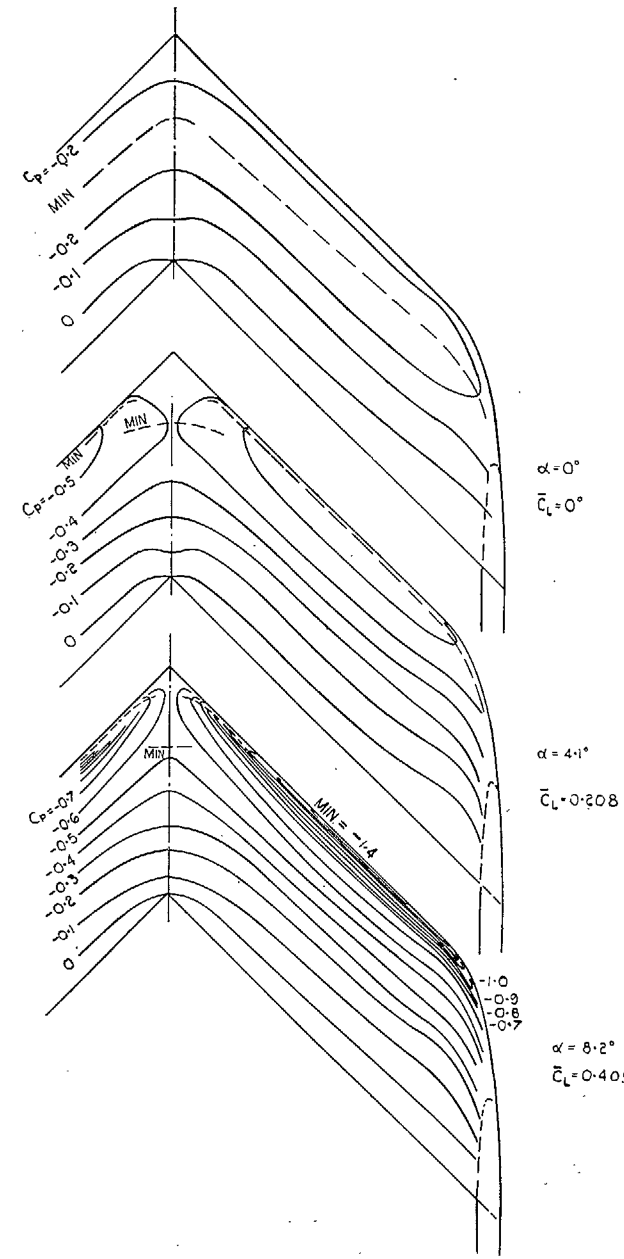

FIG. 32. Isobars on upper surface.
$A = 3.$

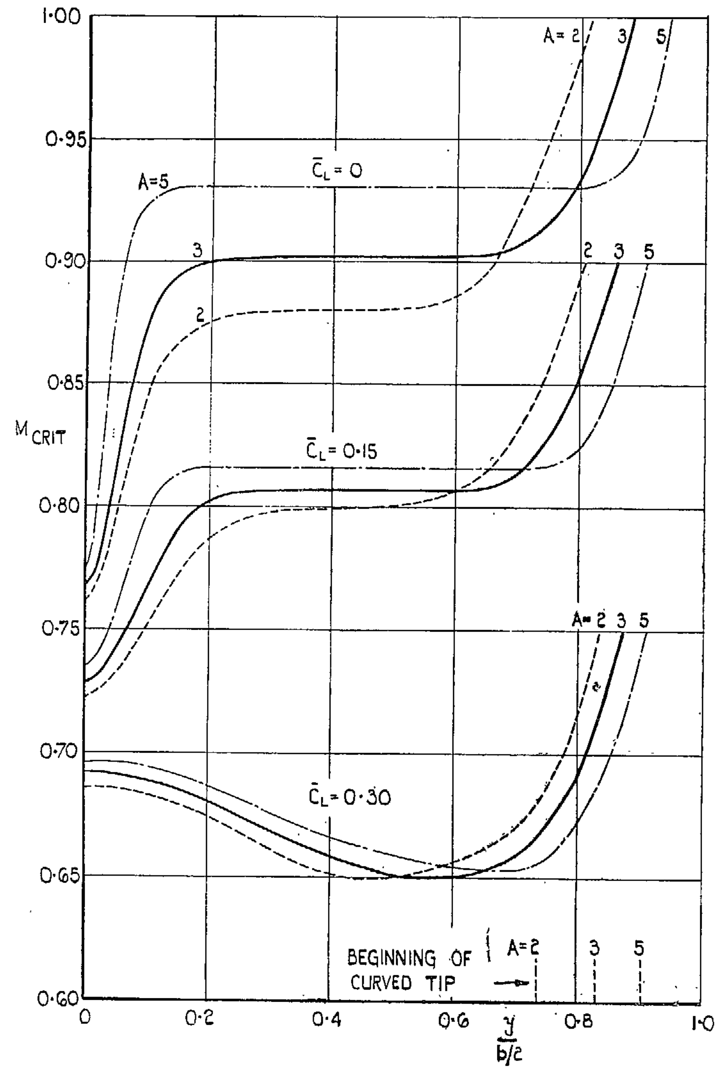

FIG. 33. Estimated critical Mach numbers.

(6705) Wt. 18/680 K7. 4/58 H.P.Co. 34-261

PRINTED IN GREAT BRITAIN

Publications of the Aeronautical Research Council

ANNUAL TECHNICAL REPORTS OF THE AERONAUTICAL RESEARCH COUNCIL (BOUND VOLUMES)—

1939 Vol. I. Aerodynamics General, Performance, Airscrews, Engines. 50*s.* (52*s.*)
Vol. II. Stability and Control, Flutter and Vibration, Instruments, Structures, Seaplanes, etc. 63*s.* (65*s.*)

1940 Aero and Hydrodynamics, Aerofoils, Airscrews, Engines, Flutter, Icing, Stability and Control, Structures, and a miscellaneous section. 50*s.* (52*s.*)

1941 Aero and Hydrodynamics, Aerofoils, Airscrews, Engines, Flutter, Stability and Control, Structures. 63*s.* (65*s.*)

1942 Vol. I. Aero and Hydrodynamics, Aerofoils, Airscrews, Engines. 75*s.* (77*s.*)
Vol. II. Noise, Parachutes, Stability and Control, Structures, Vibration, Wind Tunnels. 47*s.* 6*d.* (49*s.* 6*d.*)

1943 Vol. I. Aerodynamics, Aerofoils, Airscrews. 80*s.* (82*s.*)
Vol. II. Engines, Flutter, Materials, Parachutes, Performance, Stability and Control, Structures. 90*s.* (92*s.* 9*d.*)

1944 Vol. I. Aero and Hydrodynamics, Aerofoils, Aircraft, Airscrews, Controls. 84*s.* (86*s.* 6*d.*)
Vol. II. Flutter and Vibration, Materials, Miscellaneous, Navigation, Parachutes, Performance, Plates and Panels, Stability, Structures, Test Equipment, Wind Tunnels. 84*s.* (86*s.* 6*d.*)

1945 Vol. I. Aero and Hydrodynamics, Aerofoils. 130*s.* (132*s.* 9*d.*)
Vol. II. Aircraft, Airscrews, Controls. 130*s.* (132*s.* 9*d.*)
Vol. III. Flutter and Vibration, Instruments, Miscellaneous, Parachutes, Plates and Panels, Propulsion. 130*s.* (132*s.* 6*d.*)
Vol. IV. Stability, Structures, Wind Tunnels, Wind Tunnel Technique. 130*s.* (132*s.* 6*d.*)

ANNUAL REPORTS OF THE AERONAUTICAL RESEARCH COUNCIL—

1937 2*s.* (2*s.* 2*d.*) 1938 1*s.* 6*d.* (1*s.* 8*d.*) 1939–48 3*s.* (3*s.* 5*d.*)

INDEX TO ALL REPORTS AND MEMORANDA PUBLISHED IN THE ANNUAL TECHNICAL REPORTS, AND SEPARATELY—

April, 1950 . . . . . . R. & M. No. 2600 2*s.* 6*d.* (2*s.* 10*d.*)

AUTHOR INDEX TO ALL REPORTS AND MEMORANDA OF THE AERONAUTICAL RESEARCH COUNCIL—

1909–January, 1954 . . . R. & M. No. 2570 15*s.* (15*s.* 8*d.*)

INDEXES TO THE TECHNICAL REPORTS OF THE AERONAUTICAL RESEARCH COUNCIL—

December 1, 1936 — June 30, 1939	R. & M. No. 1850	1*s.* 3*d.* (1*s.* 5*d.*)
July 1, 1939 — June 30, 1945	R. & M. No. 1950	1*s.* (1*s.* 2*d.*)
July 1, 1945 — June 30, 1946	R. & M. No. 2050	1*s.* (1*s.* 2*d.*)
July 1, 1946 — December 31, 1946	R. & M. No. 2150	1*s.* 3*d.* (1*s.* 5*d.*)
January 1, 1947 — June 30, 1947	R. & M. No. 2250	1*s.* 3*d.* (1*s.* 5*d.*)

PUBLISHED REPORTS AND MEMORANDA OF THE AERONAUTICAL RESEARCH COUNCIL—

Between Nos. 2251–2349	R. & M. No. 2350	1*s.* 9*d.* (1*s.* 11*d.*)
Between Nos. 2351–2449	R. & M. No. 2450	2*s.* (2*s.* 2*d.*)
Between Nos. 2451–2549	R. & M. No. 2550	2*s.* 6*d.* (2*s.* 10*d.*)
Between Nos. 2551–2649	R. & M. No. 2650	2*s.* 6*d.* (2*s.* 10*d.*)
Between Nos. 2651–2749	R. & M. No. 2750	2*s.* 6*d.* (2*s.* 10*d.*)

Prices in brackets include postage

HER MAJESTY'S STATIONERY OFFICE

York House, Kingsway, London, W.C.2; 423 Oxford Street, London, W.1; 13a Castle Street, Edinburgh 2; 39 King Street, Manchester 2; 2 Edmund Street, Birmingham 3; 109 St. Mary Street, Cardiff; Tower Lane, Bristol 1; 80 Chichester Street, Belfast *or through any bookseller.*

S.O. Code No. 23-2882